Use of volume-based 3-D seismic attribute analysis to characterize physical property distribution:

A case study to delineate reservoir heterogeneity at the Appleton Field, SW Alabama

By

Juliana M. TEBO

Department of Earth and Planetary Sciences

McGill University, Montréal, Canada

March 2003

A thesis submitted to the Faculty of Graduate and Postdoctoral Studies McGill University in partial fulfillment of the degree of Master of Science.

Your file Votre référence
ISBN: 0-612-88314-0
Our file Notre référence
ISBN: 0-612-88314-0

ABSTRACT

The use of seismic attribute studies in the petroleum industry is fast spreading. Seismic attribute studies entail the integration of derived attributes from 3-D seismic data with well log, core and/or outcrop data (through multivariate linear regression, neural networks, etc.) to estimate and project physical properties in areas of sparse data control. Because of the accuracy of this technique in predicting the subsurface distribution of physical properties in 3-D space, and delineating depositionally and non-depositionally controlled trends not readily apparent from other methods commonly used in sedimentary geology (e.g., facies modeling, geostatistics, and sequence stratigraphy), it becomes an important tool for sedimentary geologists.

We illustrate the techniques and advantages of the approach to predict 3-D distribution of porosity in stratigraphically complex carbonate buildups of the Upper Jurassic Smackover Formation at Appleton Field, southwest Alabama. This research shows the usefulness of multiple seismic attributes, which may have diverse physical relationships to the physical properties of a stratigraphic interval, to predict porosity. It also sheds light on the causes of facies heterogeneity observed in the porous interval at Appleton Field. Statistics and forward modeling are used to validate the robustness of the multiattribute results. We predict that porosity is thicker on the forereef flanks than on the crest of paleostructure. This conclusion is geologically reasonable in terms of the sequence stratigraphic framework, and agrees with core and facies analyses from earlier studies.

This study indicates that primary depositional facies play a critical role in determining porosity formation and its distribution in this and other Smackover fields of the basement-ridge play. Images obtained from this volume-based method, never before applied at Appleton Field, improved our understanding of the geologic factors controlling facies deposition in this field. It further augments the applicability of seismic attribute analysis in defining physical property distribution in the subsurface.

SOMMAIRE

L'utilisation des attributs sismiques pour l'estimation des propriétés du réservoir devient de plus en plus répandue dans l'industrie pétrolière. Les études basées sur cet approche requièrent l'intégration de données du forage, du carottage et/ou d'affleurement avec les attributs sismiques obtenus à partir de données sismiques en 3-D. Pour cela, des méthodes en régression linéaire multidimensionnelle et réseaux neuronaux ont été proposés.

La capacité de cet approche à prédire la distribution des propriétés physiques, ainsi qu'à définir les tendances qui sont contrôlées ou non par l'environnement géologique, rend cet approche un outil important pour les géologues sédimentaires. L'obtention de tels résultats n'étant pas évidente par des méthodes d'analyse généralement employées en géologie sédimentaire (i.e., modélisation des faciès, géostatistique et/ou stratigraphie séquentielle).

Lors de cette étude, nous mettons en évidence les avantages des attributs sismiques générés à partir du volume de données sismiques afin de prédire la distribution de la porosité dans les dépôts carbonatées de la Formation Smackover Jurassique Supérieur dans l'Appleton Field au sud-ouest de L'Alabama. Nos résultats montrent l'existence d'une relation empirique entre certains attributs sismiques et la porosité de l'intervalle stratigraphique analysé. Dans le but de corroborer la robustesse de nos résultats, nous avons utilisé la modélisation numérique et des méthodes statistiques. À partir de nos résultats, nous prédisons que la porosité est plus épaisse sur le talus du récif que sur la crête. De plus, ceux-ci éclaircissent les causes de l'hétérogénéité des faciés observées dans l'intervalle poreux d'Appleton Field. Cette conclusion est géologiquement raisonnable car elle correspond aux résultats obtenus par d'autres études.

Notre recherche indique aussi que la nature des faciés de dépôt primaire joue un rôle critique lorsqu'il s'agit de déterminer l'origine et la distribution de la porosité dans l'Appleton Field et comme d'autres zones dans le Smackover du socle rocheux. De plus, les images obtenues à partir de ce volume représentent une première application de cette approche dans cette région, et celles-ci ont contribué à mieux comprendre les éléments géologiques contrôlant la formation et la distribution de la porosité. Les résultats démontrent l'applicabilité d'attributs sismiques afin de déterminer la distribution des propriétés physiques du sub-surface.

CONTRIBUTIONS OF AUTHORS

I hereby declare that all practical and analytical aspects of the studies described in this thesis were carried out by me. Dr. Bruce Hart supervised the investigational work and ensured that a critical and coherent scientific approach was maintained throughout the study.

DEDICATION

To my late aunt, Ruth Tebo-Ngwa, and late uncle, David Tebo. Rest in peace.

ACKNOWLEDGEMENTS

Funded, primarily, by a U.S. Department of Energy award to Dr. E. Mancini of the University of Alabama, Tuscaloosa, this study is part of an ongoing research project to characterize and model reservoir architecture of the Upper Jurassic reef and shoal grainstone reservoirs associated with basement paleohighs. I would like to thank the companies that provided the well, core, and seismic data made available to us by Dr. Mancini and Brian Panetta of the University of Alabama, Tuscaloosa.

Thanks also to Geographix and Hampson-Russell Inc. for providing the necessary seismic attribute extraction and analysis, modeling and interpretation software packages; and also the software support that was required during various phases of my analysis. Much appreciation goes to Venetia Bodycomb, Robin Pearson, Ivan Marroquin, Kamal Al Troshi, Emmanuel Sakoma, and Henri Nfon for providing useful insights on applied analytical techniques and assistance in revising this thesis.

I would like to thank my family and friends whose constant support/encouragement, love, advice, and trust in my capabilities will always be appreciated.

Special thanks go to Prof. Eric Mountjoy of the Earth and Planetary McGill University for valuable critique on my work and for introducing me to a new world of carbonates.

Most importantly, I wish to express immense gratitude to my supervisor, Dr. Bruce Hart, for making me a part of this outstanding project. I would also commend him for his constant support, guidance, teaching, knowledge, and logical approach to problem definition throughout my stay at McGill.

TABLE OF CONTENTS

LIST OF FIGURES

LIST OF TABLES

LIST OF APPENDICES

CHAPTER 1

1.1 General Introduction

The Upper Jurassic (Oxfordian) Smackover Formation is a stratigraphically complex carbonate formation. This formation is a major producer of hydrocarbons in the northeastern Gulf of Mexico (Baria *et al.*, 1982; Salvador, 1991; Mancini, 2000). One of the main reservoir facies in the Smackover Formation are the microbial and microbial-coral reefs, which extend from Arkansas to Florida. Pioneer studies to examine the Smackover reefs were carried out by Baria *et al*, (1982), and Crevello and Harris, (1984). Baria *et al.*, (1982) defined the reefal facies as occurring principally on the seaward flanks of paleostructures, and to consist of digitate and branching blue-green algae, or diverse coral assemblages. Crevello and Harris (1984) assigned the Smackover Formation to a gently sloping ramp depositional setting. Although several studies have been carried out to describe and characterize physical properties of the Smackover reservoir interval in the northeastern Gulf of Mexico, their heterogeneity is yet to be properly defined (Baria *et al*, 1982; Crevello and Harris; Benson, 1985, 1988; Mancini and Benson, 1980; Benson *et al*, 1996, 1997; Mancini *et al.*, 1999; Mancini, 2000; Parcell, 1999, 2000; Hart and Balch, 2000).

The study area for this project encompasses Appleton Field, a Smackover oil field of the basement ridge play in southwestern Alabama. Numerous studies have been carried out with an attempt to define the spatial distribution of depositional facies of the Appleton Field. The spatial distribution of facies is the major factor controlling reservoir heterogeneity in this field (Benson, 1988).

Facies heterogeneity should be defined in 3-D space in order to optimize field development strategies.

Core and log data were used to produce a detailed description of the reefal interval, which comprises of 14 lithofacies: carbonate mudstone, peloidal wackestone, peloidal packstone, peloidal/oncoidal packstone, peloidal/oolitic packstone, peloidal grainstone, oncoidal grainstone, oolitic grainstone, oncoidal/peloidal/oolitic grainstone, algal grainstone, microbial boundstone (bafflestone), microbial bindstone, algal laminite, and anhydrite (Benson, *et al.*, 1996; Markland, 1992). These lithofacies were assigned to four time-equivalent genetic depositional systems: reef/subtidal, shoal, lagoon/tidal flat, and sabkha (Benson *et al*, 1996). Log and core data capture vertical changes in facies and their associated physical property variation, but they cannot be used to unambiguously quantify such changes in inter-well areas unless they are very closely spaced (Dubrule, 1998).

Hart and Balch (2000) used forward modeling (*c.f.*, Neidell and Poggiagliolmi, 1977) to seismically image Smackover stratigraphy at Appleton Field. Forward modeling showed that the top of the Smackover could not be defined seismically. They were able however, to distinguish and map seismically the top of the porous unit (a trough) within the Smackover Formation. The thickness and large acoustic impedance difference between the porous unit (reefal) and the overlying non-porous unit (lagoon/tidal flat) of the Smackover Formation made it possible to map this top. In addition, computer modeling to simulate carbonate production and deposition during the Late Jurassic using fuzzy logic (*c.f.* Chang *et al.*, 1997) suggested that the thickness and distribution of the reefal facies were controlled by paleobasement topography, rate of sea level rise, carbonate productivity, and duration of reef growth (Kopaska-Merkel, 1994; Mancini *et al.*, 1999; Parcel, 2000). Although these modeling efforts could be used to predict the presence and/or extent of reservoir facies, they do not provide quantitative 3-D information on porosity distribution within the reservoir. As such, they cannot be used for planning drilling strategies or reserve estimation.

The microbial buildups in northeastern Gulf of Mexico are primarily thrombolitic[1] (Crevello and Harris, 1984; Markland, 1992; Parcell, 2000). The controls on the formation and the character of the thrombolitic facies in the Appleton Field are poorly understood due to insufficient core data. Also, there are no surface exposures for the Smackover Formation in the northeastern Gulf of Mexico. Hence, Parcell (2000), and Mancini and Parcell (2001) have used outcrop analogues for the microbial reefs from Western Europe (Algarve Basin of southern Portugal) to characterize the origin, composition, geometry, extent, and to model subsurface facies relationship at the Appleton Field. They show that low background sedimentation, increased alkalinity, substrate availability, and low oxygen and nutrient levels were the major factors controlling thrombolite formation. Furthermore, the growth forms of these thrombolites were dependent

---

[1] Earlier works referred to the reefal buildups as blue-green algae. Later, they were interepreted to be of cyanobacteria or microbial origin. Most recently, these reefal buildups have been referred to as thrombolites.

on the carbonate productivity and wave energy within the depositional system. Their study highlights factors to consider when modeling thrombolite reservoirs.

Hart and Balch (2000) conducted the only study, besides the current project, that has attempted to directly image the porosity distribution for Appleton Field. They used a horizon-based seismic attribute study to predict porosity thickness (c.f., Hart and Balch, 2000). Although the results of their work were quantitative, and were used to recommend the successful drilling of a new well (permit # 3854-B), they could not effectively depict porosity distribution in 3-D within the Smackover Formation.

1.2 Thesis Objectives

The principal objectives of this study are to:

(1) Quantitatively estimate porosity for the stratigraphically complex Smackover Formation at Appleton Field using a volume-based 3-D seismic attribute study.

(2) Create a 3-D porosity model to examine causes of heterogeneity in porosity distribution in the Smackover Formation at Appleton Field.

(3) Illustrate how applying a method that integrates geology, geophysics, and geostatistics can improve uncertainty associated with physical property prediction in areas of limited well control.

(4) Validate our porosity predictions with previous geologic information obtained from log, core, and outcrop data, and principles governing

porosity formation in this field (e.g., sequence stratigraphy, sedimentology, etc).

1.3 Thesis Outline

This study is presented in three parts: Chapter 1 gives a brief summary of the work done in an attempt to characterize physical property distribution (e.g., lithology, porosity) in the Smackover Formation at the Appleton Field. Chapter 2, the main focus of this study, gives a summary of the geology at Appleton Field, the database available for this analysis, and a breakdown of the methods used to achieve the objectives. It also illustrates the use of seismic attributes in physical property estimation by showing the contribution of each predicting attribute in delineating porosity distribution. In addition, it suggests probable causes for porosity development in these buildups. Finally, it proposes other areas in which this method can be applied. The last chapter, Chapter 3 gives the conclusions derived from analyzed results and their implications

References

BARIA, I.R., STOUDT, D.I., HARRIS, P.M., and CREVELLO, P.D., 1982, Upper Jurassic reef of the Smackover Formation, United States Gulf Coast: *American Association of Petroleum Geologists Bull.,* v. 66, no. ??, p. 1449-1482.

BENSON, D.J., 1985, Diagenetic controls on reservoir development and quality, Smackover Formation of southwest Alabama: *Transactions, Gulf Coast Association of Geological Societies*, v. 35, p. 317-326.

BENSON, D.J., 1988, Depositional history of the Smackover Formation in southwest Alabama: *Transactions, Gulf Coast Association of Geological Societies*, v. 38, p. 197-205.

BENSON, D.J., PULTZ, L.M., and BRUNNER, D.D., 1996, The influence of paleotopography, sea level fluctuation, and carbonate productivity on deposition of Smackover and Buckner Formations, Appleton Field, Escambia county, Alabama: *Transactions, Gulf Coast Association of Geological Societies*, v. 46, p. 15-23.

BENSON, D.J., MANCINI, E.A., GROSHONG, R.H., FANG, J.H, PULTZ, L.M., and CARLSON, E.S., 1997, Petroleum Geology of Appleton Field, Escambia County, Alabama: *Transactions, Gulf Coast Association of Geological Societies*, v. 47, p. 35-42.

CHANG, H., CHEN, H., and FANG, J.H., 1997, Lithology determination from well logs with fuzzy associative memory neural network: IEEE: *Transactions on Geoscience and Remote Sensing*, v. 35, no. 3, p. 773-780.

CREVELLO, P.D., and HARRIS, P.M., 1984, Depositional models for Jurassic reefal buildups: *In* W.P.S. Ventress, D.G. Bebout, B.F. Perkins, and C.H. Moore (eds.) The Jurassic of the Gulf Rim: Proceedings of the Third Annual Research Conference, Gulf Coast Section, *SEPM Foundation*, p. 57-102.

DUBRULE, O., 1998, Geostatistics in petroleum Geology: *American Association of Petroleum Geologists Continuing Education Course Note Series*, no. 38, 52p.

KOPASKA-MERKEL, D.C., MANN, S.D., and SCHMOKER, J.W., 1994, Controls on reservoir development in a shelf carbonate: Upper Jurassic Smackover Formation of Alabama: *American Association of Petroleum Geologists Bull.*, v. 78, no. 6 (June 1994), p. 938-959.

HART, B.S., and BALCH, R.S., 2000, Approaches to defining reservoir physical properties from 3-D seismic attributes with limited well control: An example from the Jurassic Smackover Formation, Alabama: *Geophysics*, v. 65, no. 2, p. 368-376.

MANCINI, E.A., 2002, Integrated geologic-engineering model for reef and carbonate shoal reservoirs associated with paleohighs: upper Jurassic Smackover Formation, NE Gulf of Mexico: Annual Report Year 2. On-line report retrieved Oct. 3, 2002, from Petrl. Techn. Trans. Council Web site: http://egrpttc.geo.ua.edu/reports/geo_eng_model2/title.html.

MANCINI, E.A., and BENSON, D.J., 1980, Regional stratigraphy of Upper Jurassic Smackover carbonates of southwest Alabama: *Transactions, Gulf Coast Association of Geological Societies*, v. 30, p. 151-165.

MANCINI, E.A., and BENSON, D.J., 1998, Upper Jurassic Smackover carbonate reservoir, Appleton Field, Escambia County, Alabama: *In* J.L. Allen and T. S. Brown (eds), 3-D case history of Gulf of Mexico, p. 1-14.

MANCINI, E.A. and PARCELL, W.C., 2001, Outcrop analogues for reservoir characterization and modeling of Smackover microbial reefs in the northeastern Gulf of Mexico: *Transactions, Gulf Coast Association of Geological Societies*, v. 51, p. 207-218.

MANCINI, E.A., TEW, B.H., and MINK, R.M., 1990, Jurassic sequence stratigraphy in the Mississippi interior salt basin: *Gulf Coast Association of Geological Societies Transactions*, v. 40, p. 521- 529.

MANCINI, E.A., HART, B.S., CHEN, H., BALCH, R.S., PARCELL, W.C., WANG, W., and PANETTA, B.J., 1999, Integrated geological, geophysical, and computer approach for predicting reef lithofacies and reservoirs: Upper Jurassic Smackover Formation, Appleton Field, Alabama. *GCSSEPM Foundation: 19th Annual Research Conference*: Advanced Reservoir Characterization. December 5-8, 1999, p. 235-247.

MANCINI, E.A., BENSON, D.J., HART, B.S., BALCH, R.S, PARCELL, W.C, and PANETTA, B.J, 2000, Appleton Field case study (eastern Gulf coastal plain): Field development model for Upper Jurassic microbial reef reservoirs associated with paleotopographic basement structures: *American Association of Petroleum Geologists Bull.*, v. 84, no. 11 (November), p.1699-1717.

MARKLAND, L.A., 1992, Depositional history of the Smackover Formation, Appleton Field, Escambia county, Alabama: Master's thesis, University of Alabama, Tuscaloosa, Alabama, 145p.

NEIDELL, S. and POGGIAGLIOLMI, E., 1977, Stratigraphic modeling and interpretation-Geophysical principles and techniques, *In* E.A. Beaumont and N.H. Foster (eds), Geophysics II-Tools for Seismic Interpretation: *Treatise of Petroleum Geology Reprint Series*, no. 13, p. 131-416.

PARCELL, W.C., 1999, Stratigraphic architecture of the Upper Jurassic (Oxfordian) reefs in the northeastern Gulf Coast, U.S. and the eastern Paris Basin, France: *Transactions, Gulf Coast Association of Geological Societies*, v. 49, p. 412-417.

PARCELL, W.C., 2000, Controls on the development and distribution of reefs and carbonate facies in the Late Jurassic (Oxfordian) of the eastern Gulf Coast, United States and eastern Paris Basin, France (PhD Thesis): University of Alabama. 226p.

CHAPTER 2

USE OF VOLUME-BASED 3-D SEISMIC ATTRIBUTE ANALYSIS TO CHARACTERIZE PHYSICAL PROPERTY DISTRIBUTION

1.1 Introduction

One of sedimentary geologist's primary roles is to predict the occurrence and distribution of physical properties of subsurface sedimentary facies (Walker, 1992; Schlager, 1999). Reasons for such predictions might be for applied (e.g., exploiting aquifers or hydrocarbon reservoirs), or for fundamental purposes (e.g., developing depositional models). The data used may include core, wireline logs, outcrop analogs, seismic data, etc. Several analytical techniques have been applied, such as facies analysis and modeling (e.g., Bádenas and Aurell, 2001; Kenter *at al*, 2002). The most important role of facies modeling in sedimentary geology is prediction (Walker, 1992), using well, core and outcrop data. Facies modeling for prediction is mainly qualitative in that, observed lithofacies are assigned to particular depositional environments. Thus, the prediction of physical properties distribution in these facies would be possible only if a given property is facies specific, which is not usually the case (Walker, 1992). Another limitation of this method is the necessity for good sampling coverage, which considering the non-linear dynamics of depositional systems can be very complex (Schlager, 1999). Therefore, facies models are better used as guides for mapping. Sequence stratigraphy (e.g., Miall, 1995; Tinker, 1998; Hampson *et al.,* 1999; Nissen *et al.,* 1999; Vecsei and Sanders, 1999; Booler and Tucker, 2002; Whalen *et al.,* 2002), is another method that has been used to help in mapping the distribution of different parameters to define or predict lithofacies relationships in 2-D or 3-D (Reading, 1978; Sarg, 1988; Van Wagoner *et al.*, 1988; Posamentier and James, 1993). As with facies modeling where log, core and outcrop data are normally used, dense data sampling is required to quantify uncertainties in physical property prediction in areas of limited data coverage. As such, sequence stratigraphy is also better applied as a mapping guide. With the advent of computers, the use of geostatistics in making predictions is another method that has gained ground in sedimentary geology (e.g., Michelena *et al.,* 1998; Richards *et al.*, 1998; Chensheng and Hiscott, 1999; Murkerji *et al.,* 2001). The application of geostatistics in sedimentary geology serves a dual purpose: 1) to construct realistic 2-D or 3-D geologic models that closely depict the heterogeneity of physical property distribution, and 2) to predict and quantify the uncertainty in physical property prediction that boosts confidence in the final models (Dubrule, 1998; Hirsche *et al.*, 1997). The usefulness of this method for defining and mapping the spatial distribution of physical properties is dependent on several factors, both geologic and statistical, which may influence the outcome of the prediction. A lack of adequate constraints in the form of dense well spacing, outcrop data, etc, to confine lateral variability, is also a potential source of error in the predicted model (Dubrule, 1998; Hirsche *et al.,* 1998).

Sedimentary geologists in the oil industry often use seismic data to make geologically meaningful sequence stratigraphic interpretations (Reymond and Stampfli, 1994; Gregersen, 1997; Nissen *et al.,* 1999; Eberli *at al.*, 2001, Eberli *et al.*, 2002). Attributes extracted from this data (e.g., phase, amplitude envelope) are sometimes an integral part of the evaluation process. High-resolution seismic data, if available, are preferentially utilized for geomorphologic interpretations (Gensous and Tesson, 1996). Seismic data images changes in physical properties across layers and not the physical properties of the layers themselves. As such, there is need to use different methods (e.g., inversion, seismic attribute studies) to predict physical properties within the layers.

Multiattribute seismic studies are another technique for predicting physical property determination, and have found widespread application in the petroleum industry. This technique seeks to find empirical correlations between seismic attributes and log-derived physical properties such as velocity, porosity, lithology, bed thickness, etc, through methods such as multivariate linear regression (MLR) and artificial or probabilistic neural networks (ANN/PNN; Schultz *et al.,* 1994a&b; Russell *et al.*, 1997; Hampson *et al.*, 2001). Seismic attributes are derivatives or mathematical transforms of a basic seismic measurement, the seismic trace (Brown, 1996a&b; Chen and Sidney, 1997; Hampson *et al.,* 2001). Relationships between seismic attributes and physical properties originate from the propagation of acoustic waves through the subsurface (Schultz *et al.*, 1994a; Anstey, 1982; Brown, 1996a). A measurement of the combined changes observed in the seismic attributes, which stem from the seismic response of lithologic and fluid characteristics, allows for the spatial interpretation of physical properties. While some of these relationships have an obvious rock physics basis (e.g., tuning effects of amplitudes and rock thickness; Robertson and Nogami, 1994; Brown, 1996a; Hilterman, 2001, acoustic impedance and porosity changes; Dedman *et* *al.,* 1975; Neidell and Poggiagliolmi, 1977), the physical basis for other relationships is more poorly understood. Accordingly, some authors have advocated statistical approaches to correlate seismic attributes with physical properties measured by logs (Schultz *et al.,* 1994; Hampson *et al.,* 2001). Of considerable importance in these studies is the mode of attribute extraction, which determines the type of attributes used. There are two main types, horizon/interval and volume-based methods (Schultz *et al.*, 1994; Brown 1996b). Horizon attributes are extracted or averaged along or between interpreted seismic horizons and then correlated to log-derived properties (e.g., average porosity, net thickness). This mode of extraction produces a map. On the other hand, volume/sample–based attributes are extracted and then correlated to log properties on a sample-by-sample basis over a window that is defined by two seismic horizons (Brown, 1996b; Chen and Sidney, 1997; Hampson *et al.,* 2001). It yields a physical property volume, and thus better defines changes in physical properties and their corresponding geometries in 3-D space. The latter method is particularly useful for property prediction in thick and complex stratigraphic sequences where lateral and vertical facies changes are frequent.

Sedimentary geologists working with logs or cores are limited in their ability to predict the distribution of rock properties (e.g., porosity). This is because well data are normally too widely spaced to adequately characterize these rock properties in structurally disturbed and stratigraphically complex formations, and the methods described above (sequence stratigraphy, facies modeling, geostatistics) often yield ambiguous results. Three-dimensional seismic data offers a continuous lateral coverage for imaging facies heterogeneity (Brown, 1996a; Hart, 1997; Wang *et al.,* 1997; Liu and Liu, 1998). Thus, integration of borehole and seismic data in multiattribute studies can be used to overcome the shortcomings of the other methods. In addition, the images obtained from such integrated analyses can give sedimentary geologists important and fundamental insights into depositional histories and processes that otherwise are not easily attainable, e.g., the study of the deposition of basin-floor fan systems by Leiphart and Hart (2001), and controls on diagenesis by Pearson and Hart (*in press*).

In this paper, we use a case study to illustrate the use of 3-D seismic attributes studies to directly image rock physical properties (porosity) in the Smackover carbonate buildups of southwestern Alabama. We further show how the application of this method has not only decreased the uncertainty associated with estimating the distribution of physical properties in stratigraphically complex formations, but has also improved confidence in our results. The volume-based method has not previously been applied to characterize porosity distribution in the Smackover Formation at Appleton Field. By examining images derived using this volume-based method, one is able to deduce relationships between the predicting attributes and features of the porous interval that were not readily apparent from using a single data type. Finally, we demonstrate the possibility of using multiattribute results to foster an understanding of depositionally oriented trends in porosity distribution that have been observed in these buildups.

1.2 Geological Overview

The study area is the Appleton Field of southwestern Alabama, located on the tectonically stable northern rim of the Gulf of Mexico basin (Fig. 1; Salvador, 1991). The Smackover Formation at Appleton Field was deposited in the Conecuh embayment, a broad paleotopographic low situated between the Conecuh Ridge (assumed to be a continuation of the Alabama Piedmont structural trend; Neathery and Thomas, 1975) and the Pensacola Arch along the western prong of the South Georgia rift system (Fig. 1). The updip basin configuration of the study area is dominated by a series of northeast trending pre-Jurassic salients and re-entrants associated with this rift system (Fig. 1). Seismic and gravity data suggest that the Conecuh Ridge acted as a stable basement high throughout Smackover deposition (Wilson, 1975a; Mancini and Benson, 1980) and that deposition setting of this field was within an inner homoclinal/distally steepened carbonate ramp defined by an inclined platform that extended basinward without a pronounced break in slope (Ahr, 1973; Mancini and Benson, 1980; Tew *et al.,* 1993).

Within Appleton Field, a combination of basement paleohighs along the pre-Smackover surface (Paleozoic/Mesozoic in age and of igneous and metamorphic origin; Kopaska-Merkel *et al.,* 1994; Benson *et al.,* 1996; Mancini, 2002), carbonate productivity/sedimentation, relative sea level and associated hydrodynamic energy changes, are collectively identified as the major controls on facies distribution (Benson *et al.,* 1996). Carbonate deposition at Appleton was essentially in a shallow marine environment. Facies distribution

Figure 1: Location map of study area showing existing structural controls at time of Smackover deposition. Adapted from Mancini (2002, Fig. 1).

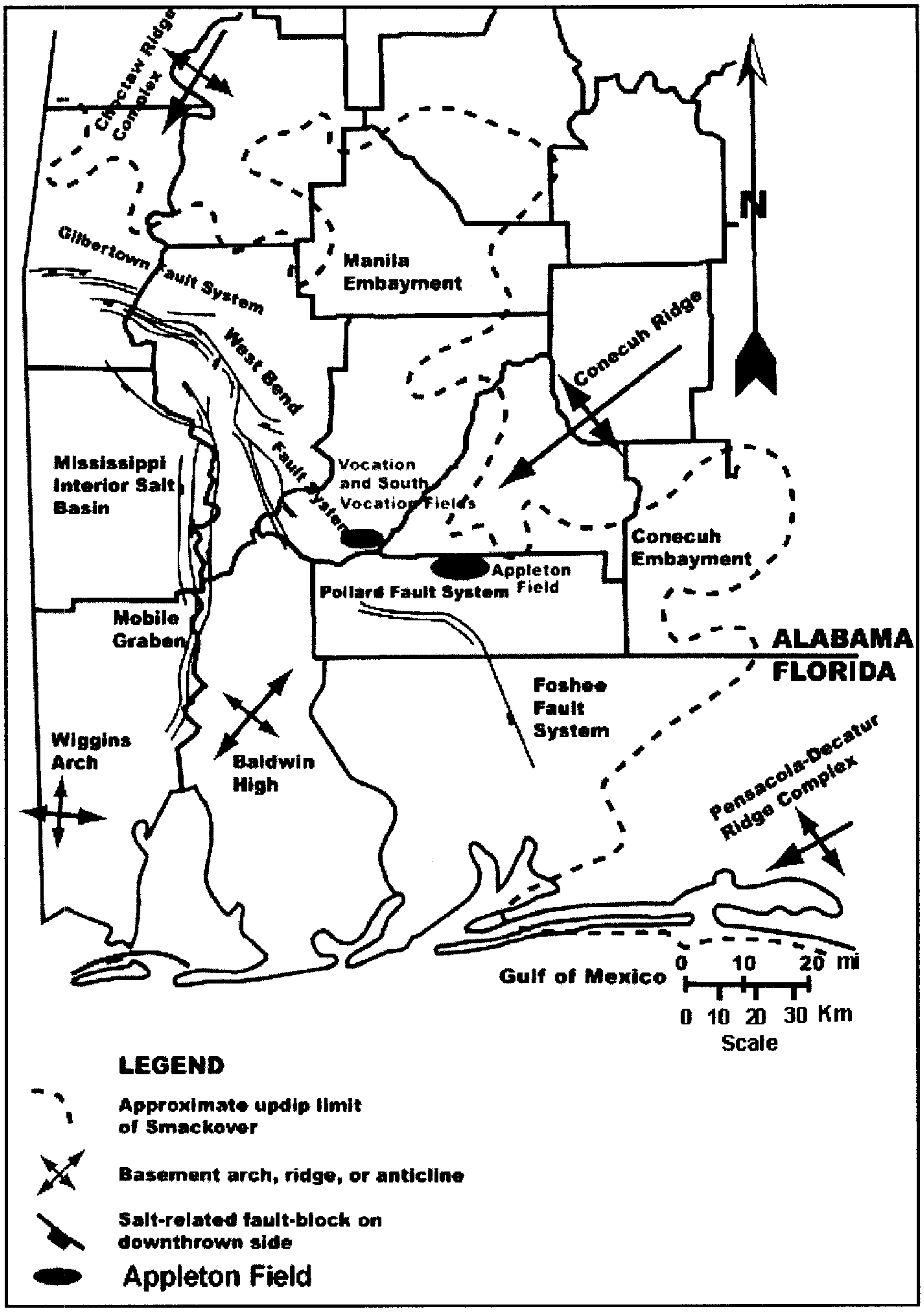

Choctaw Ridge Complex
Gilbertown Fault System
West Bend Fault System
Manila Embayment
Conecuh Ridge
N
Mississippi Interior Salt Basin
Vocation and South Vocation Fields
Conecuh Embayment
Appleton Field
Pollard Fault System
Mobile Graben
ALABAMA
FLORIDA
Foshee Fault System
Wiggins Arch
Baldwin High
Pensacola-Decatur Ridge Complex
Gulf of Mexico
0 10 20 mi
0 10 20 30 Km
Scale
LEGEND
Approximate updip limit of Smackover
Basement arch, ridge, or anticline
Salt-related fault-block on downthrown side
Appleton Field

ranged from shelf and banks, through marginal reefs and back reef lagoons, to subtidal and supratidal sub-environments (Benson *et al.,* 1997).

Initial deposits (Fig. 2) in the study area were derived from the Appalachian Mountains during Mid- to Late Jurassic, leading to deposition of the siliciclastic Norphlet Formation (Callovian to Oxfordian) in the topographically lower areas of the Conecuh Embayment (Mancini and Benson, 1980; Mancini *et al.*, 1999). These siliciclastic materials supplied by intermittent streams were deposited as a basal fluvial facies. Due to their abrupt contact with underlying marine-derived Werner Anhydrites and Louann Salt, Wade and Moore (1993) interpreted the fluvial facies as constituting the lowstand system tract (LST). Mancini *et al.* (1990) on the other hand, have interpreted them as belonging to a highstand systems tract (HST). The siliciclastics of the Norphlet Formation were later marine-reworked during early Oxfordian sea level transgression and were interpreted to form the base of the transgressive systems tract (TST; Wade and Moore, 1993) and shelf margin systems tract (Mancini *et al*, 1990) respectively. At Appleton Field, pre-Smackover (Norphlet) siliciclastics are absent over basement highs (paleohigh/on-structure) but thicken off-structure towards the embayment center. Continued sea incursions led to the drowning of the paleohighs and deposition of the lower Smackover carbonates, which onlap the basement rock on-structure (Prather, 1992a).

The Smackover Formation can be subdivided into 3 members (Lower, Middle and Upper Smackover) based on temporal variations in depositional conditions and consequent lithofacies (Mancini and Benson, 1980; Benson,

Figure 2: Lithostratigraphic and sequence stratigraphic interpretation for the Appleton Field, SW Alabama. Adapted from Parcell (2000).

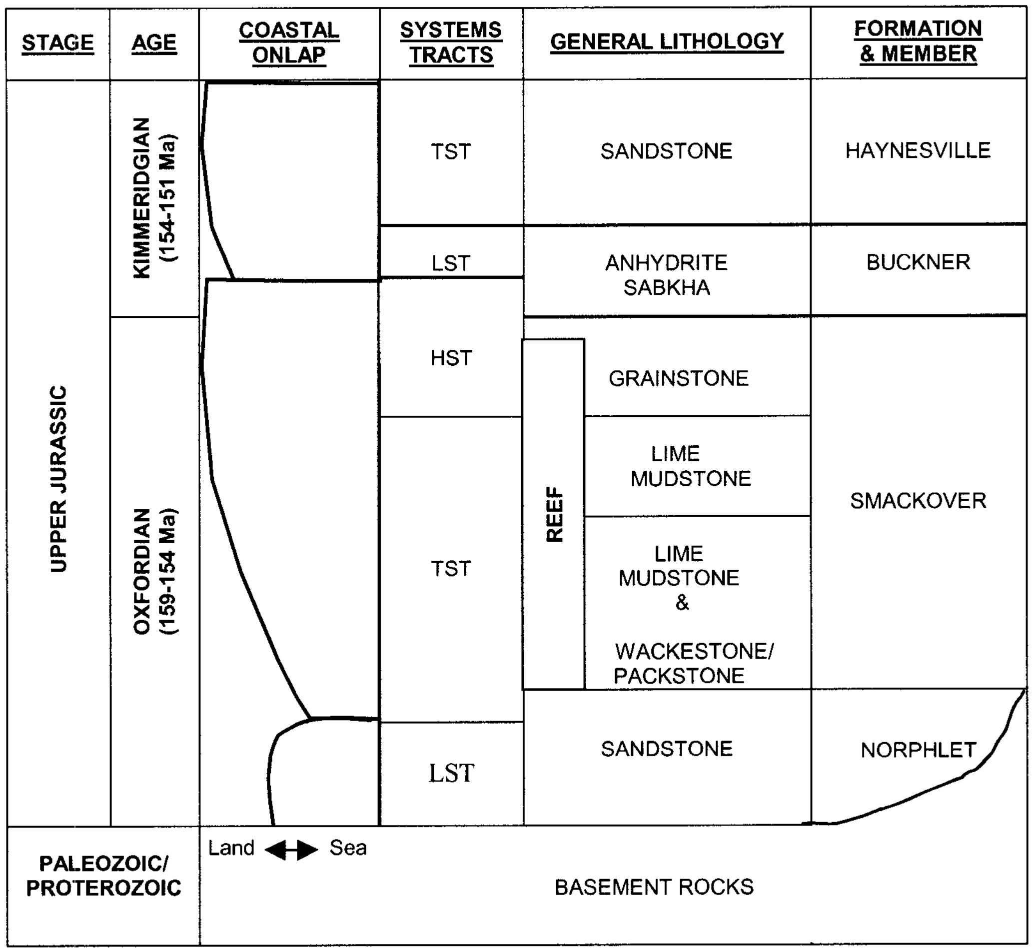
STAGE
AGE
COASTAL ONLAP
SYSTEMS TRACTS
GENERAL LITHOLOGY
FORMATION & MEMBER
UPPER JURASSIC
KIMMERIDGIAN (154-151 Ma)
OXFORDIAN (159-154 Ma)
TST
SANDSTONE
HAYNESVILLE
LST
ANHYDRITE SABKHA
BUCKNER
HST
GRAINSTONE
REEF
LIME MUDSTONE
SMACKOVER
TST
LIME MUDSTONE & WACKESTONE/ PACKSTONE
LST
SANDSTONE
NORPHLET
PALEOZOIC/ PROTEROZOIC
Land
Sea
BASEMENT ROCKS

1988). Though absent at Appleton Field, the Lower Smackover facies is found mainly in embayment centers and ranges from fenestrae-laden algal laminites (Esposito and King, 1987), through intraclast wackestones/packstones, to peloidal-oncoidal packstones/wackestones that have been interpreted as tidal flat to subtidal deposits (Benson, 1988; Benson *et al.,* 1996). With a continued rise in sea level, microbial patch reefs of the Middle Smackover developed over the basement highs, updip of shallow near-shore areas. These reefs consist of boundstone (bafflestone) in the deeper water reef front, and bindstone along the shallower reef crest. They constitute the best reservoirs in the field with porosities and permeabilities of 9 - 26% and 1 – 4106 md, respectively (Benson *et al.,* 1996, 1997; Hart and Balch, 2000; Mancini *et al*, 2000). These facies grade off-structure into peloidal packstone and wackestone typical of deeper water, low energy subtidal environments. The Lower and Middle Smackover members represent the transgressive system tract (TST; Mancini *et al.,* 1990).

Slowing of sea level rise allowed the Smackover reefs to grow to sea level, accrete laterally and prograde seawards, changing the system from one dominated by aggradation to that of progradation. Subsequent fall in sea level led to increased energy levels, limited growth and eventually exposure and subsequent death of reef organisms. Characteristic on-structure facies include high-energy ooid grainstones, that are flanked seaward by sub-wave base peloidal wackestone or packstone facies, and landward by lagoonal peloid packstone, where they occur in deeper water, and by peloid/oncoidal packstone where they occur in shallow water (Saller and Moore, 1986; Benson et al, 1996;

Mancini, 2002). During this period, the Late Oxfordian, sea level was relatively stable, with short-term fluctuations giving rise to shallowing upward parasequences (Vail *et al.*, 1984; Benson *et al.,* 1997).

The Buckner Anhydrite Member of the Haynesville Formation overlies the Smackover sediments and is interpreted as being deposited in a salina or sabkha environment (Benson *et al.,* 1997). The Upper Smackover unit and Buckner Anhydrite Member of the Haynesville Formation together characterize the late highstand (sabkha) to early lowstand system tract/prograding phase of TST (salina; Mancini *et al.,* 1990).

1.3 Database

Available borehole data from 12 wells within and around the study area (Fig. 3) contained a varied suite of logs. Sonic logs of 11 wells were converted from depth to time to calibrate log and seismic data. Six of these wells with good ties to the seismic data, and containing the desired property log (density porosity) were chosen for multi-attribute analyses (Appendix A). The subset of seismic data used consisted of an approximately 5 x 3.5 km grid of a 13 x 12 km post-stack time-migrated 3-D volume, with a 4 ms sample rate, a bin spacing of 165 x 165 ft (~50 x 50 m), and a 4 seconds two-way travel time (TWT) trace length. We used a larger seismic volume than that previously used by Hart and Balch (2000) to include a paleohigh to the northwest of the Appleton Field. Supplementary data in the form of production data and core analyses (Parcell 2000; Mancini 2002) were also used.

Figure 3: Seismic grid showing the areal coverage of current survey area and well locations. Strike (A - A'), and dip (B - B' and C – C') transects are also shown. The Buckner/Smackover top has been used to show better the location of wells with respect to existing structure. The presence of structure and location of porous reservoir facies (reef and grainstone) on them provide excellent drilling targets.

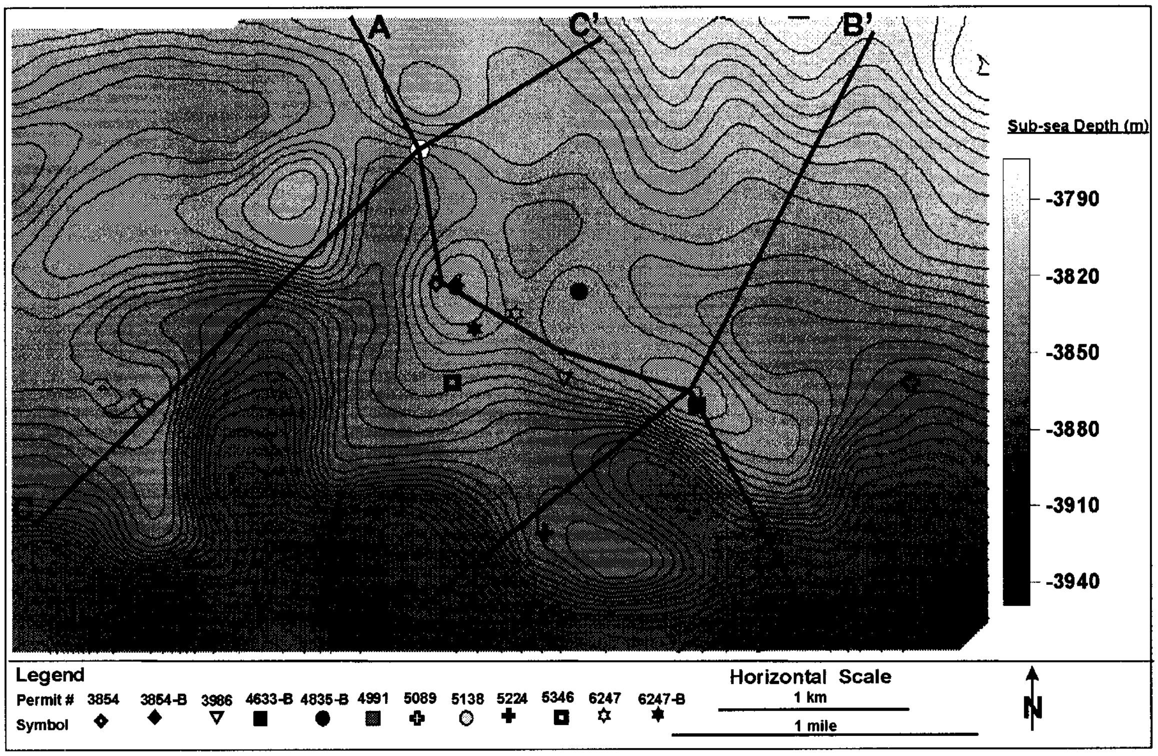
A
C'
B'
Sub-sea Depth (m)
-3790
-3820
-3850
-3880
-3910
-3940
Legend
Permit #
Symbol
3854
3854-B
3986
4633-B
4835-B
4991
5089
5138
5224
5346
6247
6247-B
Horizontal Scale
1 km
1 mile
N

1.4 Methodology

1.4.1 Log analysis

Log analysis was the first step towards structural and stratigraphic interpretation of the various formations in the study area. Logs were edited to correct irregularities in measured values emanating from tool failure or borehole conditions (e.g., vugs, washouts, etc). If not available among suite of logs, sonic and density logs were estimated using Gardner *et al.'s,* 1974 pre-defined equations (Eq. 1, 2, 3), based on their empirical relationship with existing logs.

$$\rho = 0.230 * v^{0.250} \tag{1}$$

where: ρ = density, v = velocity, 0.230 = constant, and 0.250 = exponent

$$v = (\rho / 0.230)^{4.0} \tag{2}$$

$$\rho = [(1 - \text{porosity}) * \text{matrix density})] + [(\text{porosity} * \text{fluid density})] \tag{3}$$

General observations showed that wells with density values estimated from sonic logs had poorer correlation to seismic data than those derived from density porosity logs. This difference was attributed to the radius of capture of the logging tool (shallower for sonic logs) and to disparities in logging methods: i.e. sonic interval transit time is dependent on porosity and lithology, and where matrix is affected by vuggy or fracture porosity, sonic-calculated density values will be low while density porosity measurements will remain unaffected (Asquith and Gibson, 1982; Doveton, 1994). These irregularities, if not corrected, lead to artificial bias in rock physical properties and, as was observed, degrade log-seismic calibration (Hirsche *et al.*, 1998). Formation tops and lithologies relating to parasequence/sequence boundaries and facies changes were mapped from logs based on their characteristic log responses (Appendix A). Geologic cross-sections drawn from well correlations (Fig. 4) and information obtained from seismic data were used to interpret the depositional history of the Appleton Field.

1.4.2 Time-depth conversion

The sonic logs were integrated with respect to depth in order to give two-way travel time; and this same time-depth relationship was applied to all the logs in the same well. Sonic logs were converted to velocity logs and together with the density logs were used to calculate acoustic impedance. The reflectivity series produced from this procedure was convolved with a zero-phased statistical wavelet extracted from the seismic data in order to create synthetic seismograms at wells and simulate the expected seismic response along formation boundaries (Fig. 5). The synthetic traces were time-shifted to the corresponding horizons in the seismic data, and depending on the quality of fit defined by the correlation coefficient, a wavelet was extracted from the seismic data along the wellbore in order to further improve the fit (see Appendix B). The well-tying procedure was critical to our analyses because it ensured that both data types were imaging and comparing the same stratigraphic intervals. Difficulties encountered during generation of the synthetic seismograms were mainly due to the limited vertical extent and deviated nature of some logs, which failed to capture rock properties effectively in the vicinity of the wellbore, or to the poor quality of the seismic data in some areas (particularly to the southern limits of the survey area). Seismic

Figure 4: NW-SE well-to-well cross-section showing major stratigraphic units and their relationships. Cross-section was obtained along strike of paleohighs (A-A' transect of Fig. 3). Note that the eastern paleohigh at well 4633-B is structurally higher than that in the west beneath well 3854. Grey curve = gamma ray, black curve = sonic.

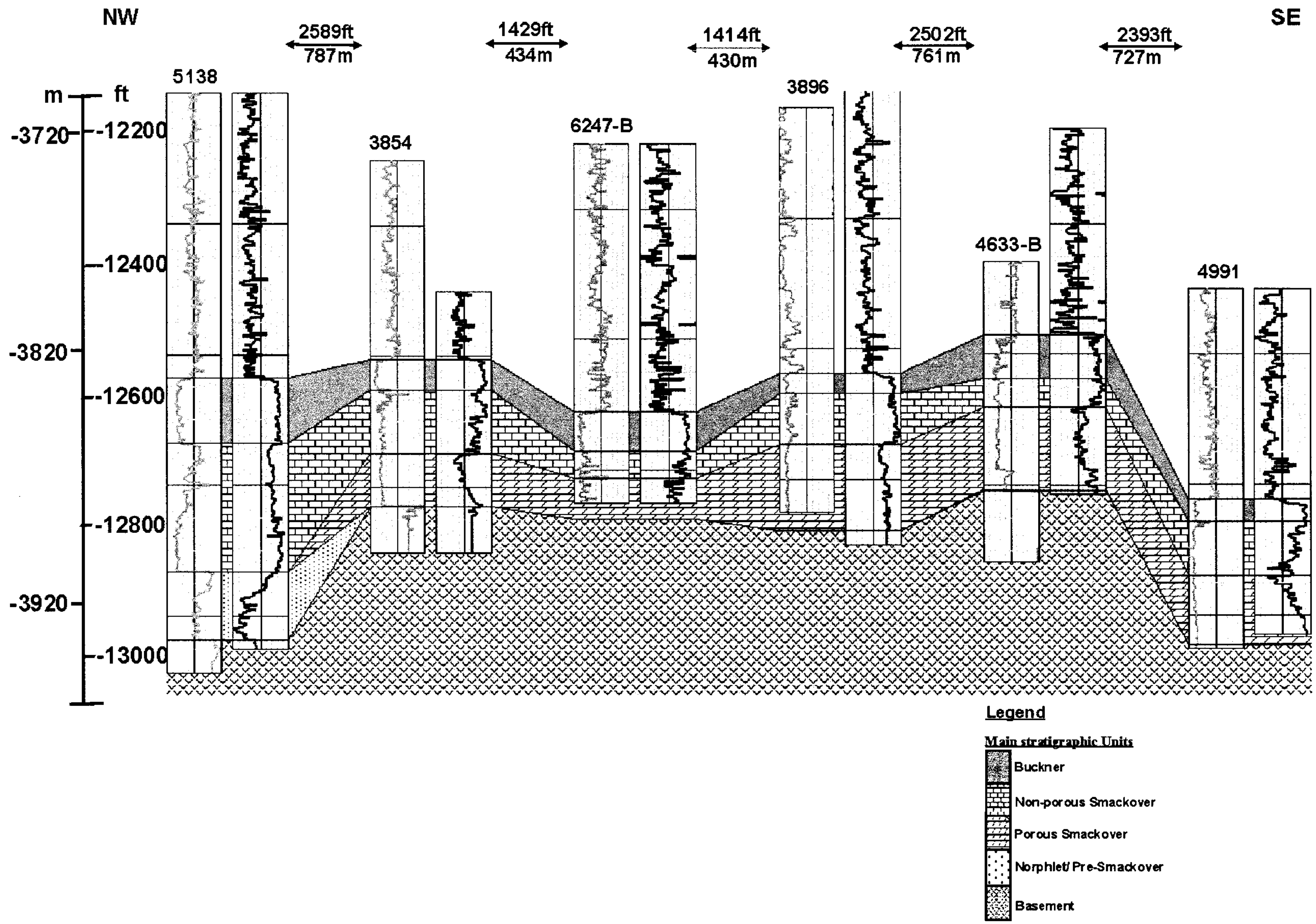

NW
SE
2589ft
787m
1429ft
434m
1414ft
430m
2502ft
761m
2393ft
727m
5138
3854
6247-B
3896
4633-B
4991
m
ft
-3720
-3820
-3920
-12200
-12400
-12600
-12800
-13000
Legend
Main stratigraphic Units
Buckner
Non-porous Smackover
Porous Smackover
Norphlet/ Pre-Smackover
Basement

Figure 5: Example of synthetic seismogram (well 4633-B) used for tying well data to seismic. Black curve = log synthetic, grey = seismic trace extracted along wellbore at well location.

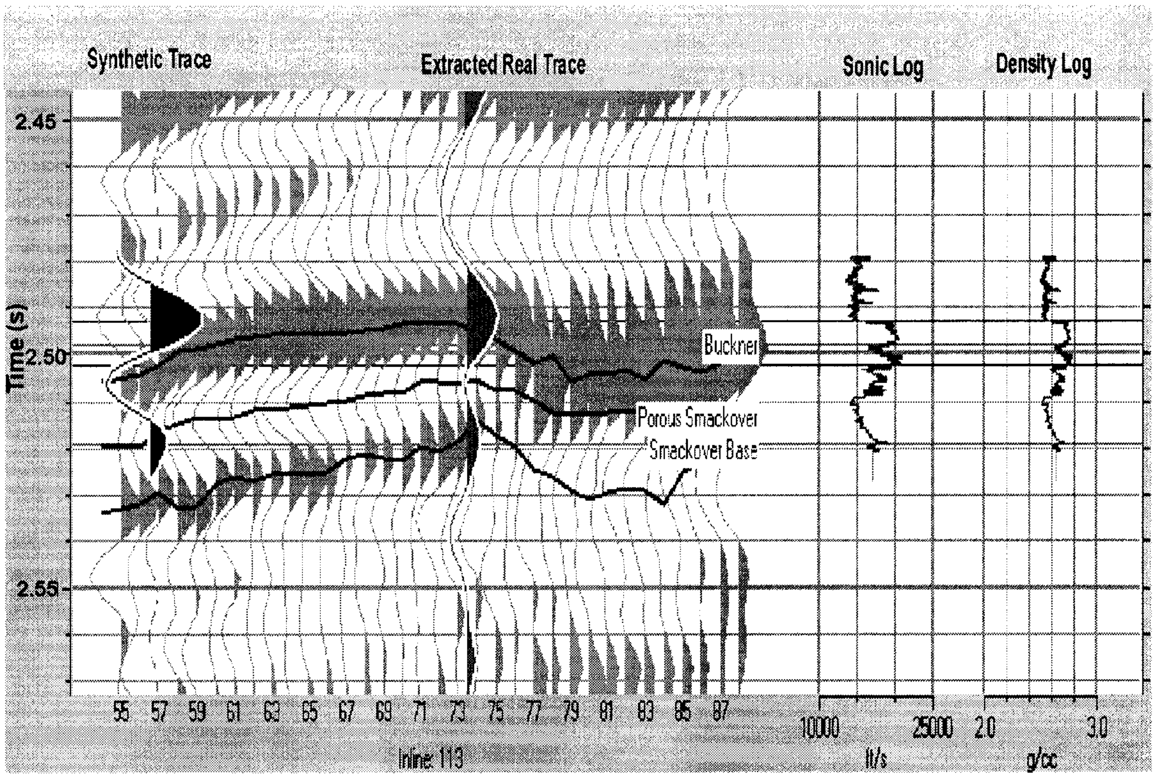

Synthetic Trace
Extracted Real Trace
Sonic Log
Density Log
Time (s)
2.45
2.50
2.55
Buckner
Porous Smackover
Smackover Base
55 57 59 61 63 65 67 69 71 73 75 77 79 81 83 85 87
Inline: 113
10000
25000
ft/s
2.0
3.0
g/cc

modeling, as performed by Hart and Balch (2000), was carried out to confirm the seismic character of the stratigraphic horizons (see Appendix C). Formation tops/ horizons (see Fig. 6) were mapped from the seismic data based on comparison of seismic traces with the modeled synthetic seismograms. The objectives for horizon mapping were to create time-structure, depth-structure, isochron and isopach maps which, together with results from log analyses, were used in geologic interpretation (see Appendix D), and to constrain attribute analysis.

1.4.3 Multiattribute studies

For the multiattribute studies, a data-driven approach was used as described by Schultz *et al.,* (1994), Hampson et al. (2001) and Murkerji et al. (2001). A volume-based method (Russell *et al.,* 1997; Hampson *et al.,* 2001), using both multiattribute step-wise linear regression and probabilistic neural network statistical techniques, was adopted due to the thickness (80 - 230ft / 24 - 70m) and stratigraphic complexity (rapid facies changes) of this interval. We sought to predict porosity, as measured by the density porosity log, because of its direct relation to depositional facies at the Appleton Field (Benson, 1988; Benson *et al.,* 1996) and the fact that it is an important variable controlling hydrocarbon production. Our window of analysis was defined by the top and base of the Smackover Formation as mapped from the seismic data. The choice of which attribute(s) to generate and use was determined by the capabilities of our software, which offered 18 attributes (Table 1). These attributes, together with the composite seismic trace at well locations, (combined seismic trace of individual bed responses at reflection boundaries) were extracted over the analysis

Figure 6: Transects showing seismic data across Appleton Field; note location of the porous Smackover on paleostructure. (a) NW-SE transect parallel to strike (A-A' in Fig. 3), and shows horizon picks and seismic character of the mapped formations (red = trough, blue = peak); (b) & (c) dip sections (B-B', C-C' in Fig. 3) across Appleton Field.

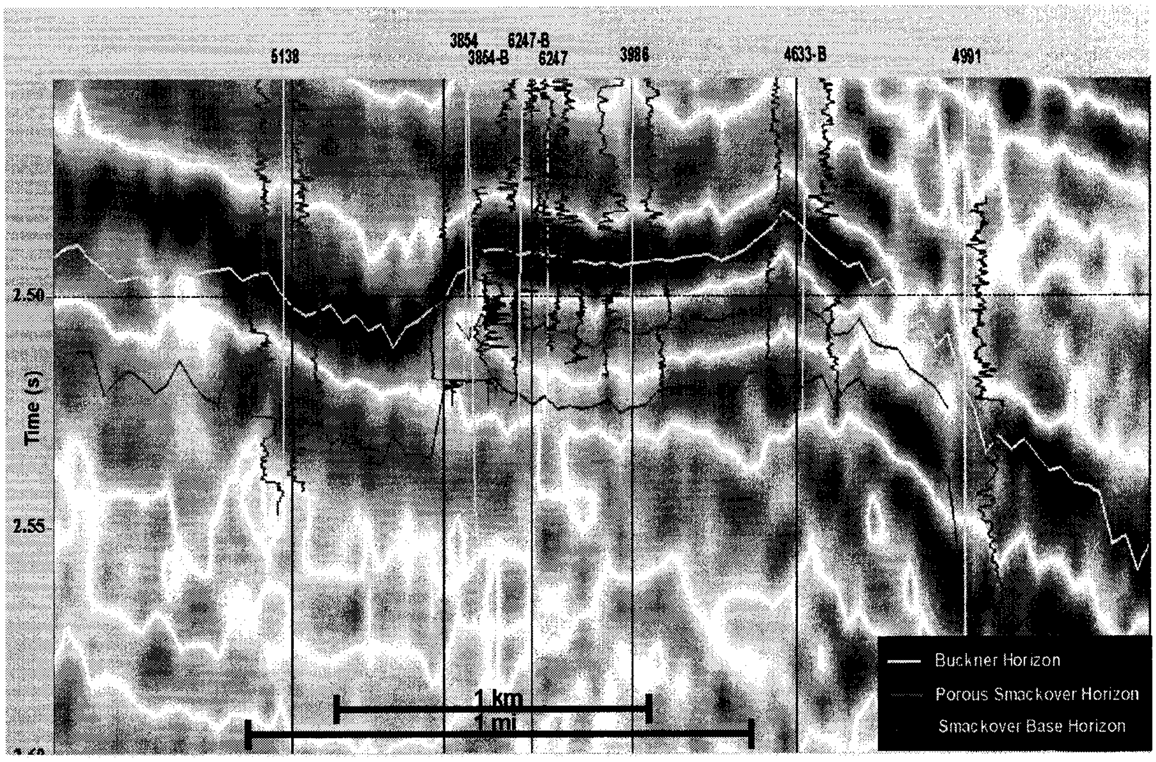
5138
3854
3854-B
6247-B
6247
3986
4633-B
4991
Time (s)
2.50
2.55
Buckner Horizon
Porous Smackover Horizon
Smackover Base Horizon
1 km
1 mi

(a)

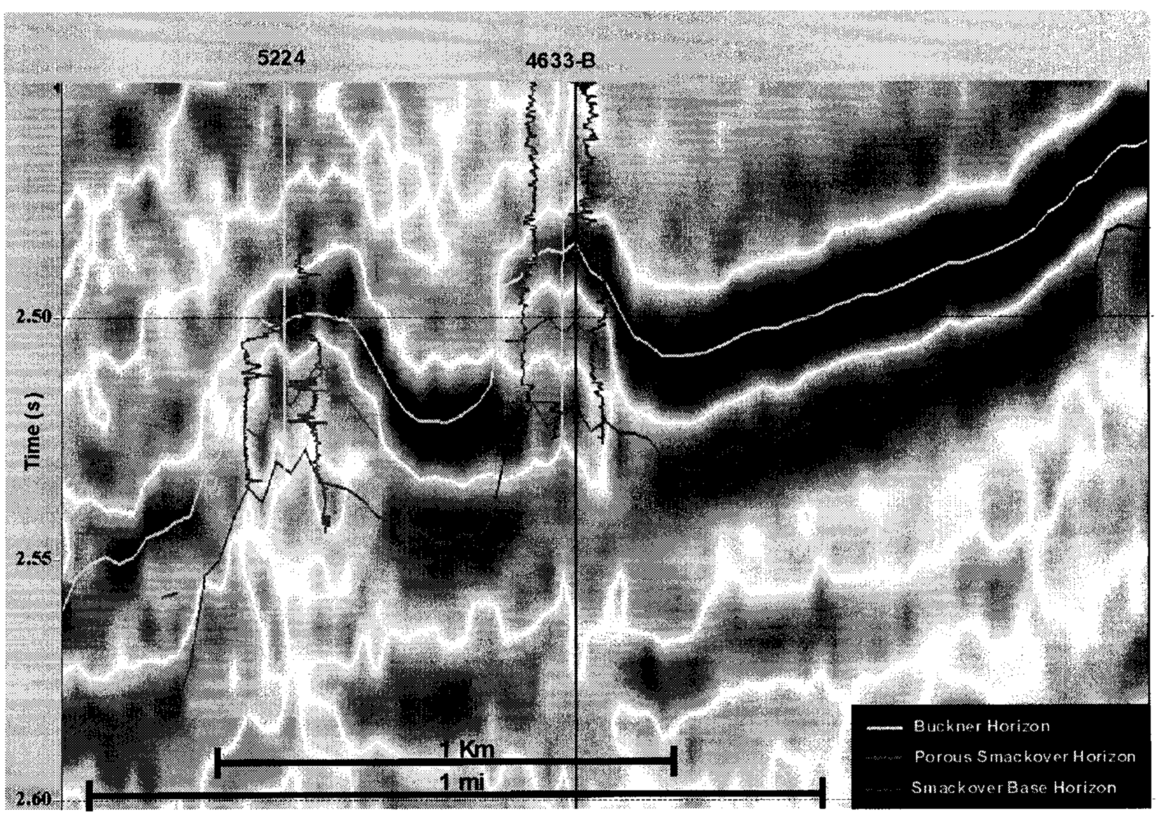
5224
4633-B
Time (s)
2.50
2.55
2.60
Buckner Horizon
Porous Smackover Horizon
Smackover Base Horizon
1 Km
1 mi

(b)

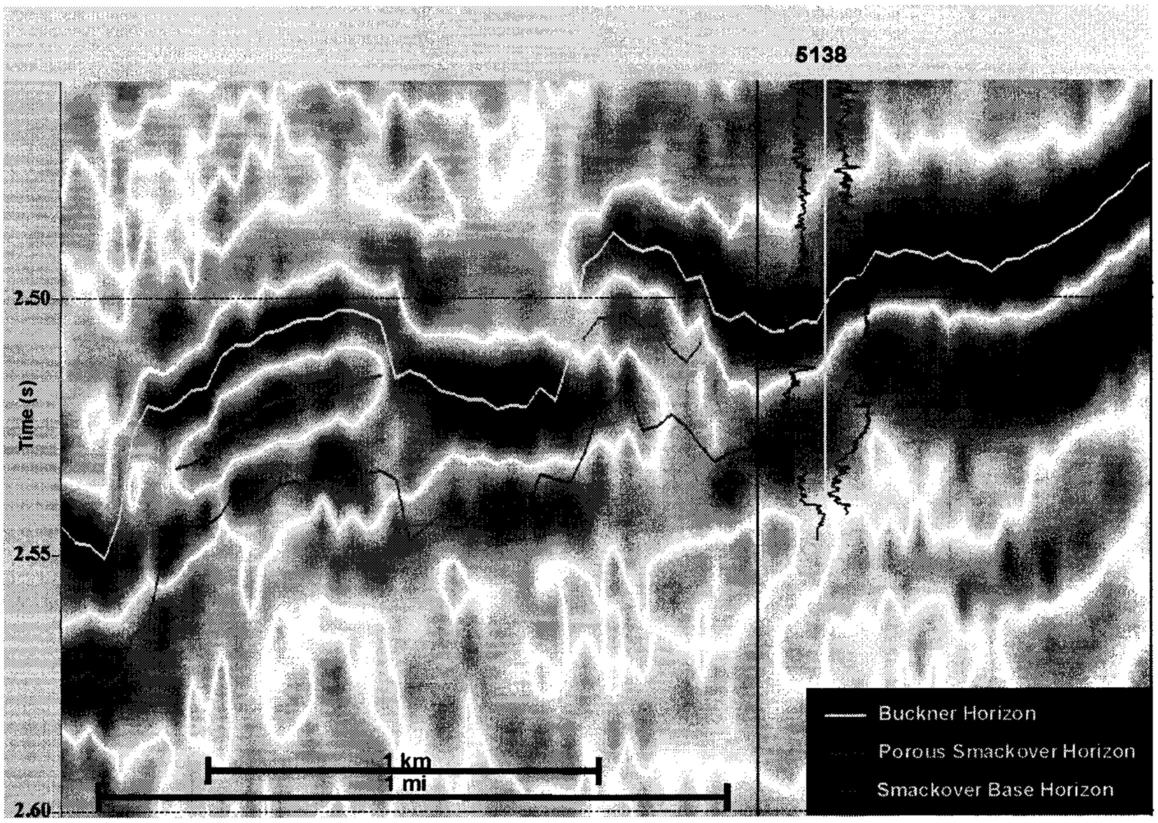
5138
2.50
2.55
2.60
Time (s)
1 km
1 mi
Buckner Horizon
Porous Smackover Horizon
Smackover Base Horizon

(c)

Table 1: Hampson - Russell internal attributes, classes and equations.

Attributes	Class	Equation
Cosine Instantaneous Phase (C(t))	Instantaneous Attributes	cos(ø(t))
Instantaneous Phase (ø (t))	"	arctan (h(t)/s(t))
Amplitude-Weighted Cosine Phase	"	A(t)cosø(t)
Amplitude-Weighted Phase	"	A(t)ø(t)
Reflection Strength (A(t))	"	$(s(t)^2+h(t)^2)^{0.5}$
Instantaneous Frequency	"	ω(t) = dø(t)/dt
Apparent Polarity	"	+/-A(t)
Amplitude-Weighted Frequency	Windowed Frequency Attributes	A(t)ω(t)
Dominant Frequency	"	Max. amplitude spectrum a given time window
Average Frequency	"	Avg. amplitude spectrum at a given time window
Derivative (D)	Derivative Attributes	s(t) – s(t-1)
Derivative Reflection Strength (DRS)	"	A(t) – A(t-1)
Second Derivative (D2)	"	D(t) – D(t-1)
Second Derivative Instantaneous Amplitude	"	DA(t) – DA(t-1)
Integrate	Integrated Attributes	Sum of s(t) – sum of smoothed s(t)
Integrate absolute Amplitude	"	Sum of A(t) – sum of smoothed A(t)
Raw Seismic (s(t))		A(t) cos(ø(t))
Time	Time	Time value of the seismic data

window. Although not considered a "true" attribute by some authors (Schultz *et al.,* 1994a; Barnes, 1998), we also included inversion results, which show the acoustic impedance structure of this interval, as an attribute.

For this multiattribute analysis, we sought to predict porosity in 3-dimensions to better characterize its heterogeneity within the field. This was accomplished by obtaining a statistical relationship between the attributes and porosity of the form:

$$P_{MLR}(z) = C + W_i\,(X(z)) + \ldots + W_m(Y(z)) \quad (4)$$

where: P_{MLR} = predicted porosity using multilinear regression, X & Y = attributes, W (i = 1…m) = weights, z = time, C = constant,

or:

$$P_{PNN}\,(z) = \frac{[P_1 e\wedge(-d^2_1/\sigma^2) + P_2 e\wedge(-d^2_2/\sigma^2) + P_3 e\wedge(-d^2_3/\sigma^2)]}{[e\wedge(-d^2_1/\sigma^2) + e\wedge(-d^2_2/\sigma^2) + e\wedge(-d^2_3/\sigma^2)]} \quad (5)$$

where: P_{PNN} = predicted property at each sample using probabilistic neural network, $P_{1\text{-}3}$ = actual porosity value, d^2_1 = distance between input point and the training data $[(X_1 - X_0)^2 + (Y_i - Y_0)^2]$, σ is a scalar.

The application of statistical relationships, derived from each of these methods, leads to the generation of a porosity volume from the seismic data volume. This is achieved by replacing each seismic trace within the analysis window by a porosity curve. This result is different to that obtained from a horizon-based attribute analysis, whereby an average porosity value might be produced at each trace location (e.g., Hart and Balch 2000). Before any statistical relationships could be obtained, the attributes and their transforms were ranked from the most to the least predicting, based on their degree of correlation with porosity values at trained interval. The quality of this correlation was determined from crossplots of attribute and log values at wells, and from the overall value of their prediction errors. The correlations were further optimized using the best single-predicting attribute that is, the attribute with maximum correlation and least predicting error; see Appendix F). These ranked attributes were used as input data for the multi-attribute analysis. The best set of predicting attributes was chosen by step-wise linear regression. The maximum number of attributes applied in the predicting relationship was determined by an all-attribute validation plot, which is taken as the maximum number of attributes at which the average error failed to decrease convincingly (Hampson *et al.,* 2001).

A probabilistic neural network (PNN) was trained using this same set of predicting attributes to improve the quality of fit. This is because PNN is a pattern recognition tool and so may better capture non-linear relationships between the attributes and log porosity than MLR. Statistical validation of selected attributes and ensuing predicting relationship was determined by visual comparison of the original and estimated density porosity logs, and crossplots of actual and predicted porosity values. Exclusion testing, wherein each of the wells used for analysis was selectively excluded from the training data and others used to predict it, was carried out to test the effectiveness of the statistical relationship in areas of sparse well control.

The porosity volumes we created were evaluated for geologic significance. Understanding the geologic applicability of the predicting attributes is the most crucial step in validating any attribute study, as it is the deciding factor when justifying the presence of trends, or lack thereof, as determined from multi-attribute analysis (Hart, 1999). The geologic interpretation of the Smackover Formation, and Appleton Field in particular, has been carried out previously by several workers: Lithofacies analysis and geologic framework: by Mancini and Benson (1980, 1998), Esposito and King (1987), Benson (1985, 1988), Mancini *et al.* (1990), Prather (1992a), Tew *et al.,* (1993), Benson *et al.* (1996, 1997), and Mancini and Parcell, (2001); depositional controls by Prather (1992b), Benson *et al.* (1996), Mancini *et al.* (1999, 2000), and Parcell (2000); and diagenesis by Benson (1985), Saller and Moore (1986), Prather (1992b), Kopaska-Merkel *et al.* (1994), and Haywick (2000).

1.5 Results and Interpretation

1.5.1 Geology

Based on lithology and rock properties, and following Hart and Balch (2000) we used logs to delineate 4 main units overlying the basement from well log analyses (Table 2). From bottom to top, they are: Norphlet Formation, Lower porous Smackover, Upper non-porous Smackover Formation, and Buckner Member of the Haynesville Formation (Fig. 7). These units are of variable thickness, depending on structural position, and some are not present everywhere in the study area (Fig. 4).

1.5.2 Seismic character of formations and their analyses

The seismic character at the interface between stratigraphic units was determined using synthetic seismograms derived from modeling log response, and well-seismic ties (Figs. 5 and 6). Seismic character as described in this paper includes reflection phase (i.e., peak/trough), amplitude and frequency, continuity of reflection events, time range of picks, and configuration of internal reflections.

(1) *Buckner/Smackover Formation* - Due to slight differences in acoustic impedance contrast, between the Buckner Member of the Haynesville Formation and the non-porous unit of the Smackover Formation, the two are indistinguishable seismically (Hart and Balch, 2000). As we observed, the

Table 2: Main stratigraphic units, their associated facies and seismic character observed at Appleton Field.

Formation (Stratigraphic Units)	**Seismic character for the top of each unit**	**Seismic Amplitude**	**Lithofacies** (Benson et al, 1997)
Buckner	Peak	Moderate - High	Anhydrite, nodular anhydrite
Non-Porous Smackover			Carbonate mudstone, algal laminite, peloidal wackestone/packstone, anhydritic dolomite
Porous Smackover	Trough	Moderate - High	Microbial bindstone/boundstone, oncoidal/peloidal/oolitic grainstone, dolomitized packstone/wackestone
Norphlet	Trough	High	Sandstone, mudstone
Basement	Peak	Low - High	Granite, Basalt, Gneiss

Figure 7 Geologic model depicting the relationship of the main stratigraphic units at Appleton Field (from Hart and Balch, 2000)

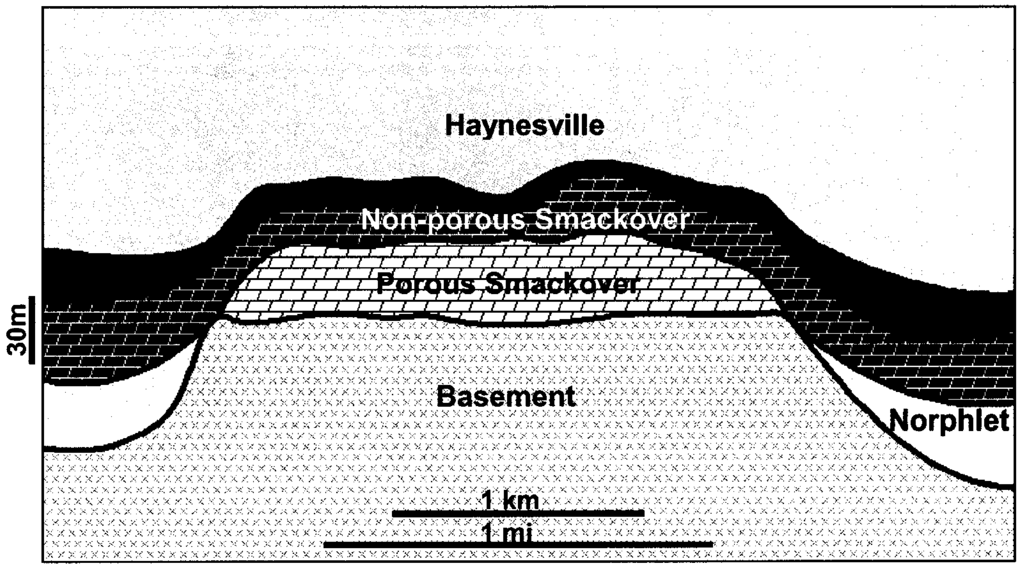

Haynesville
Non-porous Smackover
Porous Smackover
30m
Basement
Norphlet
1 km
1 mi

imaging of the Buckner and Non-porous Smackover Formations as a single layer is also dependent on the thickness variations, frequency changes of the wavelet, and interference of individual bed responses of these two units. Where these contrasts (i.e., impedance contrast and thickness) are least observed, the interface with the overlying lower impedance sandstones of the Haynesville Formation constitutes a high amplitude peak. Amplitudes were observed to be generally lower on-structure where the Buckner Member is thinnest and higher off-structure, in the landward direction, where the Buckner Member is thicker. The seismically mapped Buckner Member is laterally continuous to the updip limit of Smackover deposition. The internal configuration is conformable with a draping appearance on-structure. Seismically, this layer is picked as a proxy for the top of the Smackover Formation and ranges in time from 2457 to 2559 ms.

(2) _Porous Smackover_ - A moderate to high amplitude and moderate frequency trough characterizes the top of the Porous Smackover. Variations in amplitude for the porous Smackover (see Fig. 6), observed from seismic modeling, are mainly due to thickness, facies and/or porosity changes. Although there is some porosity in the grainstone facies of the Upper Smackover, this facies could not be imaged seismically, thus the Porous Smackover unit as defined here is composed exclusively of the reefal facies. Amplitudes and frequency were generally found to be lower on the flanks of the paleohighs, where the porous interval was thickest. The horizon is discontinuous with an onlapping to conformable configuration and the top is relatively flat, perhaps indicating the abrupt termination of reef growth (Fig. 6). The location of this porous unit, solely on the

crests and flanks of basement paleohighs during Smackover deposition, gives it a distinctly mounded appearance. Time range of picks for the porous Smackover is from 2488 to 2574 ms.

(3) <u>*Norphlet Formation*</u> - Overlain by the Buckner/non-porous Smackover Formation and possibly underlain by the basement, this boundary constitutes a very high amplitude and low frequency trough. Its internal configuration is discontinuous, onlapping at paleohighs, and conformable in embayment centers.

(4) <u>*Basement*</u> - Found directly beneath the Porous Smackover unit and the Norphlet, basement rocks constitute structural paleohighs and were seismically characterized by a high frequency and low to moderately high amplitude peak. Together with the Norphlet Formation, where present, the basement represents the lower limit of Smackover deposition in the Appleton Field and ranges in time from 2480 to 2586 ms.

Five main structural culminations occur in and around the Appleton Field, with four of these (Figs. 3 and 8) being present during Smackover deposition. Their NE-SW orientation is parallel to structural paleostrike and perpendicular to the direction transgression. Individual facies thicknesses correlated to the presence of basement paleohighs (Fig. 4). The Porous Smackover is thickest on the southward flanks and thinner on the crests of paleohighs (Fig. 4, see isopach in Appendix D). While earlier studies on these patch reefs of the Smackover Formation at Uriah, Vocation, and Huxford Fields in Alabama had predicted greater thickness of porous facies on the flanks rather than on crests of paleohighs, most wells drilled at these locations were unproductive due to lack of

Figure 8: Structure map (depth sub-sea) of the base of the Smackover Formation. This shows main pre-existing structural culminations that controlled facies deposition, three at the Appleton Field in the east, and one to the NW. The structural high to the SW had no closure prior to Smackover deposition.

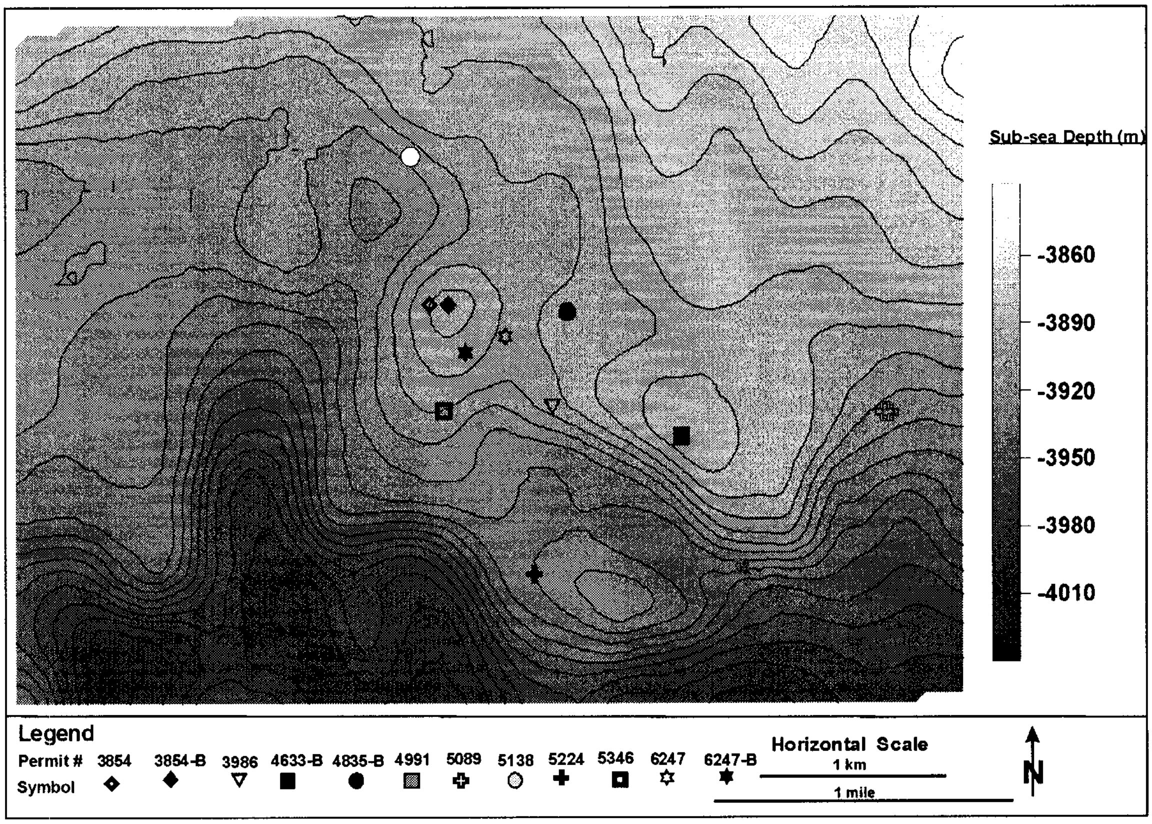
Sub-sea Depth (m)
-3860
-3890
-3920
-3950
-3980
-4010
Legend
Permit # 3854 3854-B 3986 4633-B 4835-B 4991 5089 5138 5224 5346 6247 6247-B
Symbol
Horizontal Scale
1 km
1 mile
N

structural closure (Benson *et al.,* 1996,1997; Mancini *et al.,* 1999). The height of paleohighs was later established to be the main control on the location of reef growth (Mancini *et al*, 1999, 2000). Because of the lower relief, the porous grainstone and reefal facies are located preferentially on the paleohighs at the Appleton Field (Mancini *et al*, 1999). We attributed the larger thickness of the reef facies in the forereef flanks (reef front, *sensu* James, 1989) to greater accommodation space and increasing water depth resulting from rising sea levels during the Oxfordian (Tucker and Wright, 1990; Leinfelder, 1993a). The combination of paleostructure, steep seaward slope and eustatic sea level rise provided optimal conditions (e.g., temperature, salinity, substrate, etc.) for reef growth. By comparing depth-structure maps of our interpreted top (Fig. 8) and base (Fig. 3) of the Smackover Formation, with isopach maps for Buckner/Smackover and the porous Smackover, we can show that a seaward shift and some lateral expansion occurred during Smackover deposition. This we conclude to be an expression of the outward growth of reef during sea level highstand. Subsequent fall in sea level was probably responsible for reef death (Wilson, 1975b; Tucker and Wright, 1990).

1.5.3 Multiattribute studies

The all-attribute validation plot (Fig. 9) indicated that four of the nineteen attributes, all of which had physical relationships with the porous interval, represent the optimum number of attributes required to predict porosity. These four attributes are discussed here:

(1) *Derivative* - Overall, this was the best single-predicting attribute, with a

Figure 9: Validation plot, showing the optimum number of attributes to use in predicting porosity from density porosity logs using stepwise multilinear regression. This optimum number of attributes is reached when the validation error (red curve) associated with adding a new attribute to the predicting relationship fails to decrease convincingly. The black curve shows the training error. The training error generally decreases with an increase in number of attributes

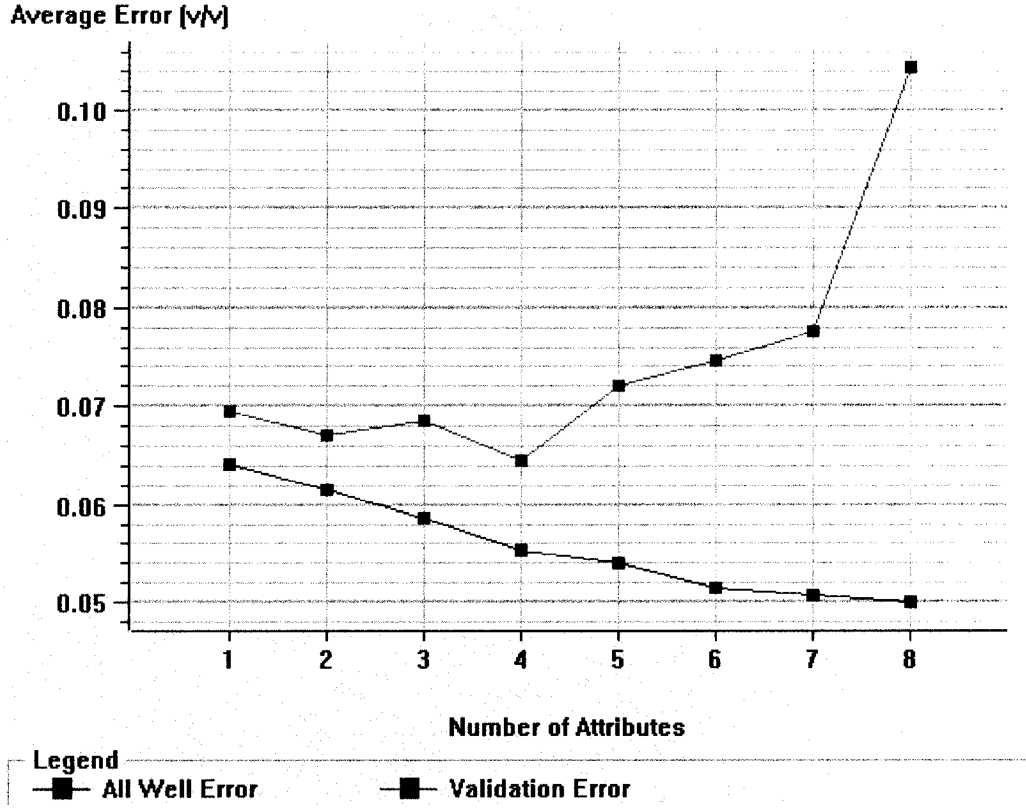

Average Error (v/v)
0.10
0.09
0.08
0.07
0.06
0.05
1
2
3
4
5
6
7
8
Number of Attributes
Legend
All Well Error
Validation Error

correlation coefficient of 73% (Fig. 10). Chen and Sidney (1997) defined derivative as the difference between the seismic trace amplitude (also known as instantaneous real amplitude, the time-domain vibration of traces at a selected sample), of one sample and the preceding sample. Calculated as such, derivative shows the onset and variation of energy for the Porous Smackover unit.

To account for the changes observed in calculated derivative values across the Porous Smackover (Fig. 11a), two models were made: The first model to demonstrate the effect of varying acoustic impedance across the porous interval on derivative (see Appendix F). First, the acoustic impedance at the Porous Smackover was varied while keeping that of Buckner and the Basement constant. Second, keeping the acoustic impedance of the Porous Smackover constant, that of the Basement was varied. The second model shows the effect of thickness variations within the porous interval on the derivative attribute. For this, a wedge model was designed with constant acoustic impedance change on either side of the progressively thickening wedge of the Porous Smackover (see Appendix F). The derivative was calculated for modeled seismograms across the Smackover Formation. The magnitude of acoustic impedance contrast, and not thickness variations, correlated strongly to changes in derivative across the Porous Smackover. As a whole, the forward attribute modeling results demonstrated that areas with highest porosity, and consequently greater acoustic impedance contrast, had the most positive derivative. These high porosities are

Figure 10: (a) Comparison of modeled porosity logs (red curve) derived from the application of the best single-predicting attribute (Derivative), and actual porosity logs (black curve). The blue line across logs defines the window for which this analysis is valid (b) Crossplot of actual porosity values from logs and derivative to illustrate relationship between this attribute and porosity. The higher the derivative, the greater the observed porosity.

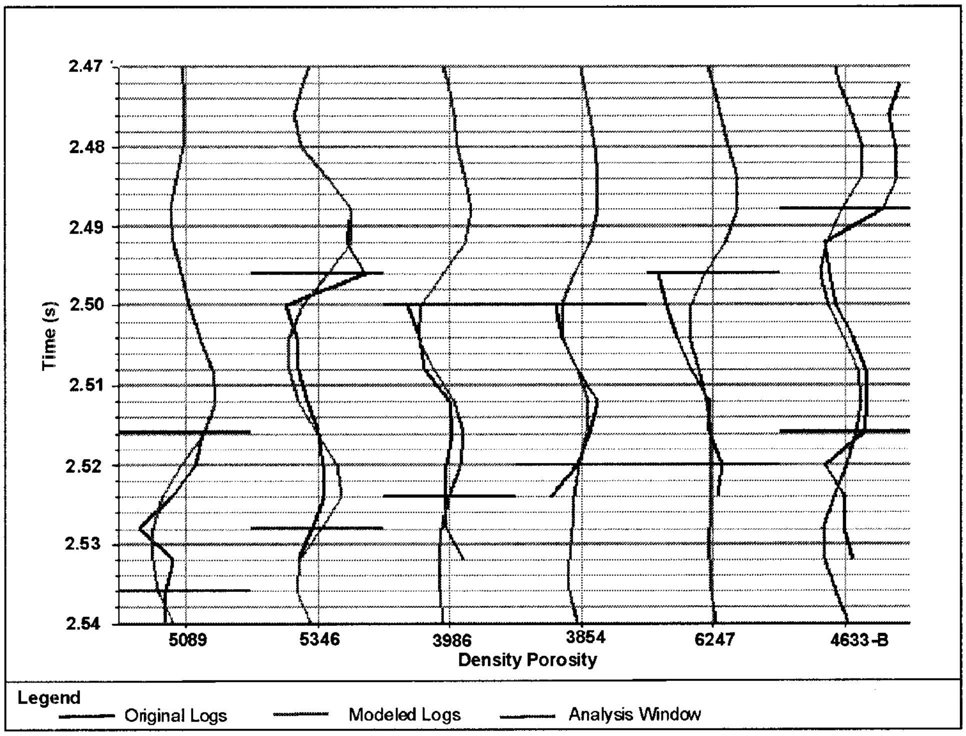

2.47
2.48
2.49
2.50
2.51
2.52
2.53
2.54
Time (s)
5089
5346
3986
3854
6247
4633-B
Density Porosity
Legend
Original Logs
Modeled Logs
Analysis Window

(a)

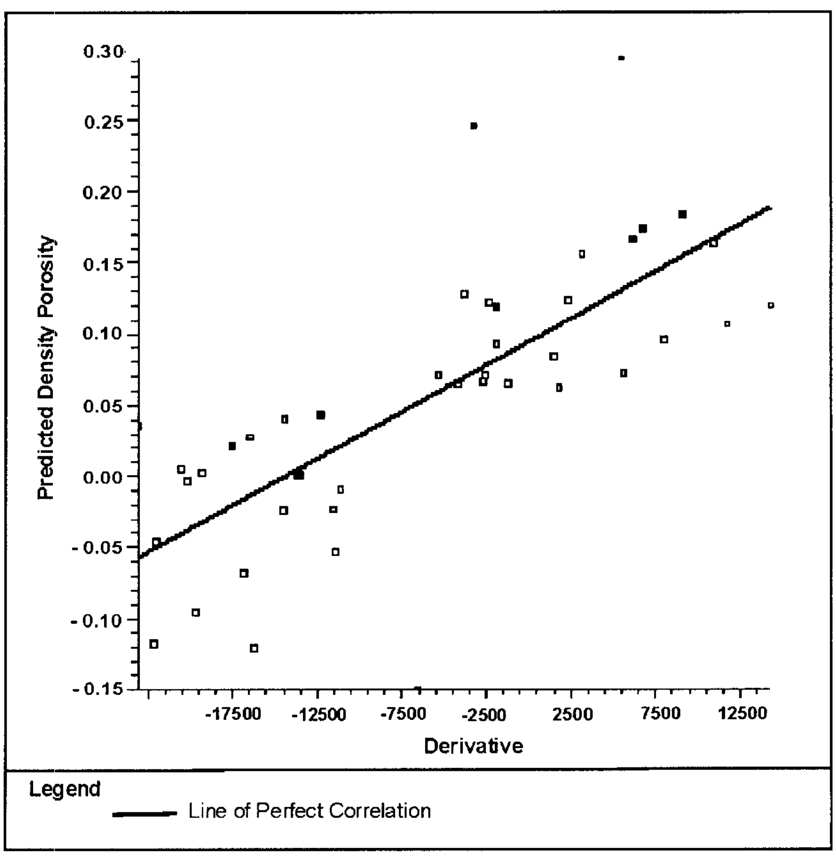

0.30
0.25
0.20
0.15
0.10
0.05
0.00
- 0.05
- 0.10
- 0.15
Predicted Density Porosity
-17500
-12500
-7500
-2500
2500
7500
12500
Derivative
Legend
Line of Perfect Correlation

(b)

Figure 11: NW-SE transects through attribute volumes corresponding to Figure 6a. These show the physical relationship between the predicting attributes and porosity within the porous interval. (a) Derivative (b) Derivative of reflection strength (c) Reflection strength (this attribute is shown to illustrate the importance of its derivative (b) in imaging vertical changes (d) Cosine instantaneous phase. See Figure 3 for location of transects.

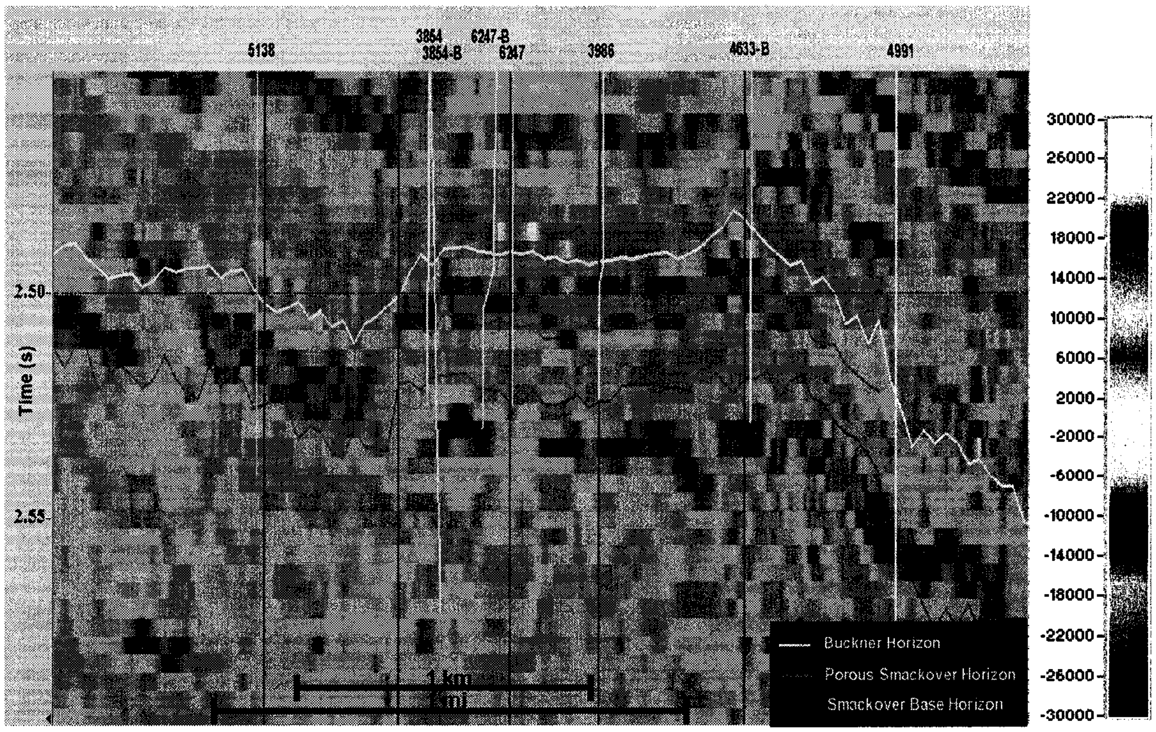

5138
3854
3854-B
6247-B
6247
3986
4633-B
4991
2.50
2.55
Time (s)
1 km
1 mi
Buckner Horizon
Porous Smackover Horizon
Smackover Base Horizon
30000
26000
22000
18000
14000
10000
6000
2000
-2000
-6000
-10000
-14000
-18000
-22000
-26000
-30000

(a)

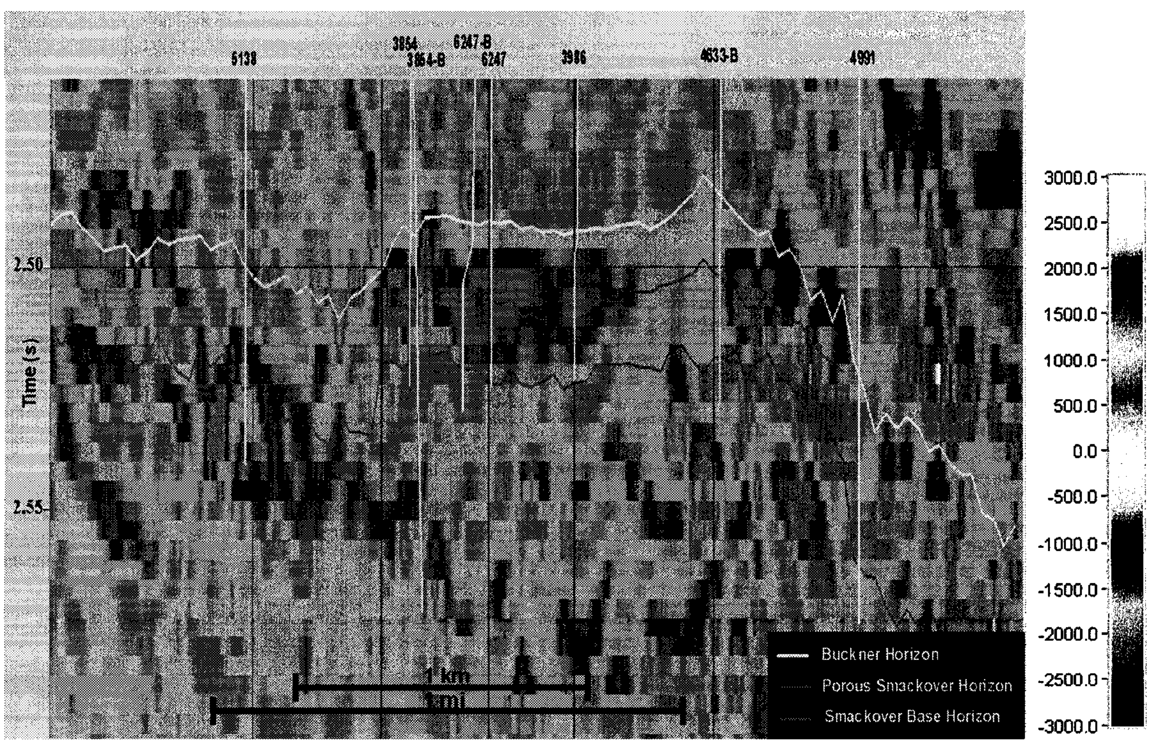

5138
3854
3854-B
6247-B
6247
3986
4633-B
4991
2.50
2.55
Time (s)
1 km
1 mi
Buckner Horizon
Porous Smackover Horizon
Smackover Base Horizon
3000.0
2500.0
2000.0
1500.0
1000.0
500.0
0.0
-500.0
-1000.0
-1500.0
-2000.0
-2500.0
-3000.0

(b)

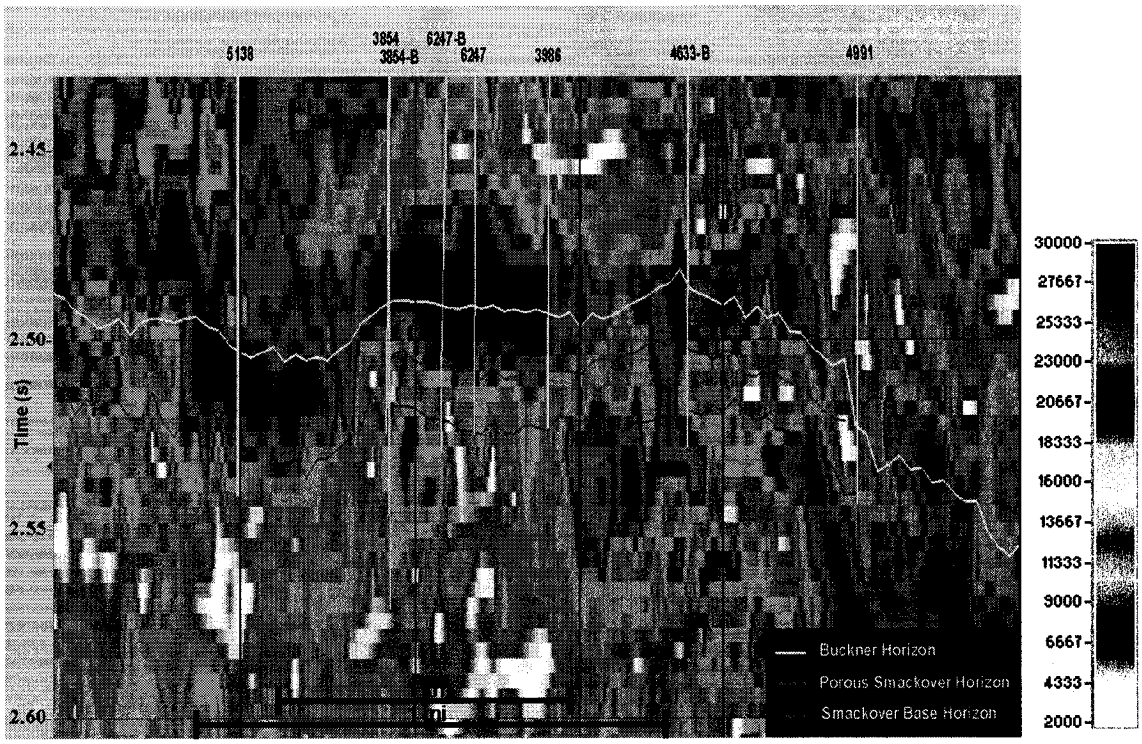
5138
3854
3854-B
6247-B
6247
3986
4633-B
4991
2.45
2.50
2.55
2.60
Time (s)
Buckner Horizon
Porous Smackover Horizon
Smackover Base Horizon
30000
27667
25333
23000
20667
18333
16000
13667
11333
9000
6667
4333
2000

(c)

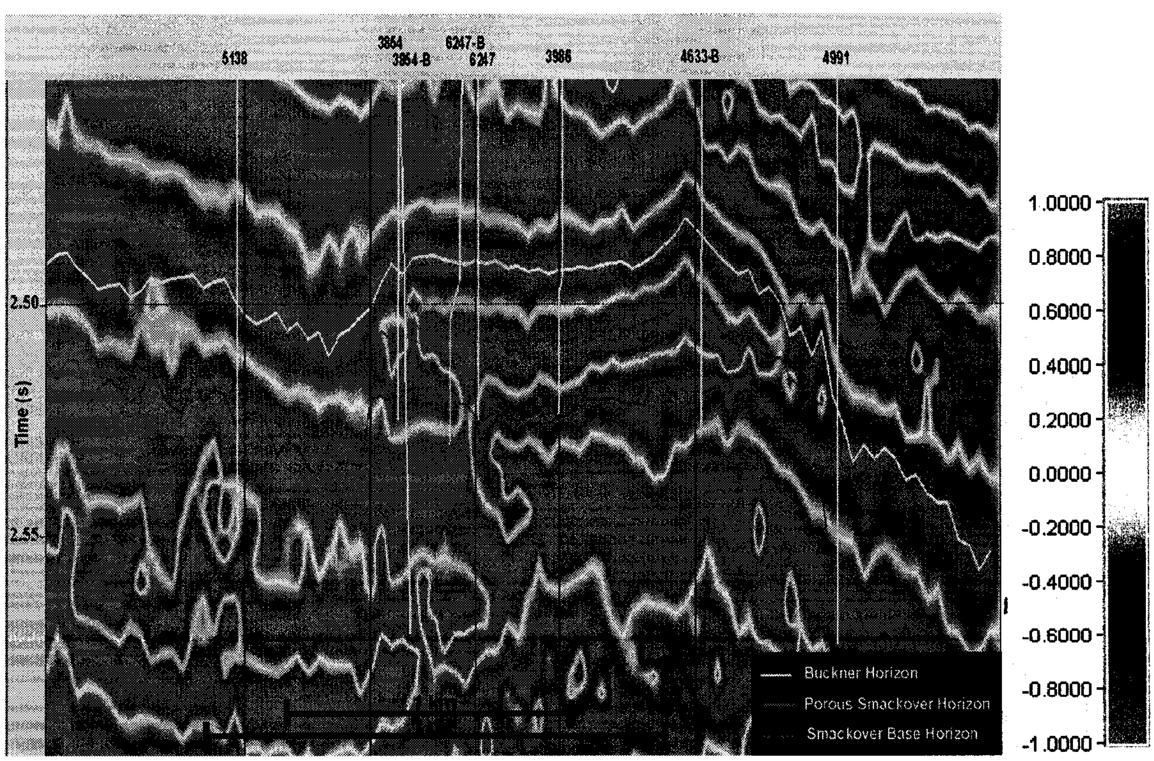
5138
3854
3854-B
6247-B
6247
3986
4633-B
4991
2.50
2.55
Time (s)
Buckner Horizon
Porous Smackover Horizon
Smackover Base Horizon
1.0000
0.8000
0.6000
0.4000
0.2000
0.0000
-0.2000
-0.4000
-0.6000
-0.8000
-1.0000

(d)

interpreted as indicative of facies changes, and/or variations in facies growth form. Derivative is given mathematically by:

$$d(t)=[s(t)-s(t-1)]/\Delta t \quad (6)$$

$$s(t)=f(t)\cos\phi(t) \quad (7)$$

where: $d(t)$ = derivative, $s(t)$ = instantaneous real amplitude (real seismic trace), Δt = sampling rate, $f(t)$ = reflection strength (instantaneous amplitude/amplitude envelope), and $\phi(t)$ = instantaneous phase.

(2) *Derivative Reflection Strength (DRS)* – This is the rate of change of reflection strength (also known as amplitude envelope or instantaneous amplitude) over time (Chen and Sidney, 1997). Reflection strength is the total energy of the seismic trace; it shows the location of maximum energy within an event, which may vary from that of the maximum amplitude (Taner *et al.*, 1979, Mar. 1997 (p.2), 2000; Partyka, 2000). This attribute may be used to examine variations in lateral fluid content (e.g., bright spots for gas detection), lithology, stratigraphy, and thickness within a porous unit (Robertson and Nogami, 1984; Liner, 1999; Yilmaz, 2001). Reflection strength as an attribute loses vertical resolution, which is therefore captured more effectively by its derivative. The derivative reflection of strength is therefore most useful in characterizing vertical interfaces and discontinuities resulting from stratigraphic (facies), lithologic, or fluid changes.

After calculating this attribute from previously described models, and also from a well-derived (model created directly from wells 4991 and 4633-B) synthetic model, the only major change observed resulted from thickness variation of the porous unit. Figures 11b and 11c show transects through DRS and reflection strength (RS) volumes respectively. High porosity areas were seen to have higher values in DRS and lower values in RS volumes (both denoted in hot colors to enhance similarities). Lateral variations in DRS observed within the porous interval show discontinuity in porosity distribution. A marked decrease in the reflection strength occurs on the seaward slope where structural dip was highest. Furthermore, sections obtained from the DRS volume not only mirrored this trend but changes in amplitude were more confined within the porous interval. This stratigraphic confinement emphasizes the effectiveness of this attribute in improving vertical resolution. Taner (Mar. 1997, p. 2) ascribed such an abrupt rise in DRS to increased absorption and attenuation of the seismic waves, changes that might result from an increase in porosity, porosity thickness or variation in fluid content. Mathematically, DRS is given as:

$$da(t)=[f(t)-f(t-1)]/\Delta t \quad (8)$$

$$f(t)=[s(t)^2+h(t)^2]^{*0.5} \quad (9)$$

where: da(t) = derivative reflection strength, h(t) = Hilbert transform

(3) _Cosine Instantaneous Phase_ – This attribute is derived from the instantaneous phase. Because cosine instantaneous phase avoids the 180° discontinuity that occurs with instantaneous phase, and hence is continually smooth, it generates a better display of phase variations. The instantaneous

phase is independent of the phase of the seismic trace amplitude and emphasizes the continuity of reflection events (Chen and Sidney, 1997; Taner, 1979, Mar. 1997 (p. 2); Yilmaz, 2001). Phase variations are most likely a result of constructive and destructive interference from other bedding contacts, a function of bed thickness (e.g., tuning), faulting, and spatial variations in the seismic wavelet (Taner *et al.,* 1979; Liner, 1999; Brown, 1996a). This attribute is useful for displaying structural information as well as subtle reservoir changes caused by disruptions in lateral continuity, which might be depositional (e.g., facies variations), or post-depositionally influenced. Within the analyzed window, changes in cosine instantaneous phase correlated in magnitude and sign to the corresponding amplitude changes of the various stratigraphic units (Fig. 11d). No criteria could be identified from this attribute volume nor from modeled results that might directly categorize changes in porosity within the porous interval. However, on the whole, this attribute defined precisely the lateral extent and stratigraphic configuration of the porous unit. Mathematically, it is given as:

$$c(t)=[\cos\phi(t)] \tag{10}$$

(4) *1/Smoothed Inversion Results* – This attribute shows the acoustic impedance structure at the reservoir interval. Acoustic impedance changes are associated with a composite effect of variations in lithologic or other rock properties such as porosity, fluid type, etc, and as a consequence play a very important role in the description of interval properties (Liner, 1999; Yilmaz, 2001).

A model-based inversion was carried out over a 700 ms window comprising the interval of interest. This inversion attempts to reconstruct an acoustic impedance and stratigraphic model for the seismic data by taking into consideration complex spatial stratigraphic relationships such as baselap, toplap, and conformity (Appendix E). Well logs provide the low frequency component that was absent from the seismic trace as a result of attenuation, and also was used to define the stratigraphic relationships (see Fig. 4). The inversion algorithm calculated the reflectivity for each seismic trace using an initial model and a statistical wavelet extracted from the amplitude spectrum of the elected time window. This initial model is a modeled acoustic impedance volume created using velocity and density information from calibrated logs in the database, with the structurally mapped seismic horizons serving as stratigraphic constraints for acoustic impedance interpolation at interwell locations (*c.f.* Francis, 1997). The modeled acoustic impedance was then gradually modified by the algorithm until the resulting synthetic trace matched the seismic trace within a given tolerance level. Our inversion results show a general reduction in acoustic impedance at the Porous Smackover unit, with a trend of decreasing impedance to the seaward flanks of the structure (Fig. 12). From first order principles, acoustic impedance is inversely proportional to porosity and thus its inverse (MLR can only be significant if all variables were assumed linear) serves as a good indicator of porosity within the Porous Smackover. Since well data are used directly in modeling the acoustic impedance structure of the seismic data, the resulting acoustic impedance volume is smoothed before use as an attribute in MLR.

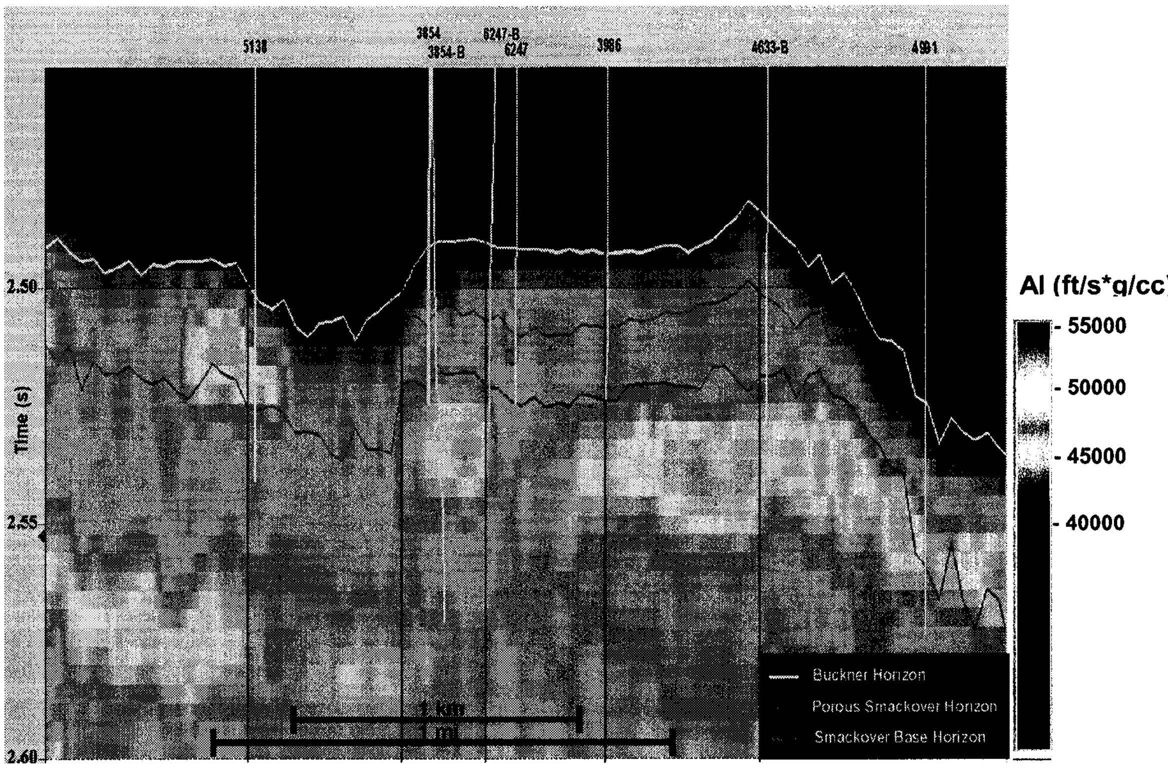
5138
3854
3854-B
6247-B
6247
3986
4633-B
4991
2.50
Time (s)
2.55
2.60
AI (ft/s*g/cc)
55000
50000
45000
40000
Buckner Horizon
Porous Smackover Horizon
Smackover Base Horizon
1 km
1 mi

(a)

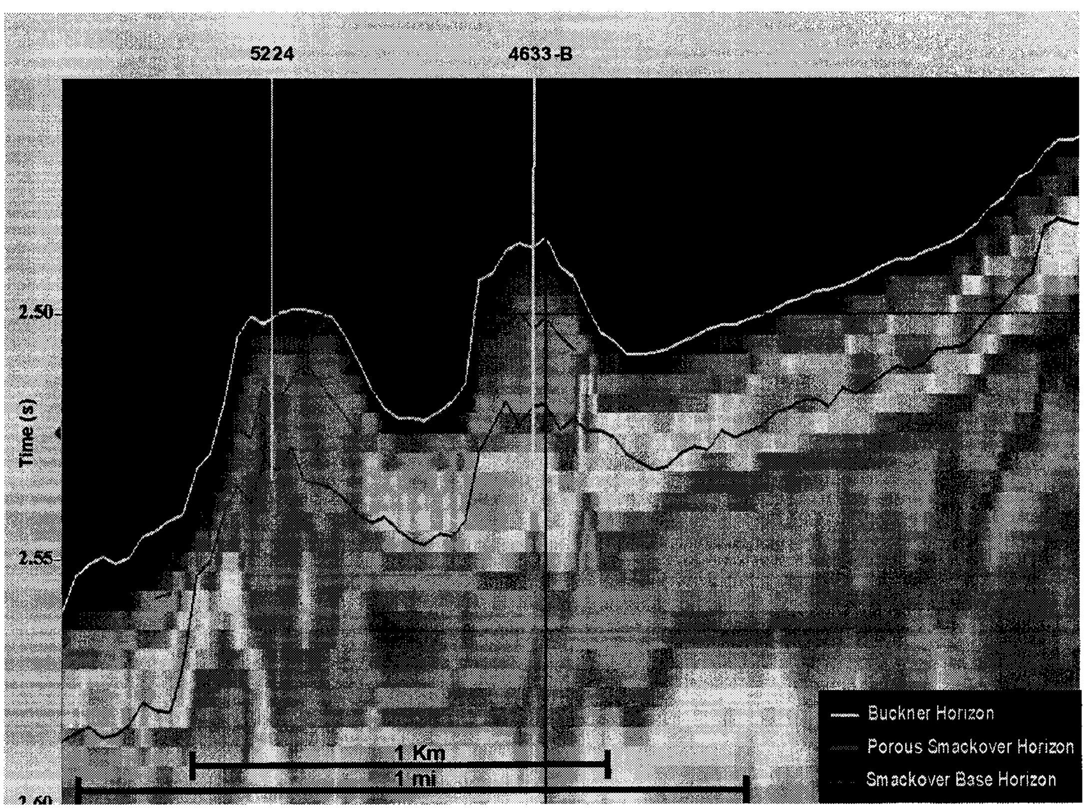
5224
4633-B
2.50
Time (s)
2.55
Buckner Horizon
Porous Smackover Horizon
Smackover Base Horizon
1 Km
1 mi

(b)

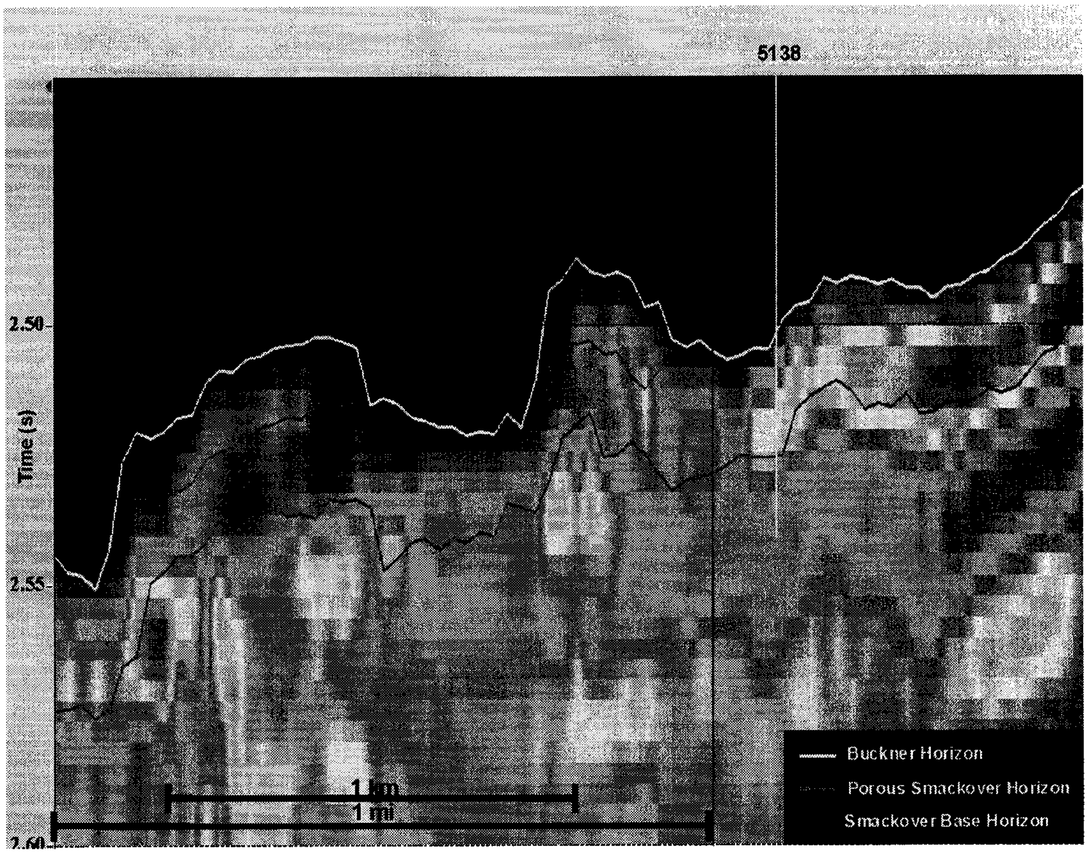
5138
2.50
2.55
2.60
Time (s)
1 km
1 mi
Buckner Horizon
Porous Smackover Horizon
Smackover Base Horizon

(c)

Figure 12: Transects, corresponding to those shown in Figure 6, showing the impedance structure of the Smackover Formation. Impedances are generally lower in the porous Smackover and the Norphlet Formation. (a) Strike section, (b) & (c) Dip sections. Units = ft/s*g/cc. See Figure 3 for location of transects.

This smoothing reduces one-to-one correlation of well and seismic acoustic impedance, which may induce bias in the attribute selection process.

Applying the empirical multi-attribute relationship to the trained wells (i.e., wells used for seismic attribute analysis), we observed an 81% correlation, 8% higher than if only the best single attribute was applied. A comparison of the modeled logs with the actual porosity logs at well locations for the single attribute (Fig. 10) and MLR (Fig. 13), and the reduction of prediction error from 6.4 % to 5.5% porosity units showed that using multi-attributes not only improves porosity prediction but also reduces uncertainty associated with the prediction. Further statistical assessment of how accurately the predicting relationship obtained from MLR-derived attributes predicts porosity, gave us confidence in our results. The 74% correlation coefficient obtained by selectively excluding each of the trained wells from the analysis and re-calculating the correlation coefficient, defines the average correlation of log and modeled porosity. This correlation coefficient gave us insights into porosity prediction in areas of limited well control (Fig. 14), which was good, considering that only six wells were used in estimating this relationship. The PNN-trained relationship provided a better correlation than the MLR-derived relationship (r = 93%, with RMS error of 1.7%). Figure 15 shows that PNN is better at predicting subtle trends in the porosity log, and thus more likely to provide greater geologic detail than MLR. It also further confirms the non-linear nature of the relationship between some of the predicting attributes and porosity (see Appendix F). Predictive equations for MLR and PNN of the

Figure 13: Visual correlation of actual and modeled/predicted porosity using MLR, on: (a) Application of multiattribute equation, (b) Crossploting actual vs predicted porosity values, based on Table 4. Correlation is only valid in interval defined by analysis window in (a). Porosity increases to the right of the curve.

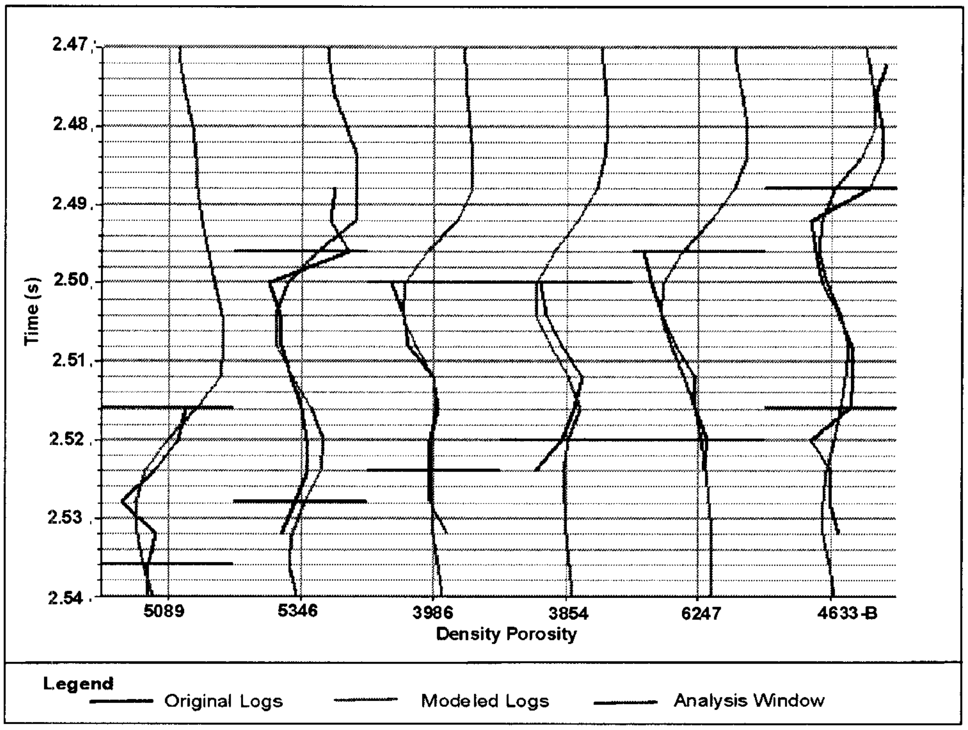

Time (s)
2.47
2.48
2.49
2.50
2.51
2.52
2.53
2.54
5089
5346
3986
3854
6247
4633-B
Density Porosity
Legend
Original Logs
Modeled Logs
Analysis Window

(a)

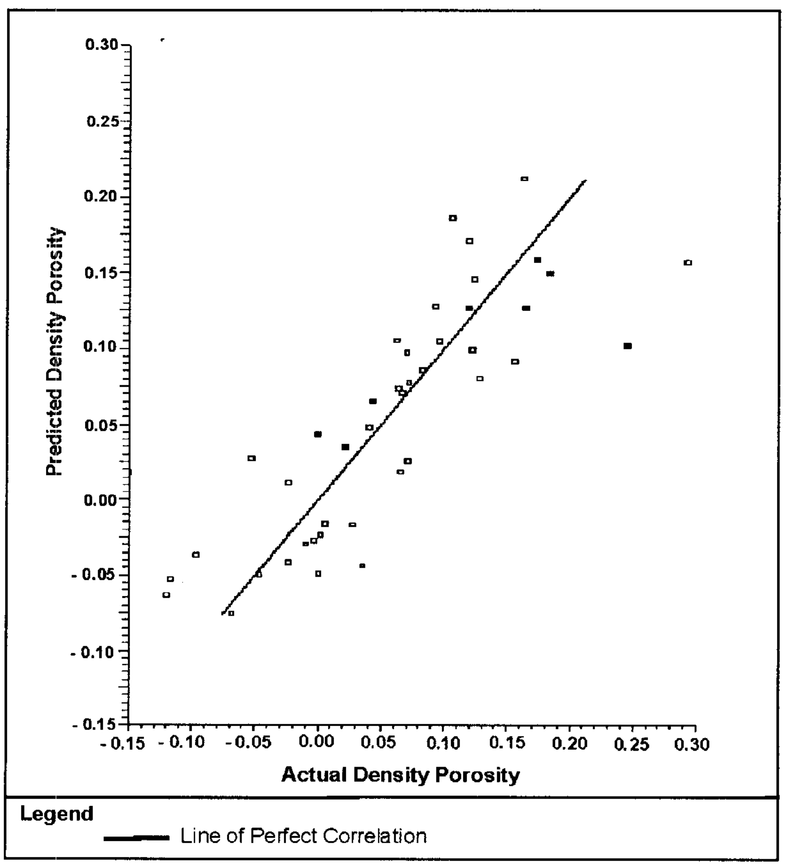

Predicted Density Porosity
0.30
0.25
0.20
0.15
0.10
0.05
0.00
-0.05
-0.10
-0.15
-0.15
-0.10
-0.05
0.00
0.05
0.10
0.15
0.20
0.25
0.30
Actual Density Porosity
Legend
Line of Perfect Correlation

(b)

Figure 14: This plot shows how accurately the porosity values of wells trained for the multilinear regression analysis (MLR) are predicted when they are excluded from the analysis and the remaining wells trained to predict them. It also gives a good approximation on how good the predicting relationship is in estimating porosity in areas of limited well control. Porosity increases to the right of the curve.

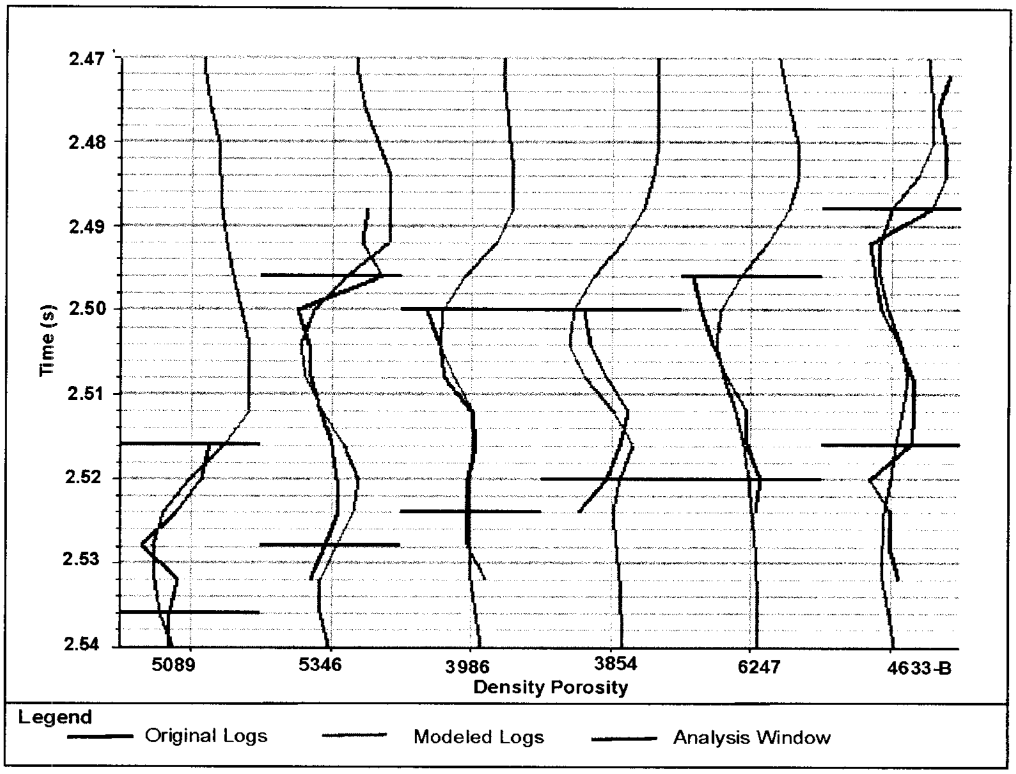
2.47
2.48
2.49
2.50
2.51
2.52
2.53
2.54
Time (s)
5089
5346
3986
3854
6247
4633-B
Density Porosity
Legend
Original Logs
Modeled Logs
Analysis Window

Figure 15: Visual correlation of actual and modeled/predicted porosity using PNN. (a) On application of multiattribute equation. Note how good the PNN-derived relationship is in modeling subtle changes in porosity within the Smackover Formation. (b) On crossploting actual vs predicted porosity values, based on Table 4. (c) As in Figure 14, this figure shows how accurately the porosity at each well can be modeled using the PNN-derived empirical relationship, when that well is excluded from the analysis. We observed a better correlation than with MLR. Porosity increases to the right of the curve.

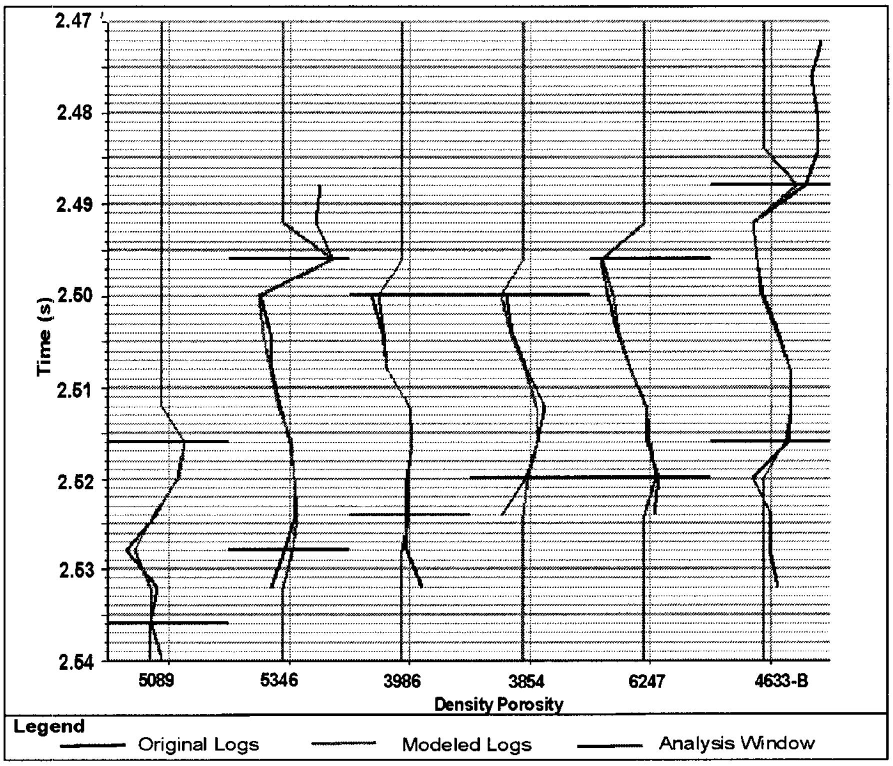

2.47
2.48
2.49
2.50
2.51
2.52
2.53
2.54
Time (s)
5089
5346
3986
3854
6247
4633-B
Density Porosity
Legend
Original Logs
Modeled Logs
Analysis Window

(a)

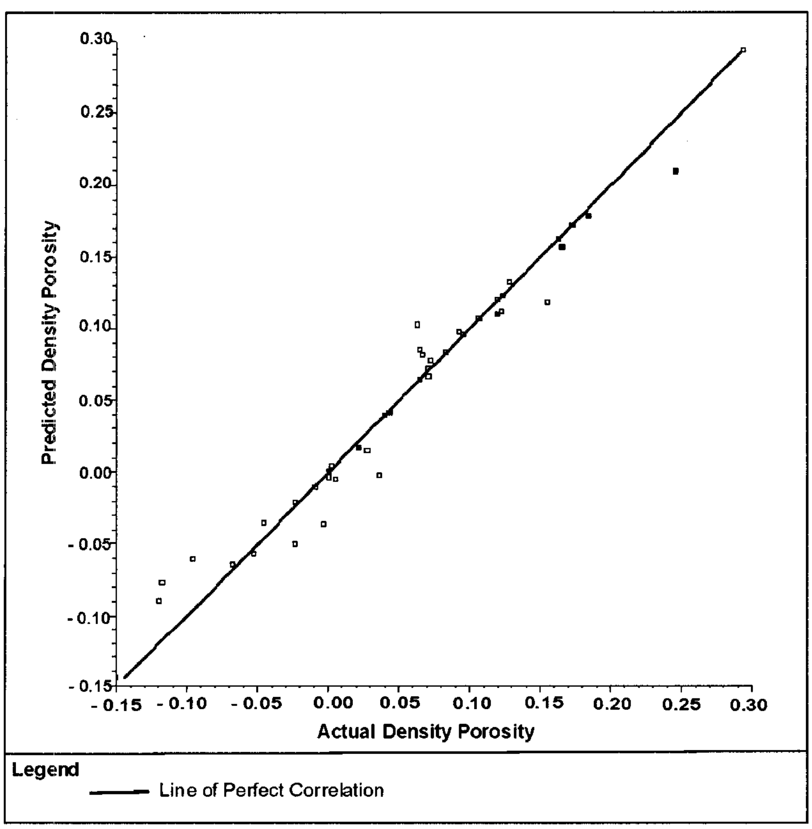

0.30
0.25
0.20
0.15
0.10
0.05
0.00
- 0.05
- 0.10
- 0.15
Predicted Density Porosity
- 0.15
- 0.10
- 0.05
0.00
0.05
0.10
0.15
0.20
0.25
0.30
Actual Density Porosity
Legend
Line of Perfect Correlation

(b)

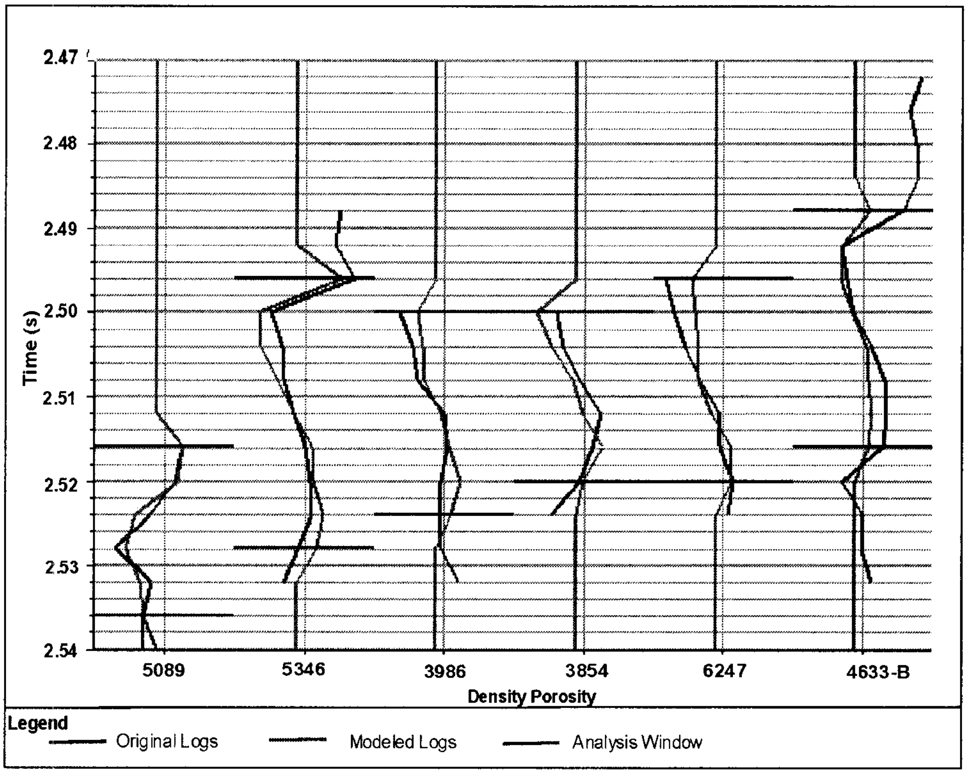

2.47
2.48
2.49
2.50
2.51
2.52
2.53
2.54
Time (s)
5089
5346
3986
3854
6247
4633-B
Density Porosity
Legend
Original Logs
Modeled Logs
Analysis Window

(c)

form of equations 5 and 11, derived from the weights obtained for each attribute in the multi-attribute analysis (Table 3) were applied to the seismic data to create porosity volumes.

P_{MLR} = -0.118 + [(5.27e-006*Derivative) + (5.42e-005*Derivative Reflection strength) + (-0.05*Cosine Instantaneous Phase) + (10263.80*(1/Smoothed Inversion Results)] (11)

From examining both the MLR- and PNN-derived values at well locations (Table 4) and volumes, the following observations are noted: First, as with thickness of the porous interval, porosity is generally higher on the forereef flanks than the crests of paleohighs, although there are other restricted areas (e.g., the highest point of the crests) of high porosity (Figs. 16 and 17). The MLR volume showed more high porosity on the flanks. Second, some areas were predicted to have high porosity by MLR, a change that was not mirrored by the PNN volume. This is attributed to an expression of non-linear relationships between porosity and the predicting attributes that is best recognized by PNN, and thus were artifacts in the MLR volume. Third, as seen in Figures 16 and 17, the magnitude and variation of predicted porosity in the porous interval strongly correlated with corresponding changes in the derivative attribute for that interval. This supports our earlier hypothesis on this attribute's (derivative) role in predicting the amount of porosity in these facies, and further adds credibility to our modeled attribute results.

Table 3: Attribute weights/sigmas applied to predicting relationships

Attribute Name	**Transform**	**Weight (MLR)**	**Sigmas (PNN)**
Derivative	None	5.26796e-006	0.212692601922194
Derivative Instantaneous Amplitude	None	5.42256e-005	0.172496042723559
Cosine Instantaneous Phase	None	-0.0467525	0.409645730267811
Smooth Inversion Results	I/X	10263.8	0.377321369776163
Constant	None-	-0.117512	0.462500001303852
Target transform	None	None	None
Trend Length	None-	1	None

Table 4: Values obtained from MLR and PNN analysis at each log location within the seismic volume. Compared with the actual density porosity values obtained from logs, PNN can be seen to model best porosity values at each sampled location. This goes to confirm that PNN best predicts porosity at log and therefore at interwell areas.

Permit #	Actual Density Porosity	Density Porosity MLR	Density Porosity PNN
5089	0.1630	0.2118	0.1630
5089	0.1281	0.0802	0.1325
5089	0.0276	-0.0166	0.0143
5089	-0.1175	-0.0533	-0.0765
5089	0.0355	-0.0440	-0.0024
5089	0.0021	-0.0237	0.0040
5346	0.2938	0.1562	0.2936
5346	-0.0530	0.0273	-0.0567
5346	-0.0037	-0.0273	-0.0359
5346	0.0053	-0.0163	-0.0052
5346	0.0401	0.0479	0.0394
5346	0.0929	0.1275	0.0980
5346	0.1066	0.1858	0.1069
5346	0.1197	0.1706	0.1203
5346	0.0625	0.1051	0.1029
3986	-0.0960	-0.0368	-0.0602
3986	-0.0461	-0.0500	-0.0354
3986	-0.0235	0.0111	-0.0212
3986	0.0833	0.0856	0.0832
3986	0.0958	0.1044	0.0959
3986	0.0720	0.0770	0.0777
3986	0.0644	0.0736	0.0852
3854	-0.0240	-0.0416	-0.0504
3854	0.0004	-0.0489	-0.0036
3854	0.0648	0.0183	0.0645
3854	0.1555	0.0913	0.1179
3854	0.1236	0.1453	0.1230
3854	0.0707	0.0969	0.0725

6247	-0.1510	0.0176	-0.1445
6247	-0.1203	-0.0635	-0.0896
6247	-0.0680	-0.0757	-0.0646
6247	-0.0097	-0.0298	-0.0107
6247	0.0710	0.0254	0.0664
6247	0.0668	0.0708	0.0818
6247	0.1221	0.0989	0.1120
4633-B	0.2452	0.1019	0.2097
4633-B	0.0003	0.0434	0.0009
4633-B	0.0215	0.0346	0.0168
4633-B	0.0430	0.0654	0.0415
4633-B	0.1192	0.1259	0.1102
4633-B	0.1729	0.1585	0.1723
4633-B	0.1835	0.1487	0.1790
4633-B	0.1651	0.1260	0.1569

Figure 16: Strike (a) and dip sections (b & c) through the MLR porosity volume. Both sections show a preference for higher porosities (hot colors) to the seaward flanks of structure, and also a landward increase in the thickness of the Buckner/Smackover horizon. Note the seaward prograding and dipping profile of the buildup in all three transects. See Figure 3 for location of transects.

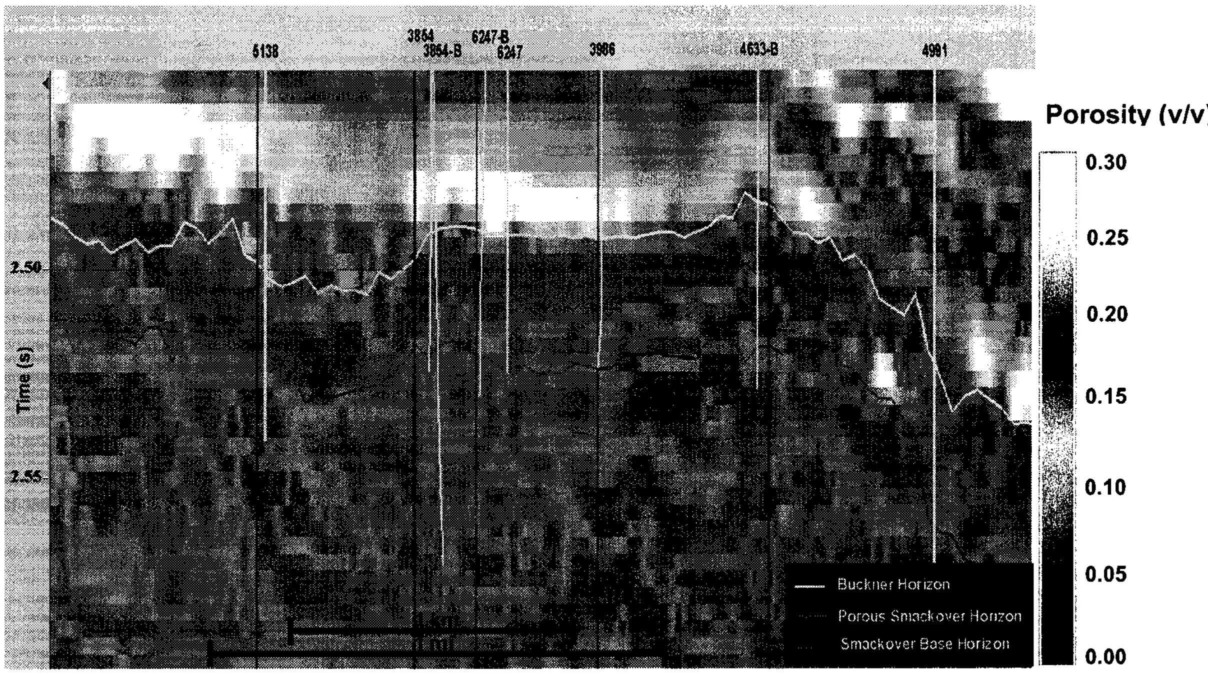
5138
3864
3864-B
6247-B
6247
3986
4633-B
4981
Porosity (v/v)
0.30
0.25
0.20
0.15
0.10
0.05
0.00
2.50
2.55
Time (s)
Buckner Horizon
Porous Smackover Horizon
Smackover Base Horizon

(a)

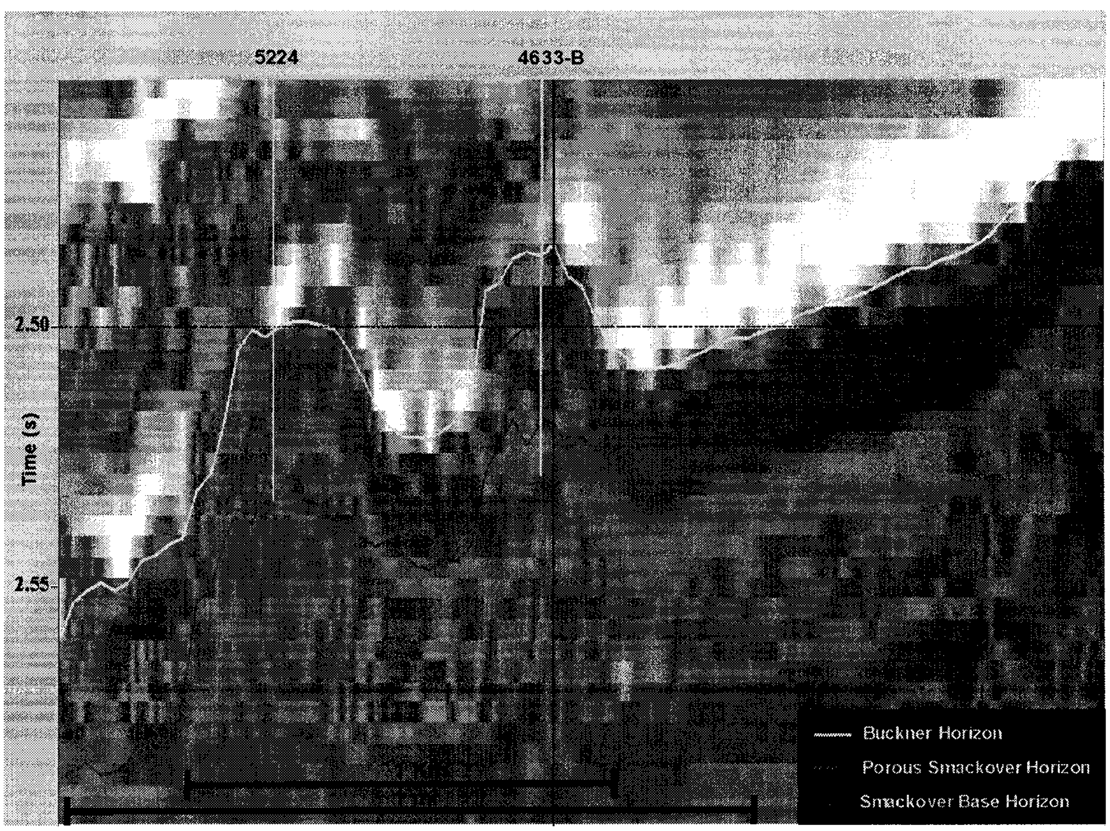
5224
4633-B
2.50
2.55
Time (s)
Buckner Horizon
Porous Smackover Horizon
Smackover Base Horizon

(b)

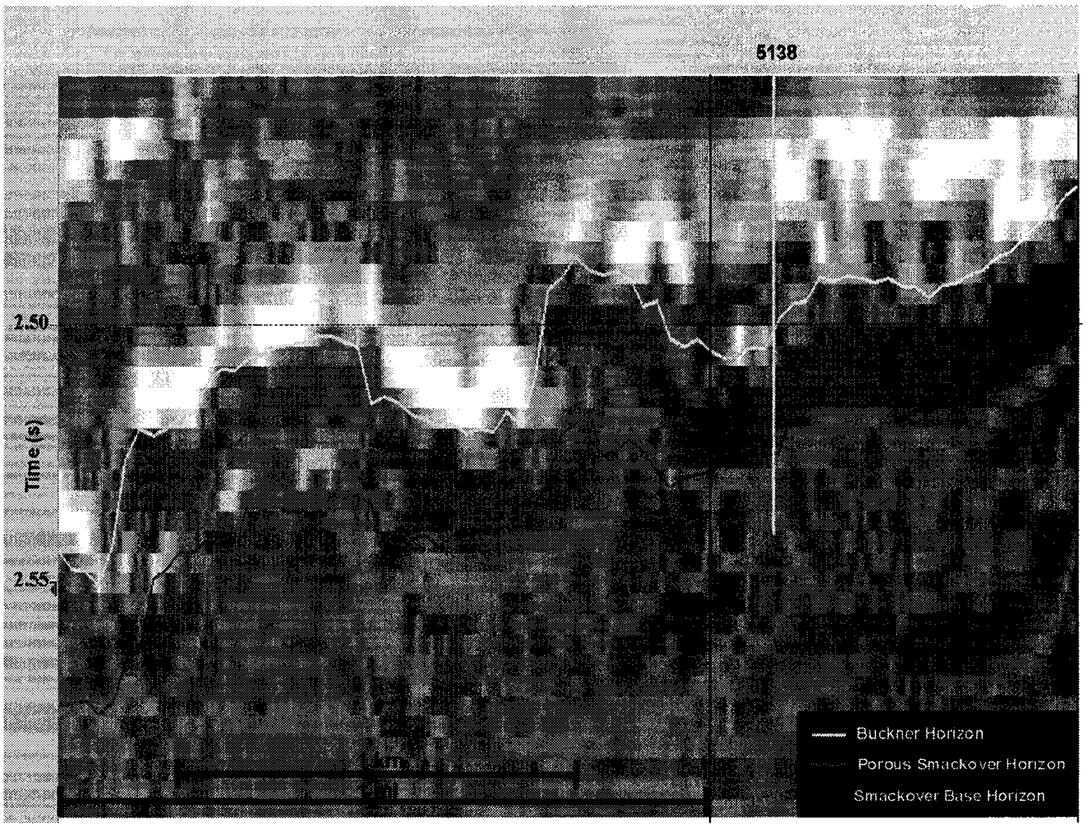
5138
2.50
Time (s)
2.55
Buckner Horizon
Porous Smackover Horizon
Smackover Base Horizon

(c)

Figure 17: Strike (a) and dip sections (b & c) through the PNN porosity volume. As with the MLR, all sections show a preference for higher porosities (hot colors) to be on the seaward flanks of structure. The porosity values in this volume at well locations (e.g. 5224) are more accurate than with the MLR. See Figure 3 for location of transects.

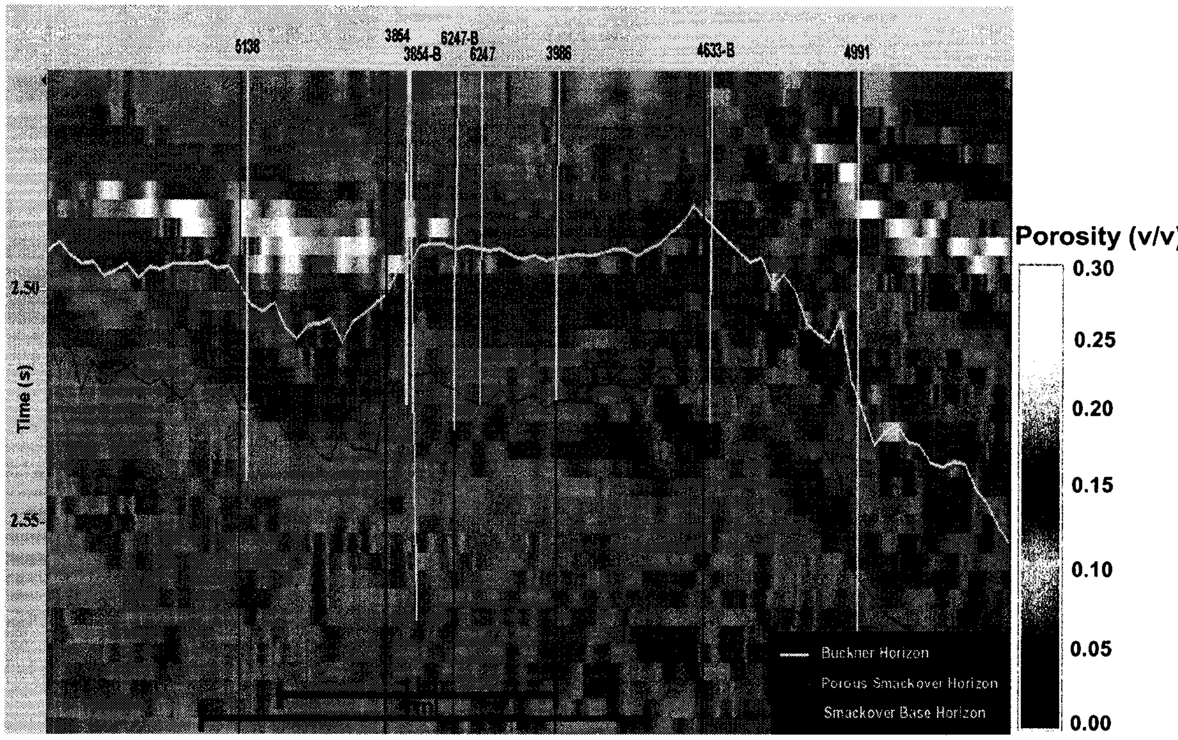
5138
3864
3854-B
6247-B
6247
3986
4633-B
4991
2.50
2.55
Time (s)
Porosity (v/v)
0.30
0.25
0.20
0.15
0.10
0.05
0.00
Buckner Horizon
Porous Smackover Horizon
Smackover Base Horizon

(a)

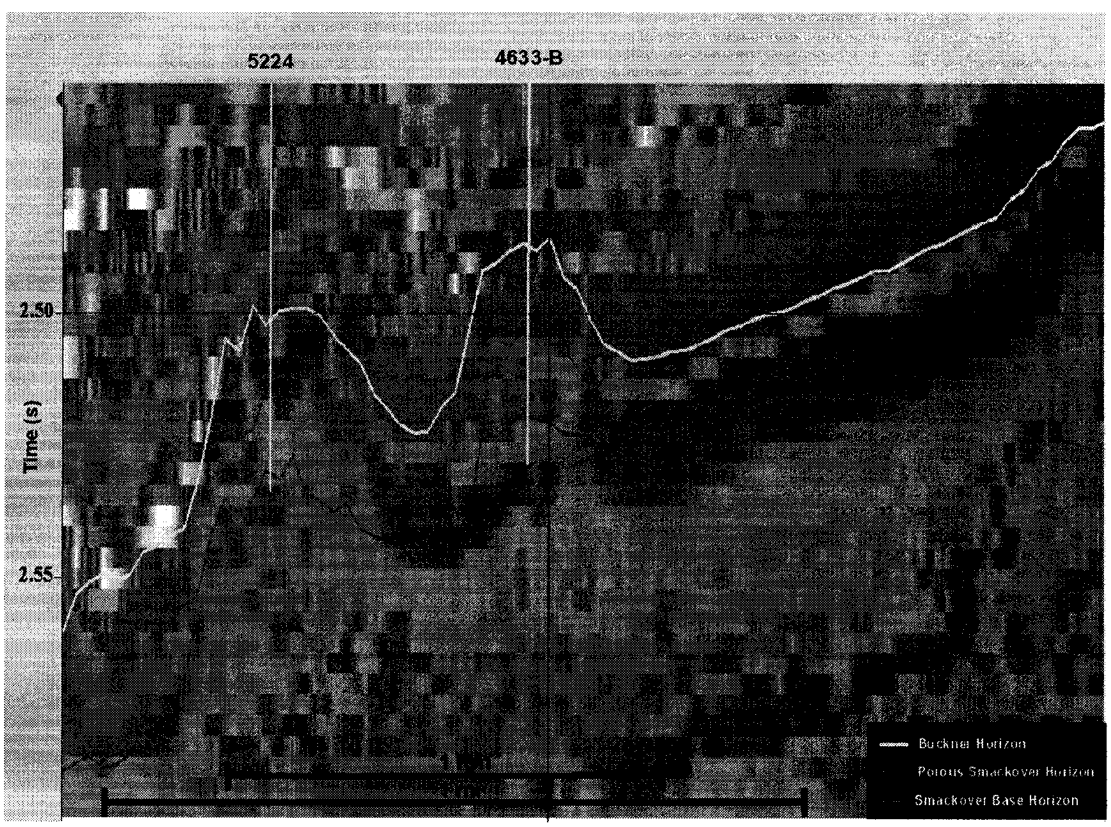
5224
4633-B
2.50
2.55
Time (s)
Buckner Horizon
Porous Smackover Horizon
Smackover Base Horizon

(b)

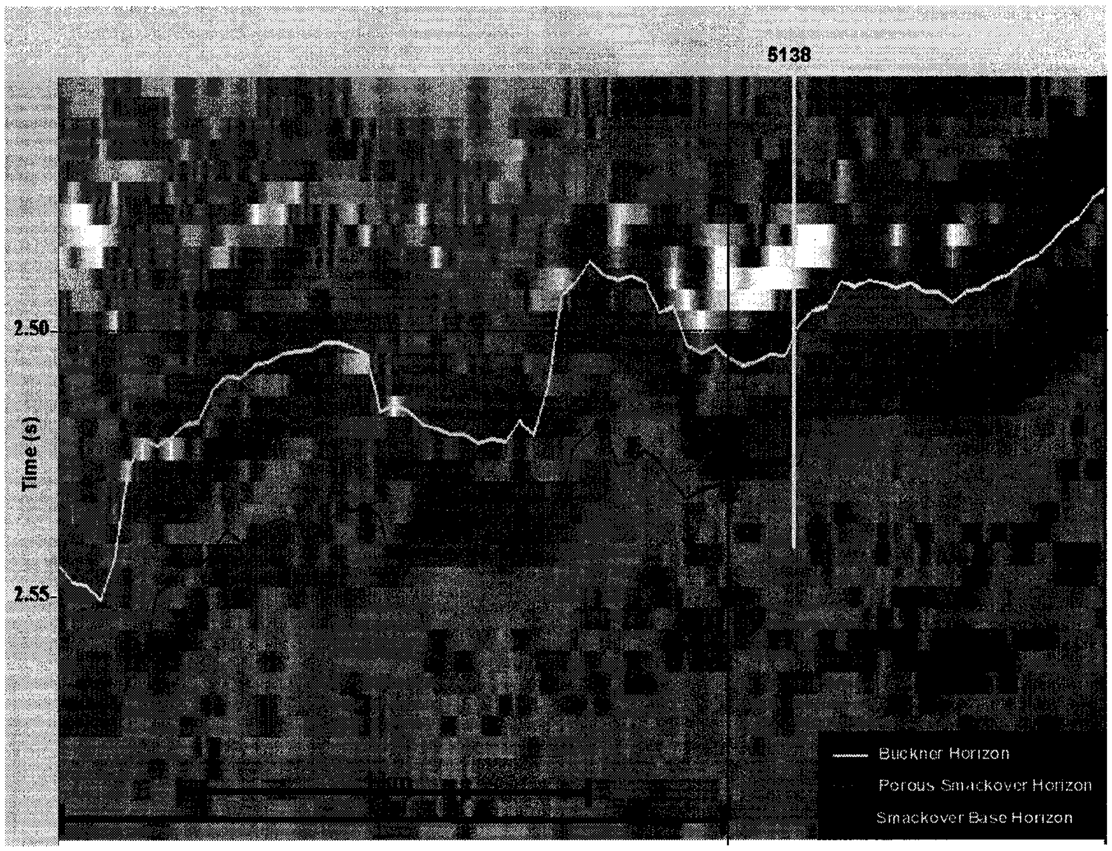
5138
2.50
2.55
Time (s)
Buckner Horizon
Porous Smackover Horizon
Smackover Base Horizon

(c)

Slices at 4 ms intervals through the reefal interval of the PNN volume (same sampling rate as seismic data, see Fig. 18), also highlight the general trend of higher porosities occurring along the southern flanks than the crests of the structure.

To better quantify the association of porosity development and paleostructure, porosity thickness (*Øh*) maps were constructed for the Smackover Formation. Initially, using a 12% porosity cut-off as our porosity indicator (12% porosity is the lower limit for production in the Appleton Field), we calculated the cumulative thickness of porosity for the Smackover Formation. Subsequently, thickness (in time, ms) was multiplied this with average velocity for the Smackover to get thickness in feet. As with the sectional views, the effects of non-linearity are readily apparent. Although both thickness maps show the predominance of porosity on the forereef flanks than the crest of structure (see Fig. 19), the PNN map is geologically more realistic given the facies types and their growth forms described from core studies (Table 5). These observations lead us to conclude that PNN best predicts the distribution of porosity in inter-well areas.

Figure 18: Slices through the porosity volume (porosity values are in decimals (v/v) i.e., volume of voids/total volume of rock, and not percentages), starting 4 ms above the porous Smackover pick. Porosity at –4 ms above this pick was attributed to shoal grainstone facies, which constitute the other major reservoir facies in the Appleton Field. Note the overall association of higher porosities (hot colors) with the southern (paleoseaward) flanks of structure, which we attribute primarily to changes in facies type and growth form. Well symbols are indicated in Figures 3 and 8.

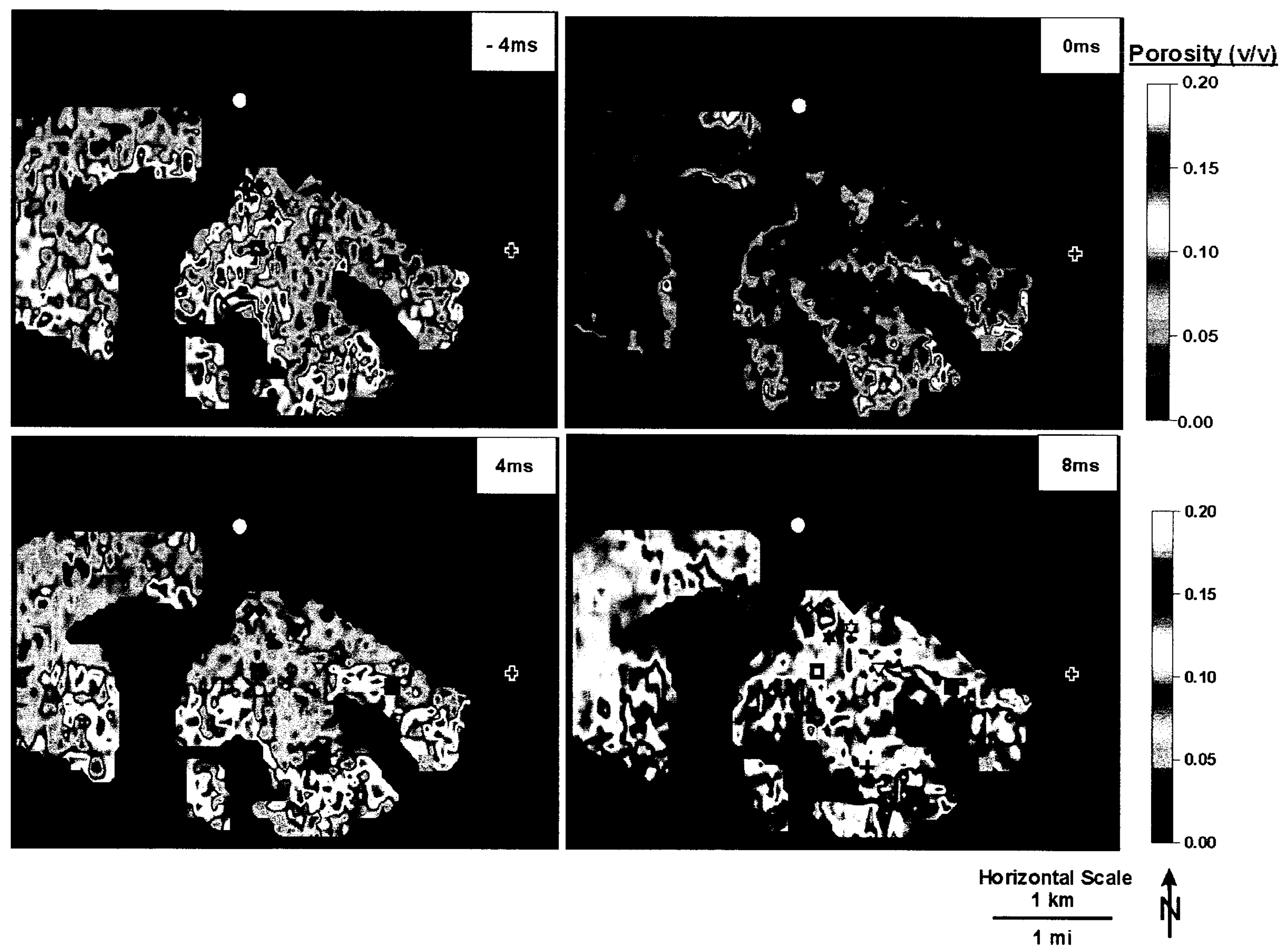

- 4ms
0ms
4ms
8ms
Porosity (v/v)
0.20
0.15
0.10
0.05
0.00
Horizontal Scale
1 km
1 mi
N

Figure 19: Porosity thickness map of the Smackover Formation overlain on the Buckner/Smackover structure map for better display. Note the overall porosity thickness (hot colors) on the southern flanks of structure. Observed differences in the distribution of porosity is mainly a result of the non-linear relationship between the predicting attributes and the seismic data. Well symbols are indicated in Figures 3 and 8.

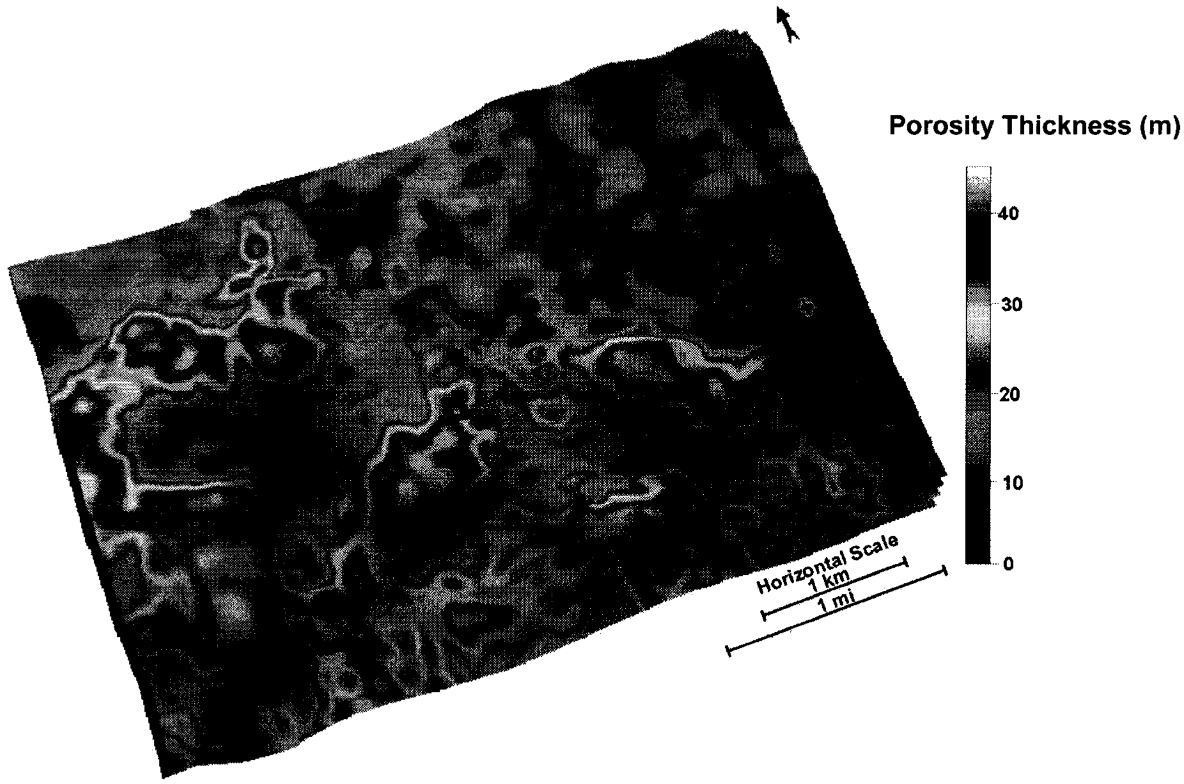
Porosity Thickness (m)
40
30
20
10
0
Horizontal Scale
1 km
1 mi

(a)

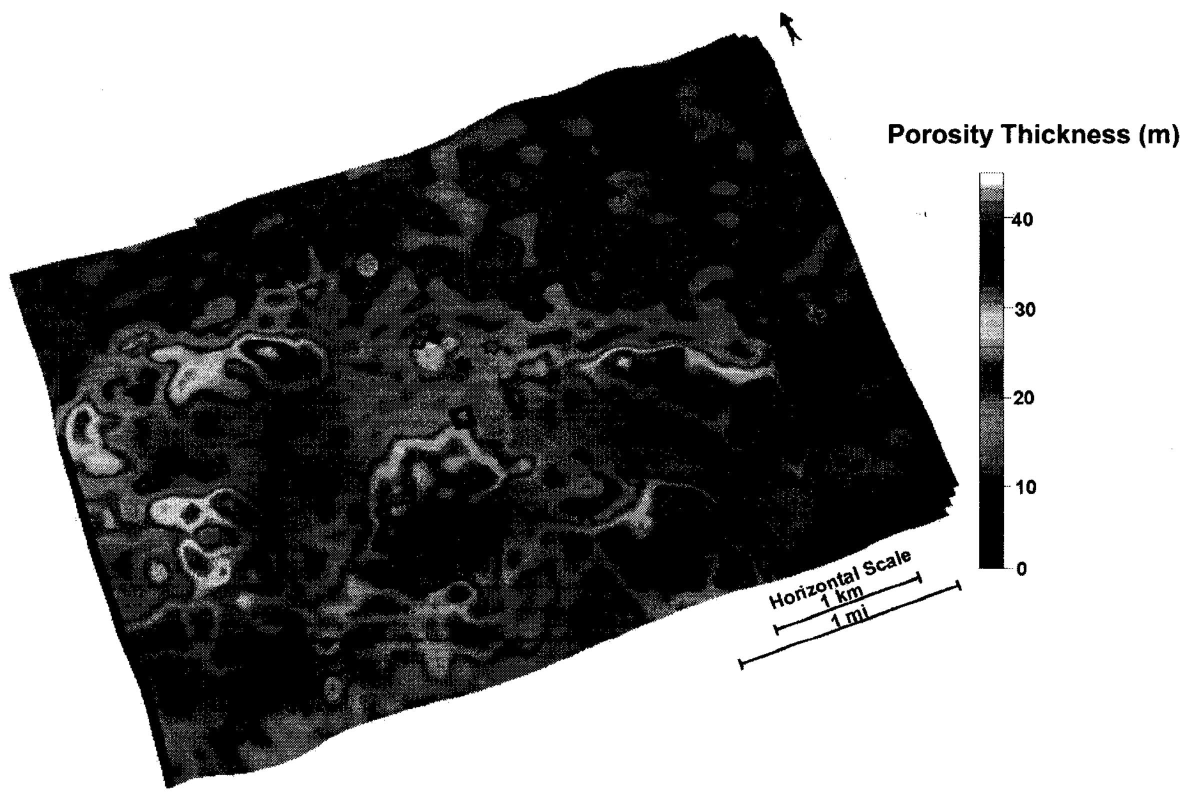
Porosity Thickness (m)
40
30
20
10
0
Horizontal Scale
1 km
1 mi

(b)

Table 5: Reef type, depositional fabric/growth forms, and their reservoir characteristics observed at the Appleton Field, SW Alabama. (Modified from Parcell, 2000).

Reef type	Depositional fabric/growth form (wave energy)	Reservoir characteristics at Appleton Field
Type I	Layered thrombolites (higher energy)	Good reservoir, lateral permeability
Type II	Reticulate/Chaotic thrombolites (moderate energy)	Good reservoir, lateral-vertical permeability
Type III	Dendroid thrombolites (lower energy)	Best reservoir, vertical permeability
Type IV	Isolated stromatolitic crusts (moderate energy)	Poor reservoir, low permeability
Type V	Oncoidal packstone/ Grainstone (higher energy)	Poor reservoir, low permeability (better if primary fabric is not occluded)

1.6 Discussion

1.6.1 Limitations and problems in assessing geologic and geophysical data

Although traditionally considered a geophysical method, multiattribute studies have far-reaching applications for the sedimentary geologist. Current methods used by sedimentary geologists to study the distribution of physical property have several deficiencies, some of which are addressed here. The application of statistical methods to a single data type, e.g., well or core data, provides little constraint in physical property distribution in interwell areas (Dubrule, 1998). Also, sample sizes are often sparse or inadequate unless there is good data control such as a large number of closely spaced wells or outcrop data. Furthermore, there is often an introduction of sampling bias in that only a limited number of facies are sampled. This is a common error because, besides exploratory wells, most wells are drilled targeting only zones of interest. This method thus show a disregard for geology (facies variation not assessed) and statistics (sampling bias), and models used in physical property prediction may be unrepresentative of field heterogeneity (Hirsche *et al.*, 1997; Dubrule, 1998; Hirsche *et al.,* 1998). In the case of applying facies analysis/modeling and sequence stratigraphy to physical property distributions, the main limitation is that there is no direct quantitative output. This limitation stems from the difficulty of characterizing facies heterogeneity in space (i.e., their geometry, physical properties, etc.) resulting from stochastic and complex interactions between factors controlling sediment deposition (e.g., reef growth, avulsion). Added to these, facies models are difficult to apply in 3-D because of the nature (gradual or abrupt) and location of physical property boundaries (e.g., lithologic transitions, porosity) that are commonly improperly characterized. Thus some ambiguity persists due to inconsistency in facies geometry and sampling. In instances where seismic data are used, sequence stratigraphy is applied mainly to predict lithology, define facies geometry and boundaries, and calibrate well data (Posamentier and James, 1993; Nissen *et al.,* 1999). Changes in physical properties within these facies cannot be adequately assessed with this method only. The interpretation of size/shape of features may be also by integration of data with models that may or may not be appropriate or adequate.

1.6.2 Multiattribute studies

The multiattribute analysis differs from the above methods mainly in the way it utilizes seismic data. Seismic data is derived from *in situ* measurements of physical properties. There is usually less ambiguity, which is peculiar to facies modeling and sequence stratigraphy, in defining geometry of targets, as most seismic data are shot to resolve critical features (e.g., channels, faults), and delineate necessary depositional trends and physical properties of the facies imaged. Because seismic data represents average rock properties across a given analysis window, while log data represents precise rock measurements at given points within this window, mapped seismic horizons helps to constrain physical property interpolation at interwell locations. The 3-D structure maps obtained from seismic mapping are more accurate than 2-D or well-based maps, as 3-D migration accurately repositions reflections diffracted from curved surfaces such as reefs and anticlines. Also, using a volume as opposed to 2-D data helps to quantify predictions in 3-D space. Additionally, the use of a volume-based as opposed to a horizon-based method increases sample size. As was observed during our multiattribute analysis, the sample size was substantially increased from six (one sample per well) to forty-three (an average of six samples per well). Hence, this method is most appropriate in areas of limited well control (Russell *et al.*, 1997; Hampson *et al.*, 2001; Hart, 2002). This increase in sample size further reduced the uncertainty, as determined from statistical correlation, associated with such comparisons of sparse well data and the densely populated seismic data. The use of both porous (producers and abandoned) and non-porous wells during our analysis also reduced the probability of our prediction being too sample-specific, as a result of facies bias.

Another major advantage of this method is that it integrates information (geology, geophysics) from a variety of data types using several analytical techniques (Schultz *et al.,* 1994a&b; Hampson *et al.,* 2001; Matteucci *et al.*, 2001). This helps limit the degree of assumption in the following manner: Seismic modeling carried out showed the expected response of formations, thus reducing the possibility of incorrect sampling resulting from mispicks of formation tops and mistie of well-seismic data. Trace inversion showed the expected acoustic impedance structure at the interval of interest. This helped define areas with marked changes in porosity. Statistics, used concurrently with analysis, provided a means for comparing both data and estimating the degree of confidence we can place in our predicted results. Furthermore, the predicting attributes have been shown to relate to different aspects of the porous interval. Thus we have sufficient evidence, and confidence, that our interpretation of the distribution of porosity adequately models the geology at Appleton Field.

1.6.3 Precautions in multiattribute studies

As with other computational methods, several precautions are necessary to ensure validity of the results:

(i) Although appropriate for areas of limited well control, the logs and seismic data used should be of the same vintage. This overcomes the influence of changes in the physical properties of facies over time (e.g., oil/water saturation) due to production.

(ii) Logs should be edited to check for borehole influences e.g., caving, washouts, vugs, etc, that might affect their readings.

(iii) Logs should contain the suite of logs whose property is being measured.

(iv) Also, the predicting log type should be reflective of the host rock type, the modeled property, and not dependent on the data available.

Care should be taken while extracting attributes from the seismic data. The quality, and hence the validity of the relationships obtained using these attributes depends on the quality of the seismic data and the mode of attribute extraction.

(i) Horizons should be properly interpreted from the seismic data. Only strong reflections should be autotracked to avoid mispicks, and consequently sampling a wrong location.

(ii) Logs should be well correlated to the seismic data. Care is required when dealing with deviated logs to avoid possibilities of spurious correlation resulting from sampling incorrect locations.

(iii) Attribute results and their interpretations are only valid within the analysis window.

Lastly, as with any statistical correlation between variables, there always is a risk of spurious correlations between any attribute and log property (Kalkomey, 1997). The probability of observing such a spurious correlation increases with the number of attributes used in the analysis, and with a corresponding decrease in the number of well samples. This risk can be limited by:

i) A direct physical, or good statistical relationship between attributes and predicted property.

ii) A geologically reasonable relationship observed between the predicting attributes and the measured physical property.

1.6.4 Porosity distribution model

Several models have been proposed to describe porosity formation, its distribution, and controls on facies distribution in the Appleton Field, with the aim of improving the understanding of the depositional history (Mancini *et al.,* 1999, 2000; Hart and Balch, 2000; Parcell, 2000). Differences between models discussed lie principally in the analytical method(s) used for the assessment of data, and their effectiveness in defining porosity distribution. Hart and Balch (2000) used a horizon-based attribute study to predict porosity thickness defined the porous Smackover unit as favoring the crests rather than flanks of the paleohighs (Fig. 20a). They suggested that porosity development on the southern flanks of structure might be related to forereef talus deposits. While much evidence points to the probability of development of talus-derived porosity e.g., distal steeping of this ramp and higher wave energy levels during late highstand/early lowstand fall in sea level provide suitable conditions for talus formation; presence of oncoids, which are characteristic to talus deposits, have been observed in cores from the Appleton Field and other Upper Jurassic reef-dominated fields (Jansa, *et al.,* 1989; Pratt *et al.,* 1992; Tew *et al.,* 1993; King, 1994; Pratt, 1995; Parcell, 2000). We believe however, that talus-derived porosity is not a major contributor to porosity development in this field, because transects through the predicted porosity volume depict porosity as better developed on the crest and forereef flanks of structure. Also, given the steepness of slope in the forereef areas, it would be difficult for talus deposits to accumulate to great thicknesses as was observed from the limited higher energy talus-derived reef facies identified from cores (see Table 5). Thus, with the lack of flexibility common to 2-D-based models, it is difficult to visualize and make suggestions on the probable controls on porosity development in this field.

Figure 20: Existing models for the Appleton field. (a) Model of Hart & Balch (2000) depicting porosity distribution in the porous unit of the Smackover Formation, Appleton Field. Map created using a horizon-based seismic attribute study. (b) Model by Mancini *et al,* 1999. This illustrates facies distribution as a function of water depth on the basement paleohigh.

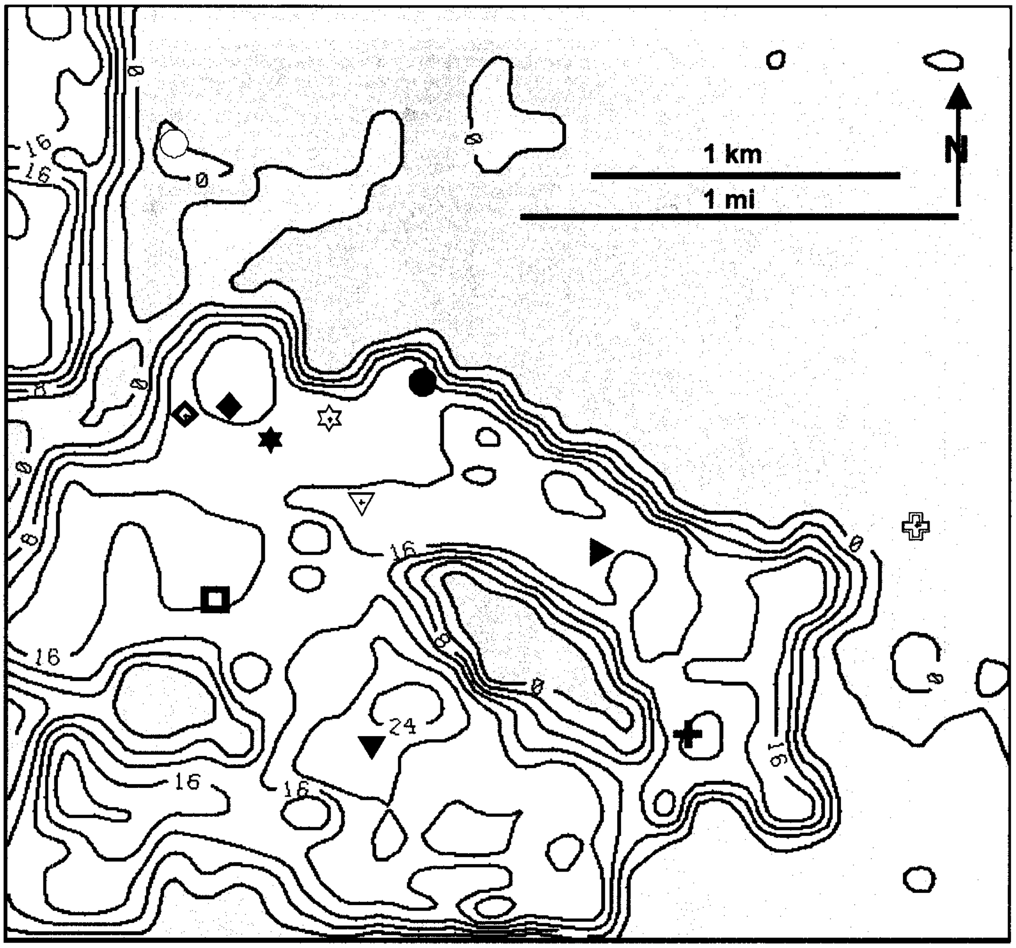

(a)

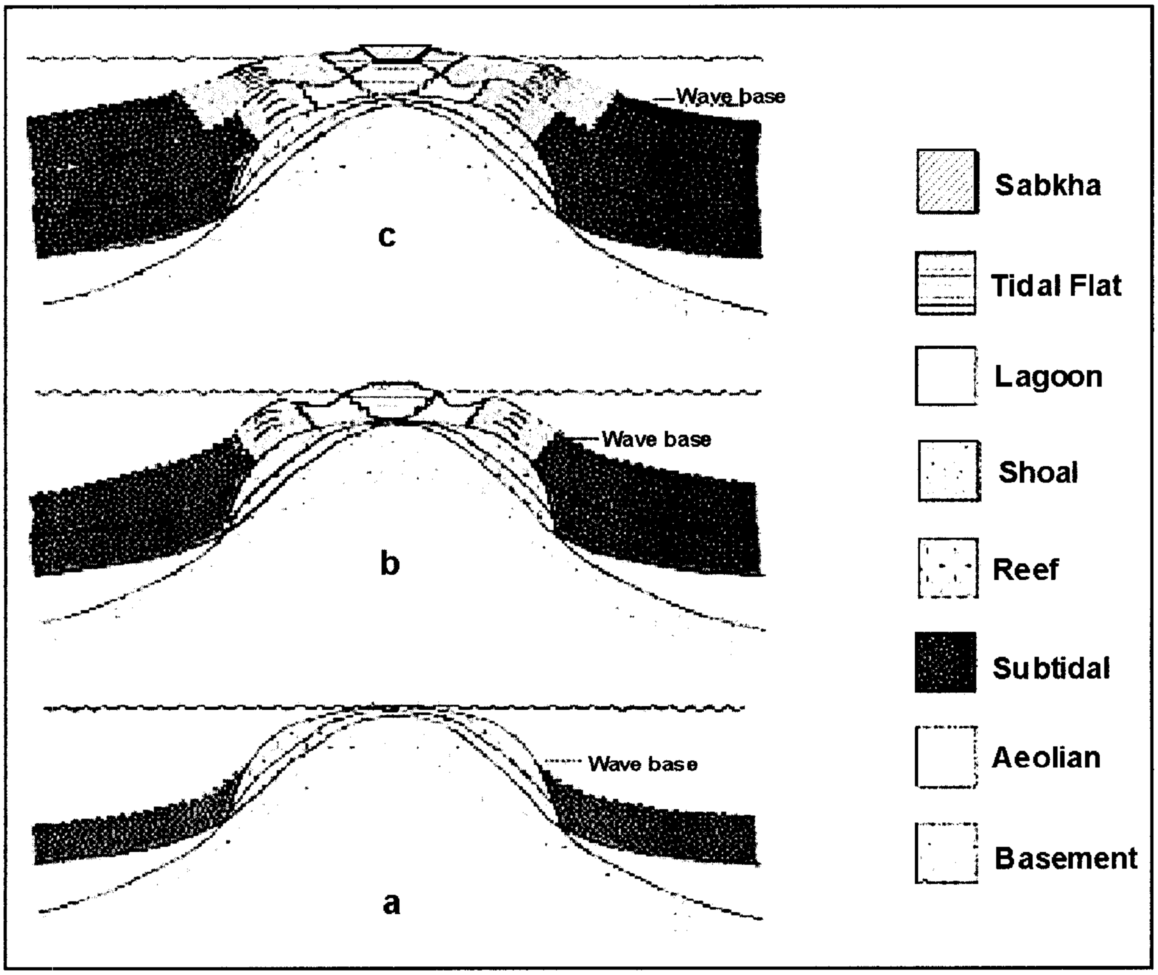
Wave base
c
Wave base
b
Wave base
a
Sabkha
Tidal Flat
Lagoon
Shoal
Reef
Subtidal
Aeolian
Basement

(b)

Conversely, the model of Mancini *et al.* (1999, 2000) suggested that the distribution of facies was dependent on the height of the paleohighs (Fig. 20b) and associated water depth. Because of the methods used (see Mancini *et al.*, 1999, 2000), it was not possible to represent the variation of these facies and calculate porosity distribution in 3-D space. Thus the proposed model is mainly conceptual geologic model and not unique to the Appleton Field. Therefore, neither model provided a detailed guide to facies heterogeneity in the Smackover of the Appleton Field. By looking at transects and slices through porosity volume, our proposed model has the advantage of capturing 3-D porosity changes, hence large-scale reservoir heterogeneities, within the Appleton Field (Figs. 17, 18, & 19). Not only does this model predict porosity and provide a 3-D perspective of porosity distribution, it also provides suggestions as to their extent, development, and quality in the Appleton Field. Therefore, it can be used to directly detect zones of bypassed hydrocarbons and/or design recovery strategies to improve production in this field.

The new geologic model presented in this paper is consistent with carbonate sedimentologic and sequence stratigraphic principles. Preferential growth of reservoir grade facies on paleohighs in this and other basement play fields has been attributed to favorable substrate provided by the basement paleohighs, relative fluctuations of sea level, and carbonate productivity (Kopaska-Merkel *et al.,* 1994; Benson *et al.,* 1996). Relative changes of sea level are controlled by eustatic sea level changes and local tectonics (Sarg, 1988; Mancini *et al.,* 1990; Schlager, 1992; Posamentier and James, 1993). This relative sea level change further controls carbonate productivity, facies distribution and platform growth by affecting intrinsic environmental factors such as salinity, wave energy, water depth, sedimentation rate, and oxygen/nutrient fluctuation (Sarg, 1988; Tucker and Wright, 1990; Leinfelder, 1993a). The overall effect is a change in character of the resulting buildups, manifested by the growth form, fabric, and as well as by later diagenetic alteration of the deposited lithofacies formed during changing sea levels. These changes in character have been described from log and core studies by Benson *et al.,* (1996), Parcell (2000), and Mancini and Parcell (2001), and are the main factors influencing reservoir formation, architecture and observed heterogeneity in this field (Benson, 1988; Mancini, 2002). Compositionally, the buildups of the Appleton Field are mainly thrombolitic (Parcell, 2000; Mancini and Parcell, 2001). Growth of this algal-related microbial morphology is favored by low background sedimentation, low oxygen, and high nutrient concentrations, conditions observed mainly during rising sea levels (Leinfelder, 1996). Each of the thrombolitic growth forms has significantly different physical characteristics (see Table 5) resulting primarily from their depositional fabric; as a consequence, they all have different reservoir quality. The thicker porosity in the forereef environment in this field, as opposed to other reef environments, is credited to the low background sedimentation and low to moderate energy, which enhanced the proliferation of deeper water dendroid thrombolites (Markland, 1992; Leinfelder, 1993a; Parcell, 2000; Mancini and Parcell, 2001). Furthermore, early cementation that is pervasive due to greater water influx, aids against compaction and also influences the reef form (James and Guinsburg, 1979; Tucker and Wright, 1990). In addition, the high accommodation potential of the forereef environment permitted these buildups to attain thicknesses in excess of 30m.

Although facies of the forereef environment are prone to early diagenesis, due to water circulation (Wilson, 1975b; Tucker and Wright, 1990), the effect of diagenesis on these facies cannot be directly determined from our porosity volume. The main effect of diagenesis (early and burial) on the reef crest and forereef facies that has been observed from core studies is dolomitization (Saller and Moore, 1986; Prather, 1992b; Kopaska-Merkel *et al.,* 1994; Haywick *et al.,* 2000). These facies have been pervasively dolomitized, and although this has failed to obliterate original primary shelter and interparticle porosity resulting from facies growth form, the major effects of dolomitization have been to improve facies porosity by stabilizing against burial compaction (because dolomites are more resistant to pressure solution; Mountjoy, *pers. comm.*), creating secondary porosity by dissolution, and increasing permeability by enlarging pore throats. The predominance of the more porous thrombolitic facies on the forereef environment might also explain the strong water drive observed for reservoir at the Appleton Field (Benson et al., 1997). This water drive due to density differences displaces oil from pore spaces to closures provided by paleohighs.

Knowledge such as the controls on thrombolite deposition gained from this study can be applied to other situations where thrombolitic facies are encountered such as; other Smackover carbonate buildups of the basement ridge play, and the Upper Jurassic carbonate buildups of the northern Tethyan ocean (e.g., Atlantic Upper Jurassic carbonate play (Jansa et al, 1989), Portugal (Leinfelder, 1993b; Parcell, 2000), etc.). This understanding of the facies can be used to develop concepts pertaining to thrombolites e.g., what part of the field to expect the different facies, what thrombolitic facies to expect better porosity development given the prevailing basinal conditions, and their probable seismic expression (properties). These concepts can further be extended to include other facies types. Additionally, this study has highlighted the relationships between porosity and the attributes that can be used to predict porosity, i.e., it shows clearly the singular aspect or aspects (continuity, magnitude and thickness of porosity, etc.) of the porous interval that is revealed by each of these predicting attributes.

1.6.5 Case studies to illustrate the applications of multiattribute studies

There are several case studies, besides this one, which go to further perpetuate the usefulness of this method to sedimentary geologist. Images derived from seismic attribute studies have been used to successfully model and reconstruct depositional histories and describe ongoing processes within the sedimentary regime. They have been used to define geometry and distribution of rock/fluid properties in the subsurface (e.g., Raeuchle *et al.*, 1997; Gastaldi *et al*, 1997; Schuelke *et al.,* 1997; Sippel, 1998; Hart and Balch, 2000; Leiphart and Hart, 2001; Carr *et al.,* 2001; Wittick, 2002; Pearson and Hart, *in press*). Attribute studies have also been used to identify and accurately delineate the depositional trends, their features and evolution over time, of complex systems such as compartmentalized carbonates, reefs, multistoried sandbodies, fluvial channels, submarine fans, turbidites, etc. (Bulloch *et al.,* 2001; Skirius *et al.,* 1999; Leu *et al.,* 1999; Sippel, 1998; Raeuchle *et al.,* 1997). Processes that affect subsurface fluid movement, and whose extents are not easily identifiable from log or outcrop data alone, such as, faulting, fracturing and diagenesis have also been characterized by this method (Hart *et al.,* 2002; Matteucci, 2001; Skirius *et al.*, 1999). Furthermore, seismic attribute studies have been used to monitor fluid movement in the subsurface (Lewis, 1997).

CHAPTER 3

1.1 Conclusions and Implications of Study

- Our main objective was to show how multiattribute seismic analysis is used to predict physical properties between well locations. We have demonstrated this approach using a volume-based method on stratigraphically complex carbonate buildups of the Smackover Formation in S.W. Alabama. Given the limited number and extent of wells, hard constraints provided by seismic and log-based mapping of the top and base of the formation were necessary to guide porosity distribution away from boreholes. The integration of various data and analytical methods in the analysis, (e.g., geophysics, geostatistics, geology) gave added confidence in our results. Predicted porosity values from multilinear regression (MLR) and probabilistic neural network (PNN) relationships show that PNN, because of its ability to capture non-linear relationships between rock properties and seismic attributes, best models porosity values observed in logs and cores. Transects, slices, and thickness maps generated from our PNN-derived porosity volume show geologically more meaningful distribution of porosity than MLR away from the borehole.
- Porosity was found to be generally greater and thicker on the forereef flanks than the crest of structure. The presence of paleostructure was yet again revealed to control porosity distribution in the Smackover Formation of this field (*c.f.* Benson *et al.*, 1996). No consistent trends were observed between the development of porosity, porosity thickness, and relief of paleohighs. On a whole, porosity thickness was found to correlate with the steepness of

slope. This is geologically reasonable as this area affords greater accommodation and optimal conditions for reef growth. Our predicted porosity distribution is also consistent with known facies types of the porous interval, their growth forms and reservoir characteristics, derived from studies of core and outcrop analogues (Parcell, 2000; Mancini and Parcell, 2001). Thus, our predicted porosity predictor also fits the known sedimentologic and stratigraphic framework for the Appleton Field (Mancini, 2002). Our results thus strongly suggest that porosity development is controlled mainly by primary depositional facies at the Appleton Field, even though these facies have been pervasively dolomitized.

- Although this is not the only porosity model proposed for the Appleton Field, it is the first to be based on a volume-based seismic attribute study. This volume model offers greater flexibility in data display and for defining vertical and lateral heterogeneity, than the 2-D map obtained from the horizon-based study of Hart and Balch (2000). Because our results are quantitative, they may be employed in calculating the extent of specific intervals for reserve estimation, and/or to plan new recovery strategies to enhance dwindling hydrocarbon production for this field, other Smackover fields of the basement play, and also other Upper Jurassic carbonate buildups of the northern Tethyan ocean (e.g., Outer Continental Shelf of the Gulf of Mexico, North Atlantic east coast, France, Portugal, Saudi Arabia, etc.).
- Conclusively, this study illustrates the adaptiveness of seismic attribute studies to resolve problems involving physical property discrimination in the

subsurface. To this end, it should be useful in other areas of study, other than geophysics and sedimentary geology, where trend delineation of physical properties is essential. From our application of this method, it has been shown that it can be extrapolated to other disciplines of interest it sedimentary geologist. Some suitable areas are:

(1) Engineering – 3-D models produced from seismic attribute studies can be used to plan drilling strategies to maximize fluid production.

(2) Geotechnical – Images obtained can be used to provide insights into geologic processes or conditions that control the occurrence, and quantify mechanics (faults, fractures, and rock or sediment properties) of slope failure.

(3) Hydrogeology – To define porous zones, and predict subsurface properties that control groundwater movement (e.g., rock permeability, porosity, faulting, etc).

(4) Environmental – From physical property predictions it should be possible to define appropriate areas for toxic waste disposal, and characterize contaminant movement in the subsurface so as to define adequate mitigating strategies.

(5) Mining – This method can be used to quantify anomalies created by the presence of minerals or ores e.g., coal.

REFERENCES

AHR, W.M., 1973, The carbonate ramp: An alternative to the shelf model: *Transactions, Gulf Coast Association of Geological Societies*, v. 23, p. 221-225.

ANSTEY, N.A., 1982, Simple Seismics: International Human Resources Development Corporation (IHRDC), 168p.

ASQUITH, G.B., and GIBSON, C.R., 1982, Basic well log analysis for geologists: Tulsa, *AAPG Methods in Exploration Series* no. 3, 216 p.

BÁDENAS, B., and AURELL, M., 2001, Proximal-distal facies relationships and sedimentary processes in a storm dominated carbonate ramp (Kimmeridgian, northwest of the Iberian Ranges, Spain); *Sedimentary Geology*, v.139, issues 3-4, 1 March 2001, p. 319-340.

BANCHS, R.F., and MICHELENA, R.J., 2002, From 3D seismic attributes to pseudo-well log volumes using neural network: Practical considerations: *The Leading Edge,* v.21, no. 10, p. 996-1001.

BARNES, A.E., 1998, The complex seismic trace made simple: *The Leading Edge,* v.17, no. 4, p. 473-476.

BENSON, D.J., 1985, Diagenetic controls on reservoir development and quality, Smackover Formation of southwest Alabama: *Transactions, Gulf Coast Association of Geological Societies*, v. 35, p. 317-326.

BENSON, D.J., 1988, Depositional history of the Smackover Formation in southwest Alabama: *Transactions, Gulf Coast Association of Geological Societies*, v. 38, p. 197-205.

BENSON, D.J., PULTZ, L.M., and BRUNNER, D.D., 1996, The influence of paleotopography, sea level fluctuation, and carbonate productivity on deposition of Smackover and Buckner Formations, Appleton Field, Escambia county, Alabama: *Transactions, Gulf Coast Association of Geological Societies*, v. 46, p. 15-23.

BENSON, D.J., MANCINI, E.A., GROSHONG, R.H., FANG, J.H, PULTZ, L.M., and CARLSON, E.S., 1997, Petroleum Geology of Appleton Field, Escambia County, Alabama: *Transactions, Gulf Coast Association of Geological Societies*, v. 47, p. 35-42.

BOOLER, J., and TUCKER, M.E., 2002, Distribution and geometry of facies and early diagenesis: the key to accommodation space variation and sequence stratigraphy: Upper Cretaceous Congost Carbonate platform, Spanish Pyrenees: *Sedimentary Geology*, v. 146, issues 3-4, 15 January 2002, p. 225-247.

BROWN, A. R., 1996a, Interpretation of Three-Dimensional Seismic Data, 4th ed.: *American Association of Petroleum Geologists Memoir* 42, 424p.

BROWN, A. R., 1996b, Interpreter's corner - Seismic attributes and their classification: *The Leading Edge*, v. 15, no. 10, p 1090.

BULLOCH, T., VONCANNON, J., MEYER, D., LORENZETTI HARVEY, E., SHEFFIELD, T., ZEITLIN, M., and ROBERSON, R., 2001, Examination of a turbidite system using 3-D visualization and multiple seismic attributes, Albacora Field, deepwater Brazil: *71st Ann, Internat. Mgt: Soc. of Expl. Geophys.*, p. 565-568.

CARR, M., COOPER, R., SMITH, M., TANER, M.T., and TAYLOR, G., 2001, The generation of rock and fluid properties volume via the integration of multiple seismic attributes and log data: *First Break.* v. 19, no. 10, p. 567-571.

CHEN, Q., and SIDNEY, S., 1997, Seismic attribute technology for reservoir forecasting and monitoring: *The Leading Edge*, v. 16, no. 5, p 445-456.

CHENSHENG, C., and HISCOTT, R.N., 1999, Statistical analysis of facies clustering in submarine fan turbidite successions: *Journal of Sedimentary Research*, v. 69, no.2, March 1999, p 505-517.

DEDMAN, E.V., LINDSEY, J.P., and SCHRAMM (Jr.), M.W., 1975, Stratigraphic modeling: A step beyond bright spot. *In*: Geophysics II: Tools for Seismic Interpretation, *In* E.A. Beaumont and N.H. Foster, (eds): *Treatise of Petroleum Geology Reprint Series*, no. 13, p. 83-105.

DOVETON, J.H., 1994, Geologic Log Interpretation: *SEPM Short Course* no. 2, 169p.

DUBRULE, O., 1998, Geostatistics in petroleum Geology: *American Association of Petroleum Geologists Continuing Education Course Note Series*, no. 38, 52p.

EBERLI, G.P., ANSELMETTI, F.S., KENTER, J.A.M., MCNEILL, D.F., and MELIM, L.A., 2001, Calibration of seismic sequence stratigraphy with cores and logs, *in:* Subsurface of a Prograding Carbonate Platform Margin, Great Bahama Bank: Results of the drilling project, *SEPM Special Publication, no. 70, p 241-265.*

EBERLI, G.P., ANSELMETTI, F.S., KROON, D., SATO T., and WRIGHT, J.D., 2002, The chronostratigraphic significance of seismic reflections along the Bahamas Transect: *Marine Geology,* v. 185, issues 1-2, 15 June 2002, p. 1-17.

EMBRY, A.F. and KLOVAN, J.E., 1971, A Late Devonian reef tract on northeastern Banks Island, Northwest Territories: *Bulletin Canadian Petroleum Geology*, v. 19, p. 730-781.

ESPOSITO, R.A. and KING, D.T., Jr., 1987, Facies analysis, sea-level history, and platform evolution of the Jurassic Smackover Formation, Conecuh Basin, Escambia County, Alabama: *Transactions, Gulf Coast Association of Geological Societies,* v. 37, p. 335-346.

EWING, T.E., 1997: Synthetic helps spot the target: *American Association of Petroleum Geologists EXPLORER*, July 1997, p. 15-17.

FRANCIS A., 1997, Acoustic impedance inversion pitfalls and some fuzzy analysis: *The Leading Edge,* v.16, no. 3, p 257-278.

GARDNER, G.H.F., GARDNER, L.W., and GREGORY, A.R., 1974, Formation velocity and density - The diagnostic basics for stratigraphic traps: *Geophysics* v. 39, no.6 December 1974.

GASTALDI, C., BIGUENET, J-P., and DePAZZIS, L., 1997, Reservoir characterization from seismic attributes: An example from the Peciko Field (Indonesia): *The Leading Edge*, v. 16, no. 3, p. 263-266.

GENSOUS, B., and TESSON, M., 1996, Sequence stratigraphy, seismic profiles, and cores of Pleistocene deposits on the Rhone continental shelf: *Sedimentary Geology,* v. 105, issues 3-4, September 1996, p. 183-190.

GREGERSEN, U., 1997, The depositional significance of 3-D attributes in the Upper Cenozoic of the Central North Sea: *Petroleum Geoscience*, v. 3, n. 4, p. 291-304.

HAMPSON, G.J., HOWELL, J.A., and FLINK, S.S., 1999, A sedimentological sequence stratigraphic re-interpretation of the Upper Cretaceous Prairie Canyon Member ("Mancos B") and associated strata, Book Cliffs area, Utah, USA: *Journal of Sedimentary Research*, v. 69, no.2, March 1999, p 414-433.

HAMPSON, B., SCHUELKE, J. and QUIREIN, J., 2001, Use of Multi-attribute Transforms to Predict Log Properties from Seismic data: *Geophysics*, v. 66, no. 1 (Jan- Feb, 2001), p. 3-46.

HAYWICK, W.D., BROWN, M.B., and PFEIFFER, L., 2000, Smackover Reservoir diagenesis in the Appleton Field, Escambia County, Alabama (Abstract): *American Association of Petroleum Geologists Bull.,* v. 84, no. 10, p. 1680.

HART, B.S., 1997, 3-D seismic: what makes interpreters tick? *The Leading Edge*, v. 16, no. 8, p. 1114-1119.

HART, B.S., 1999, Geology plays key role in seismic attribute studies: *Oil & Gas Journal,* p. 76- 80.

HART, B.S., 2002, Validating seismic attribute studies: Beyond statistics: *The Leading Edge*, 21, no. 10, p. 1016-1021.

HART, B.S., and BALCH, R.S., 2000, Approaches to defining reservoir physical properties from 3-D seismic attributes with limited well control: An example from the Jurassic Smackover Formation, Alabama: *Geophysics*, v. 65, no. 2, p. 368-376.

HART, B.S, PEARSON R., and RAWLING, G.C., 2002, 3-D seismic horizon-based approaches to fracture-swarm sweet spot definition in tight gas reservoirs: *The Leading Edge*, v. 21, no. 1, p. 28-35.

HILTERMAN, F.J., 2001, Seismic amplitude interpretation: 2001 Distinguished Instructor Short Course, *Distinguished Instructor Short Course Series*, no. 4, SEG and EAGE, 9 sections.

HIRSCHE, K., PORTER-HIRSCHE, J., MEWHORT, L., and DAVIS, R., 1997, The use and abuse of Geostatistics: *The Leading Edge*, v. 16, no. 3, p. 253-260.

HIRSCHE, K., BOERNER, S., KALKOMEY, C., and GASTALDI, C., 1998, Avoiding pitfalls in geostatistical reservoir characterization: A survival guide: *The Leading Edge*, v. 17, no. 4, p. 493-504.

JAMES, N.P., 1984, Reefs: In, Facies models. R.G. Walker (ed.), *Geoscience Canada*, p. 229-244.

JAMES, N.P., 1989, Structure and stratigraphy of modern and ancient reefs, *In:* P.A. Scholle, N.P. James, and J.F. Read (eds). Carbonate Sedimentology and Petrology, *American Geophysical Union (AGU) Short Course in Geology*, v. 4, p. 1-40.

JAMES, N.P. and GINSBURG R.N., 1979, The seaward margin of Belize barrier and atoll reefs: *International Association of sedimentologists, Special Publ.*,no. 3, 191p.

JAMES, N.P., and. MACINTYRE, I.G., 1985, Carbonate depositional environments, modern and ancient. Part 1- Reefs, zonation, depositional facies and diagenesis: *Quart. J. Colorado Sch. Mines* 80, 70.

JANSA, L.F., PRATT, B.R., and DROMART, G., 1989, Deepwater thrombolite mounds from Upper Jurassic of Offshore Nova Scotia, *In*: Reefs, Canada and Adjacent Areas. H.H. Geldsetzer, N.P. James, and G.E. Febbutt (eds.): *Canadian Society of Petroleum Geologists Memoir*, n. 13, 1989, p. 725-735.

KALKOMEY, C.T., 1997, Potential risks when using seismic attributes as predictors of reservoir properties: *The Leading Edge*, v. 16, no. 3, p. 247-251.

KENTER, J.A.M., ANSELMETTI, F.S., KRAMER, P.H., WESTPHAL, H., and VANDAME, M.G.M., 2002, Acoustic properties of "young' carbonate rocks, ODP leg 166 and borehole clino and unda, western Great Bahama bank: *Journal of Sedimentary Research*, v. 72, no.1, January 2002.

KING, D.T., Jr., 1994, Smackover Sedimentology in Alabama's Conecuh and Manila Basins. Retrieved July 3, 2002, from, Auburn University Web site: http://www.auburn.edu/~kingdat/smackover.html.

KOPASKA-MERKEL, D.C., MANN, S.D., and SCHMOKER, J.W., 1994, Controls on reservoir development in a shelf carbonate: Upper Jurassic Smackover Formation of Alabama: *American Association of Petroleum Geologists Bull.*, v. 78, no. 6 (June 1994), p. 938-959.

LAVERGNE, M., AND WILLM, C., 1977, Inversion of Seismograms and Pseudo velocity logs, *In* E.A. Beaumont and N.H. Foster (eds), Geophysics II-Tools for Seismic Interpretation: *Treatise of Petroleum Geology Reprint Series*, no. 13, p. 25-44.

LEINFELDER R.R., 1993a, Upper Jurassic reef types and controlling factors: A preliminary report: *Profil 5*, p. 1-45.

LEINFELDER R.R., 1993b, A sequence stratigraphic approach to the Upper Jurassic mixed carbonate-siliciclastic succession of the central Lusitanian Basin, Portugal: *Profil 5*, p. 119-140.

LEINFELDER, R.R., WERNER, W., NOSE, M., SCHMID, D.U., KRAUTTER, M., LATERNSER, R., TAKACS, M., and HARTMENN, D., 1996, Paleoecology, Growth Parameters and Dynamics of Coral, Sponge and Microbolites Reefs from the Late Jurassic: In:. J. Reitner, F. Neuweiler, and F. Gunkel (eds.): Global and Regional Controls on Biogenic Sedimentation. I. Reef Evolution. *Research Reports. Göttinger Arb. Geol. Paläontl.*, Sb2, p., 227-248, Göttingen.

LEIPHART, D.J., and HART, B.S., 2001, Comparison of linear regression and probabilistic neural network to predict porosity from 3-D seismic attributes in Lower Brushy Canyon channeled sandstones, southeast New Mexico: *Geophysics,* v. 66, n. 5 (September-October 2001), p. 1349-1358.

LEU L-K, McPHERSON, J.G., and KAN, Y., 1999, Integration of 3-D seismic attributes with core and wireline log data for detailed modeling of Cretaceous fluvial reservoirs: *The Leading Edge*, v.18, no. 6, p. 730-738.

LEWIS, C., 1997, Seismic attributes for reservoir monitoring: A feasibility study using forward modeling: *The Leading Edge*, v.16, no. 5, p. 459-469.

LINER, C.L., 1999, Elements of 3-D Interpretation: PennWell Publishers, 438p.

LIU, Z., and LIU, J., 1998, Seismic-controlled non-linear extrapolation of well parameters using neural networks: *Geophysics*, v. 63, no. 6 (November-December 1998), p. 2035-2041.

MANCINI, E.A. 2002, Integrated geologic-engineering model for reef and carbonate shoal reservoirs associated with paleohighs: upper Jurassic Smackover Formation, NE Gulf of Mexico: Annual Report Year 2. Online Report retrieved Oct. 3, 2002, from Petrl. Techn. Trans. Council Web site: http://egrpttc.geo.ua.edu/reports/geo_eng_model2/title.html

MANCINI, E.A., and BENSON, D.J., 1980, Regional stratigraphy of Upper Jurassic Smackover carbonates of southwest Alabama: *Transactions, Gulf Coast Association of Geological Societies*, v. 30, p. 151-165.

MANCINI, E.A., and BENSON, D.J., 1998, Upper Jurassic Smackover carbonate reservoir, Appleton Field, Escambia County, Alabama: *In* J.L. Allen and T. S. Brown (eds.), 3-D case history of Gulf of Mexico, p. 1-14.

MANCINI, E.A. and PARCELL, W.C., 2001, Outcrop analogues for reservoir characterization and modeling of Smackover microbial reefs in the northeastern Gulf of Mexico: *Transactions, Gulf Coast Association of Geological Societies*, v. 51, p. 207-218.

MANCINI, E.A., TEW, B.H., and MINK, R.M., 1990, Jurassic sequence stratigraphy in the Mississippi interior salt basin: *Gulf Coast Association of Geological Societies Transactions*, v. 40, p. 521- 529.

MANCINI, E.A., HART, B.S., CHEN, H., BALCH, R.S., PARCELL, W.C., WANG, W., and PANETTA, B.J., 1999, Integrated geological, geophysical, and computer approach for predicting reef lithofacies and reservoirs: Upper Jurassic Smackover Formation, Appleton Field, Alabama. *GCSSEPM Foundation: 19th Annual Research Conference*: Advanced Reservoir Characterization. December 5-8, 1999, p. 235-247.

MANCINI, E.A., BENSON, D.J., HART, B.S., BALCH, R.S, PARCELL, W.C, and PANETTA, B.J, 2000, Appleton Field case study (eastern Gulf coastal plain): Field development model for Upper Jurassic microbial reef reservoirs associated with paleotopographic basement structures: *American Association of Petroleum Geologists Bull.*, v. 84, no. 11 (November), p.1699-1717.

MARKLAND, L.A., 1992, Depositional history of the Smackover Formation, Appleton Field, Escambia county, Alabama: Master's thesis, University of Alabama, Tuscaloosa, Alabama, 145p.

MATTEUCCI, G., CASSIANI, D., and MOHAMMED, A., 2001, Using seismic attributes and forward modeling to characterize producibility in a fractured carbonate reservoir: *71st Ann, Internat. Mgt: Soc. of Expl. Geophys.*, p. 536-539.

MIALL, A.D., 1995, Wither stratigraphy? *Sedimentary Geology*, v. 100, issues 1-4, December 1995, p. 5-20.

MICHELENA, R.J., GONZÁLEZ, S.M., and CAPELLO De P., 1998, Similarity analysis: A new tool to summarize seismic attributes confirmation: *The Leading Edge*, v. 17, no. 4, p. 545-548.

MULHOLLAND, J.W. (1998) Sequence Stratigraphy: Basic elements, concepts and terminology. *The Leading Edge:* v. 17, no. 1, p 37-40.

MUKERJI, T., JØRSTAD, A., MAVKO, G., and. GRANLI, J.R., 1998, Applying statistical rock physics and seismic inversion to map lithofacies and pore fluid probabilities in a North Sea reservoir: *68th Ann. Internat. Mgt. Soc. of Expl. Geophys.,* p. 894-897.

MUKERJI, T., AVSETH, P., MAVKO, G., TAKAHASHI, I., and GOREE, W.S., 2001, Statistical rock physics: Combining rock physics, information theory, and Geostatistics to reduce uncertainty in seismic reservoir characterization: *The Leading Edge*, v., 20, no. 3, p. 313-319.

NEATHERY, T.L., and THOMAS, W.A., 1975, Pre-Mesozoic basement rocks of Alabama coastal plain: *Transactions, Gulf Coast Association of Geological Societies*, v. 25, p. 86-99.

NEIDELL, S. and POGGIAGLIOLMI, E., 1977, Stratigraphic modeling and interpretation-Geophysical principles and techniques, *In* E.A. Beaumont and N.H. Foster (eds), Geophysics II-Tools for Seismic Interpretation: *Treatise of Petroleum Geology Reprint Series*, no. 13, p. 131-416.

NISSEN, S. A., COMBES, J.M., and NEKUT, A.G., 1999, Acquisition, processing, and analysis of shallow, high-resolution seismic data from the outer continental shelf and upper slope, Offshore Louisiana: *Journal of Sedimentary Research*, v. 69, no.2, March 1999, p 300-316.

PARCELL, W.C., 2000, Controls on the development and distribution of reefs and carbonate facies in the Late Jurassic (Oxfordian) of the eastern Gulf Coast, United States and eastern Paris Basin, France (PhD Thesis): University of Alabama. 226p.

PARTYKA, G., 2000, Seismic attribute sensitivity to energy, bandwidth, phase, and thickness: *70th Ann. Internat. Mgt. Soc. of Expl. Geophys.,* p. 2405-2408.

PEARSON, R.A., and HART, B.S., *in press*, 3-D seismic attributes help define controls on reservoir development: case study from the Red River Formation, Williston Basin. *In:* G.P. Eberli, J.L. Masaferro, and J.F. Sarg (eds.), Seismic Imaging of Carbonate Reservoirs and Systems: *American Association of Petroleum Geologists Memoir.*

POSAMENTIER, H. and JAMES, D.P., 1993, An overview of sequence stratigraphic concepts: Uses and abuses: *Spec. Publs. Int. Ass. Sediment.* , v. 18, p. 3-18.

PRATHER, B.E., 1992a, Evolution of a late Jurassic carbonate/ evaporite platform, Conecuh Embayment, Northeastern Gulf Coast, U.S.A: *American Association of Petroleum Geologists Bull.,* v. 76, no. 2, p. 164-190.

PRATHER, B.E., 1992b, Origin of dolostone reservoir rocks, Smackover Formation (Oxfordian), Northeastern Gulf Coast, U.S.A: *American Association of Petroleum Geologists Bull.,* v. 76, no. 2, p. 133-163.

PRATT, B.R., 1995, The origin, biota, and evolution of deep-water mud-mounds: *Spec. Publs. Int. Ass. Sediment.* , v. 23, p. 49-123.

PRATT, B.R., JAMES, N.P., and BOURQUE, P., 1992, Reefs and Mounds: *In* Walker, R. G and N. P. James (eds.), Facies Models: Response to Sea Level Change: GEOTEXT**1**, p. 323-348.

RAEUCHLE, S.K., HAMILTON, D.S., AND UZCÁTEGUI, M., 1997, Case history: Integrating 3-D seismic mapping and seismic attribute analysis with genetic stratigraphy: Implications for infield reserve growth and field extension, Budare Field, Venezuela: *Geophysics*, v. 62, no. 5 (September-October 1997), p. 1510-1523.

READ, J.F., 1985, Carbonate platform facies models: *American Association of Petroleum Geologists Bull.,* v. 69, p. 1-21.

READING, H.G., 1978, Sedimentary Environments and Facies: New York, *Elsevier*, 557p.

REYMOND, B.A., and STAMPFLI, G., 1994, Sequence stratigraphic interpretations of 3-D seismic data offshore Louisiana - a case study: *First Break.* v. 12, no. 9, p. 453-462.

RICHARDS, M., BOWMAN, M., and READING, H., 1998, Submarine-fan systems I: characterization and stratigraphic prediction: *Marine and Petroleum Geology,* v. 15, issue 7, 15 November 1998, p. 689-717.

ROBERTSON, J.D. and NOGAMI, H.H., 1984, Complex seismic trace analysis of thin beds: *Geophysics*, v. 49, no. 4 (April 1984), p. 344-352.

RUSSELL, B., HAMPSON, D., SCHUELKE, J., and QUIREIN, J., 1997, Multi-attribute Seismic Analysis: *The Leading Edge*, v. 16, no. 10, p. 1439-1443.

SALLER, A.H., and MOORE B.R., 1986, Dolomitization in the Smackover Formation, Escambia County, Alabama: *Transactions, Gulf Coast Association of Geological Societies,* v. 36, p. 275-282.

SALVADOR, A., 1991, Triassic-Jurassic: *In* A.R. Palmer and J.O. Wheeler (eds.), The Geology of North America Volume J: The Gulf of Mexico Basin: *The Geological Survey of America DNAG*, p.131-180.

SARG, J.F., 1988, Carbonate sequence stratigraphy: *In* C.K. Wilgus, B.S. Hastings, C.G.St.C. Kendall, H.W. Posamentier, C.A. Ross, and J.C. Van Wagoner (eds.), Sea-Level Changes: An Integrated Approach: *SEPM Special Publication*, no. 42, p.155-182.

SCHLAGER, W., 1992, Sedimentology and sequence stratigraphy of reefs and carbonate platoforms: *American Association of Petroleum Geologists Continuing Education Course Note Series*, no. 34, 71p.

SCHLAGER, W., 1999, Sequence stratigraphy of carbonate rocks: *The Leading Edge*, v.18, no. 8, p. 901-907.

SCHUELKE, J.S., QUIREN, J.A., SAG, J.F., ALTANY, D.A., and HUNT, P.E., 1997, Reservoir architecture and porosity distribution, Pegasus Field, West Texas – an integrated sequence stratigraphic – seismic attribute study using neural networks: *67th Ann. Internat. Mgt. Soc. of Expl. Geophys.*, p. 668-671.

SCHULTZ, P.S, RONEN, S., HATTORI, M., and CORBETT, C., 1994, Seismic-guided estimation of log properties: Part 1: A data-driven interpretation methodology: *The Leading Edge*, v. 13, no. 5, p. 305-315.

SCHULTZ, P.S, RONEN, S., HATTORI, M., and CORBETT, C., 1994, Seismic-guided estimation of log properties: Part 2: Using artificial neural networks for nonlinear attribute calibration: *The Leading Edge*, v. 13, no. 6, p. 674-678.

SIPPEL, M.A., 1998, Exploitation of reservoir in the Red River Formation, southern Williston Basin, *in*, R.M. Slatt (ed.), Compartmentalized Reservoirs in Rocky Mountain Basins, *Proceedings 1998 Rocky Mountain Association of Geologists Symposium*, p. 151-170.

SKIRIUS, C., NISSEN, S., HASKELL, N., MARFURT, K., HADLEY, S., TERNES, D., MICHEL, K., REGLAR, I., D'AMICO, D., DELIENCOURT, F., ROMERO, T., D'ANGELO, R., and BROWN, B., 1999, 3-D seismic attributes applied to carbonates: *The Leading Edge*, v.18, no. 3, p. 384-393.

TANER, M.T., Sept. 2000, Attributes Revisited: Retrieved May 16, 2002 from http://www.rocksolidimages.com/pdf/attrib_revisited.htm.

TANER, M.T., Mar. 1997, Seismic trace attributes and their projected use in prediction of rock properties and seismic facies: *Rock Solid Images*, retrieved May 16, 2002 from http://www.rocksolid images.com/tech_pub_1.htm.

TANER, M.T., KOEHLER, F., and SHERIFF, R.E., 1979, Complex seismic trace analysis: *Geophysics*, v. 44, no. 6 (June 1979), p. 1041-1063.

TEW, B.H., MINK, R.M., MANCINI, E.A., MANN, S.D., and KOPASKA-MERKEL, D.C., 1993, Geologic framework of the Jurassic (Oxfordian) Smackover Formation, Alabama and panhandle Florida coastal waters area and adjacent federal waters area: *Transactions, Gulf Coast Association of Geological Societies*, v. 43, p. 399-411.

TINKER, S.W., 1998, Shelf-to-basin facies distributions and sequence stratigraphy of a steep-rimmed carbonate margin: Capitan depositional system, McKittrick Canyon, New Mexico and Texas: *Journal of Sedimentary Research*, v. 68, no. 6, November 1998, p. 1146-1174.

TUCKER, M.E., and WRIGHT, V.P., 1990, Carbonate Sedimentology: Oxford, Blackwell Scientific Publications. 482 p.

VAIL, P.R., HARDENBOL, J., and TODD, R.G., 1984, Jurassic unconformities, chronostratigraphy, and sea-level changes from seismic stratigraphy and biostratigraphy: *In* J.S. Schlee (ed.) International unconformities and hydrocarbon accumulations: *American Association of Petroleum Geologists Memoir* 33, p. 129-144.

VAN WAGONER, J.C., POSAMENTIER, H.W., MITCHUM, R.M., VAIL, P.R., SARG, J.F., LOUTIT, T.S., and HARDENBOL, J., 1988, An overview of the fundamentals of sequence stratigraphy and key definition: *In* C.K. Wilgus, B.S. Hastings, C.G.St.C. Kendall, H.W. Posamentier, C.A. Ross, and J.C. Van Wagoner (eds.), Sea-Level Changes: An Integrated Approach: *SEPM Special Publication*, no. 42, p.39-45.

VECSEI, A., and SANDERS, D.G.K., 1999, Facies analysis and sequence stratigraphy of a Miocene warm-temperature carbonate ramp, Montagna della Maiella, Italy: *Sedimentary Geology*, v. 123, issues 1-2, January 1999, p. 103-127.

WADE, W.J., and MOORE, C.H., 1993, Sequence stratigraphy of Middle and Upper Jurassic strata of southwestern Alabama*: American Association of Petroleum Geologists Bulletin (abs.)*, v. 77, no. 9, p. 1602.

WALKER, R.G., 1992, Facies, facies models and modern stratigraphic concepts: *In* Walker, R.G and N.P. James (eds.), Facies Models: Response to Sea Level Change, *GEOTEXT**1***, p. 1-14.

WANG, Z., 1997, Seismic Properties of Carbonate Rocks: *In* Ibrahim Palaz and Kurt J. Marfurt, eds., Carbonate Seismology: *Geophysical Development Series*, no. 6 (*Soc. of Expl. Geophys.*), p. 29- 52.

WHALEN, M.T., DAY, J., EBERLI, G.P., and HOMEWOOD, P.W., 2002, Microbial carbonates as indicators of environmental change and biotic crises in carbonate systems: examples from Late Devonian, Alberta basin Canada: *Palaeogeography, Palaeoclimatology, Palaeoecology,* v. 181, issues 1-3, 20 June 2002, p. 127-151.

WILSON, G.V., 1975a, Early differential subsidence and configuration of the northern Gulf Coast basin in southwest Alabama and Northwest Florida: *Transactions, Gulf Coast Association of Geological societies*, v. 25, p. 196-206.

WILSON, J.L., 1975b, Carbonate Facies in Geologic History: Berlin Springer-Verlag, 471p.

WITTICK, T., 2002, Subsurface data integration – multiple attributes improve accuracy – multiple seismic attributes improve the estimation of reservoir thickness: *Hart's E & P.*, v. 75, no. 6, p. 57-59.

YILMAZ, Ö, 2001, Seismic data analysis: *In*, Cooper, M.R. and Doherty S. M. (eds.), Seismic Data Analysis: Processing, inversion, and interpretation of seismic data. *Soc. of Expl. Geophys.*, Tulsa, Ok, p. 1001-2027.

Appendix A

LOG CURVES

Table A1: Showing suite of log curves used (original and estimated), and their frequency

Well Name	Permit#	X	Y	KB	TD	DT	GR	CALI	SP	RHOB	ILM	ILD	ResS	ResD	RWA	RFOC	SFLU	NPHI	DPHI
McMilan 2-15ST	6247 B	615261	453791	267.82	13156	x	x	0	x	x	x	x	x	0	x	0	0	0	0
McMilan 2-15	6247	615261	453791	267.82	13130	x	x	x	x	x	x	x	0	0	x	x	0	x	x
McMillan 2-14#1	3854	613902	454234	242	13114	x	x	0	x	x	x	x	0	0	x	0	x	0	E-RHOB
McMillan 2-14ST	3854B	613902	454234	242	13100	0	0	0	0	0	0	0	0	0	0	0	0	x	x
McMillan D	4991	619560	450473	246.7	13246	x	x	0	x	x	x	x	0	0	x	0	x	0	0
McMillan Trust	5089	621889	452748	258	13108	x	x	0	0	E-DT	0	0	0	0	0	0	0	x	x
McMillan 2-6#1	5138	613689	456814	245	13240	x	x	0	0	E-DT	0	0	0	0	0	0	0	x	x
Graham 2-16	4835 B	614861	454591	244	13286	ITT	x	0	x	0	x	x	0	0	x	x	0	x	x
McMillan	5346	614239	452788	241	13090	E-PHID	x	0	0	E-PHID	0	0	0	0	0	0	0	x	x
McMillan 11-1#2	3986	616261	452791	254	13100	x	x	x	x	E-DT	x	x	0	0	x	0	x	x	x
Blair D	5224	615774	450148	244.8	13184	x	x	x	x	E-DT	0	0	0	0	0	0	0	x	x
McMillan 12-4#3	4633 B	618761	452691	245.31	13170	x	x	x	0	E-DT	0	x	0	0	0	0	0	x	x

x = curve
0 = no curve
E- = estimated from

Table A2: Formation tops/stratigraphic units and their characteristic log response at the Appleton field

Formation/ Stratigraphic unit	**Gamma Ray (GR)**	**Resistivity (ILD)**	**Sonic Log (DT)**	**Velocity (1/DT)**	**Neutron Porosity (NPHI)**	**Density Porosity (DPHI)**
Buckner	Decrease	Sharp Increase	Sharp Decrease	Sharp Increase	Decrease	Decrease
Non-Porous Smackover	Increase	Sharp Decrease	Slight Increase	Decrease	Increase	Increase
Porous Smackover	Slight Decrease	Slight Increase	Slight Increase	Decrease	Separation of 12 units for dolomite and no separation for limestone	
Norphlet	Sharp Decrease	Increase	Increase	Decrease	Higher DPHI, hence crossover	
Basement	Sharp Increase	Sharp Increase	Sharp Decrease	Sharp Increase	Neutron / Density Cross-over	

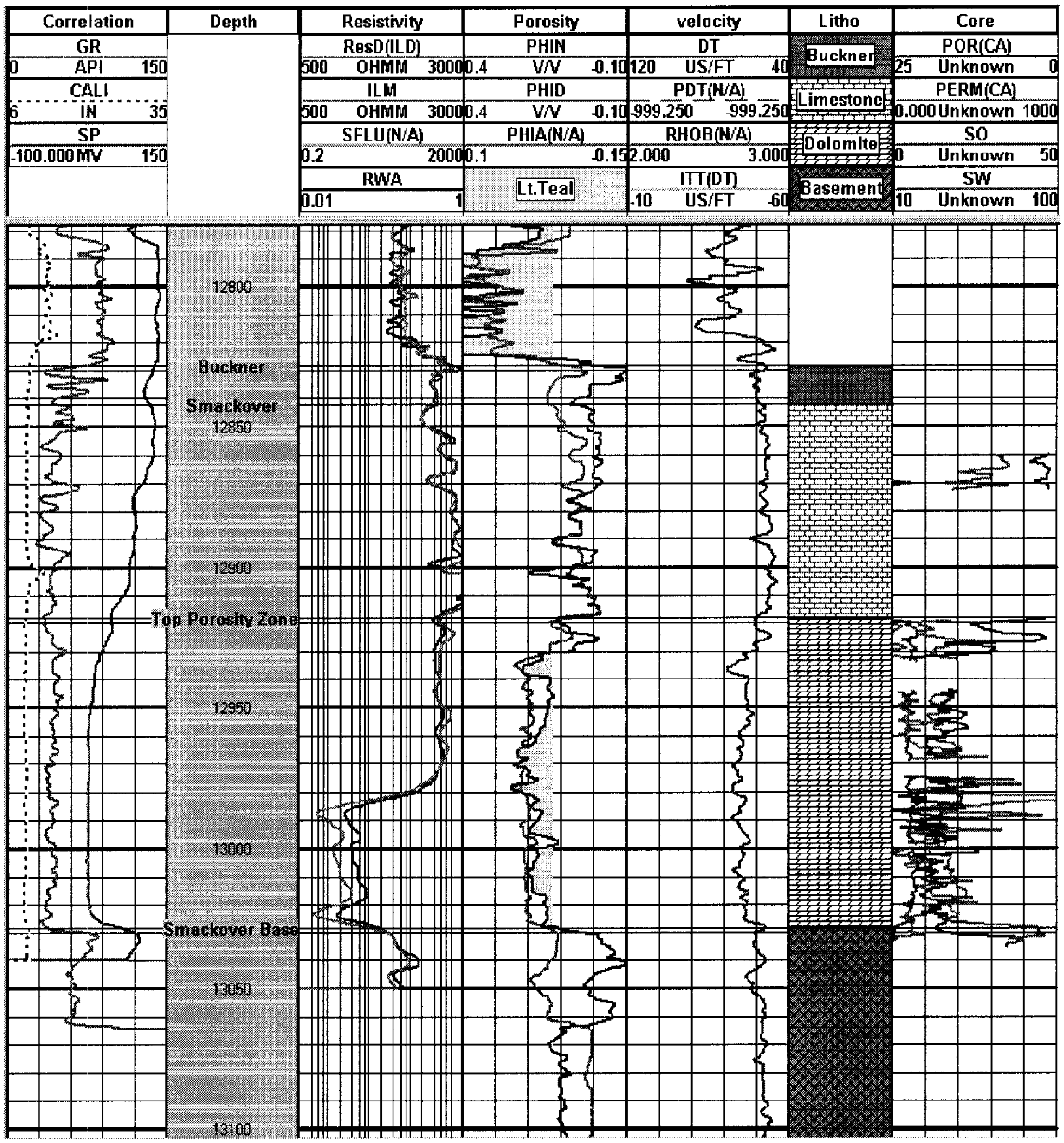

Figure A1: Sample of available logs used for analysis. Note character of response at top of stratigraphic units

Table A3: Characteristics of Smackover lithofacies in the Appleton Field area (Benson *et al*, 1996; Mancini *et al.*, 2000)

Lithofacies	Lithology	Allochems	Pore Types	Porosity	Permeability
Carbonate mudstone	Dolostone and anhydritic	None	Intercrystalline	Low (1.2 to 2.5%)	Low (<0.01 md)
Peloidal wackestone	Dolostone to calcareous	Peloids, ooids, intraclasts	Intercrystalline, moldic	Low to moderate (2.6 to	Low (<0.01 to 0.11 md)
Peloidal packstone	Dolomitic limestone	Peloids, ooids, oncoids,	Interparticulate, moldic,	Low to moderate (1.1 to	Low to moderate (<0.01 to
Peloidal/oncoidal packstone	Dolostone to calcareous	Peloids, oncoids, intraclasts	Interparticulate	Low (1.2 to 6.1%)	Low (<0.01 md)
Peloidal/oolitic packstone	Dolostone	Peloids, ooids, skeletal	Moldic, intercrystalline,	Low (1.3 to 4.5%)	Low (<0.01 md)
Peloidal grainstone	Calcareous dolostone	Peloids, oncoids, algal	Interparticulate, fenestral,	Low to high (1.0 to 19.9%)	Low to high (<0.01 to 722
Oncoidal grainstone	Calcareous dolostone to	Oncoids, peloids, intraclasts	Interparticulate,	Low to moderate (1.4 to	Low to high (<0.01 to 8.27
Oolitic grainstone	Dolostone to limestone	Ooids, peloids, oncoids,	Interparticulate, moldic,	Moderate to high (8.3 to	Moderate to high (3.09 to 406
Oncoidal/peloidal/oolitic	Dolostone to calcareous	Oncoids, peloids, ooids, algal	Interparticulate, moldic,	Low to high (1.9 to 19%)	Low to high (<0.01 to 219
Algal grainstone	Dolomitic limestone to	Algal grains, oncoids,	Interparticulate, moldic,	Low to high (1.7 to 23.1%)	Low to high (<0.01 to 63 md)
Microbial boundstone	Dolostone	Algae, intraclasts, oncoids,	Shelter, vuggy,	High (11.0 to 29.0%)	High (8.13 to 4106 md)
Microbial bindstone	Dolostone	Algae, peloids, ooids	Shelter, vuggy, fenestral,	High (11.9 to 20.7%)	High (11 to 1545 md)
Algal laminite	Dolostone to dolomitic	Algae, peloids, oncoids,	Interparticulate,	Low (1.1 to 7.0%)	Low (<0.01 md)
Anhydrite	Anhydrite	None	None	Low (<1.0%)	Low (<0.01 md)

APPENDIX B

Time-depth Conversion

Synthetic seismograms are a widely useful way to calibrate seismic time to log depth (Fig. B1). The necessary calibration between arrival time of the seismic data and depth of logs are established using velocity information from near-by log measurements (sonic logs). Well-seismic tie allows for depth-to-time conversion of logs, thus allowing for display of log data on the seismic data (means of integrating the two datasets). Visual matching of seismic and the synthetic can reliably identify the target reflector (Ewing, 1997). The synthetic also shows how the detailed waveform and amplitude of the reflectors near the target are generated from the lithology. On the minus side, synthetics do not give absolute time-depth equivalence; and the synthetic may be a poor match for the real data. Synthetics may be used with a velocity survey, if present, to give best possible time-depth values and information on reflection character To ensure accurate time-depth conversion, the sonic log has to be edited for unrealistic values (spikes, etc, resulting from washouts, vugs).

All the wells required a static time shift in Hampson Russell's STRATA package (software used to calibrate well data to seismic data) due to incorrect velocity information, which might be as a result of the limited extent of the logs. On applying the single checkshot survey available, some of the wells were overcorrected while others were undercorrected (i.e., depth to targeted formation from logs did not correspond to expected time on the seismic data). Thus the checkshot survey was used only for the well for which it was collected. A static shift was applied to correct this. The Buckner/Smackover top, because of its marked continuity observed from synthetic seismograms was used as tie point.

Format for loading data

Information needed for depth-time conversion were loaded in following order:

(i) Deviation surveys; containing the N-S, E-W offsets for deviated wells.

(ii) Wells (with X- and Y-coordinates, units and KB depths) and log curves, density and sonic (Table A1)

(iii) Checkshot survey

(iv) Seismic data

(v) Horizon picks (Formation tops)

On loading the logs, the software automatically converts the travel time from sonic logs to velocity using the equation:

$$v = d/(\Delta t/2) \qquad \text{B1}$$

Where: v = velocity (ft/s), d = depth (ft)

The velocity is multiplied by density log to give an acoustic impedance (AI) log.

$$AI = \rho v \qquad \text{B2}$$

$$RC = (\rho_2 v_2 - \rho_1 v_1)/(\rho_2 v_2 + \rho_1 v_1) \qquad \text{B3}$$

$$r(t) = (\rho_2 v_2(t+1) - \rho_1 v_1(t))/(\rho_2 v_2 (t+1) + \rho_1 v_1 (t)) \qquad \text{B4}$$

Where: ρ = density, v = velocity, AI = acoustic impedance, RC = reflection coefficient, r(t) = reflectivity

The reflectivity series (a time series of reflection coefficients (RC)) was subsequently calculated from these logs, by placing each RC at its appropriate time.

Wavelet Extraction

The next step involved wavelet extraction (Russell et al., 1997). Two types of wavelet extraction were carried out:

Statistical wavelet extraction:

Here, the amplitude spectrum was estimated from the seismic data by autocorrelation. The phase is assumed known and to be zero.

Several parameters were necessary for proper wavelet extraction:

(i) Time window - the window chosen contained the interval of interest. A 700ms window was used (2100 - 2800ms). This time window was dependent on the wavelength, and had to be about twice the wavelength.

(ii) Wavelet length – this was calculated based on relationship given in Eq. C2 (see Appendix C). A wavelength of 250ms and a taper of 50ms (less than a quarter the wavelet length) were used, giving a total length of approximately 350ms.

(iii) Phase of wavelet was set at 0^{o} and constant, on assumption that the embedded wavelet might have been processed before stacking (Dedman et al., 1975). This though wasn't true at all well location. The phase of the extracted statistical wavelet was adjusted until the log synthetic matches the seismic reflection at the given reflector.

The individual wavelet from each trace along the wellbore (for deviated wells), specified in the number of inlines and crosslines, was summed to produce the final wavelet that was convolved onto the reflectivity series to create a synthetic seismogram (same as for model).

The aim of a preliminary well-seismic tie was at remove static time shifts, which without use of a checkshot or VSP (vertical seismic profile) survey was substantial (~1000ms at some wells). The well tie was assessed by visual inspection, cross correlation plots, and correlation coefficients between log-derived synthetic trace and real seismic trace at well location (Table B1, Fig. B1).

Semi-deterministic wavelet extraction:

This mode of extraction involved using both well and seismic data. It is carried out after preliminary ties with the statistical wavelet to improve ties with minor inter-reservoir events. Due to the limited extent of some velocity logs (<100ms), and the poor correlation obtained after using the statistical wavelet to tie the seismic data, this was not possible and so not extracted for all logs. Some ties were bad due to the poor quality of the dataset, especially to the southern limits of the Appleton Field.

Procedure adopted for well – seismic ties

(i) Use a statistical wavelet extraction to determine a preliminary wavelet, with the assumption that the approximate phase of the wavelet is known.Stretch/squeeze the logs to tie well synthetic response at prominent formation tops (i.e., tops that can clearly mapped due to their large acoustic impedance contrast resulting from marked changes in lithology, e.g. Buckner) to the seismic data.

(iii) Extract a deterministic wavelet using the well logs.

(iv) Possibly repeat steps (i) and (ii).

Table B1: Well – seismic tie correlation window and coefficient

Permit #	Correlation Window (ms)	Correlation Coefficient
4991	2478 - 2542	0.72
5089	2430 - 2538	0.77
5138	2424 - 2536	0.57
5224	2478 - 2538	0.74
5346	2486 – 2532	0.91
4835-B	2410 - 2546	0.59
3854	2482 - 2530	0.92
6247	2436 - 2512	0.81
6247-B	2436 - 2506	0.87
3986	2372 - 2522	0.86
4633-B	2442 - 2518	0.72

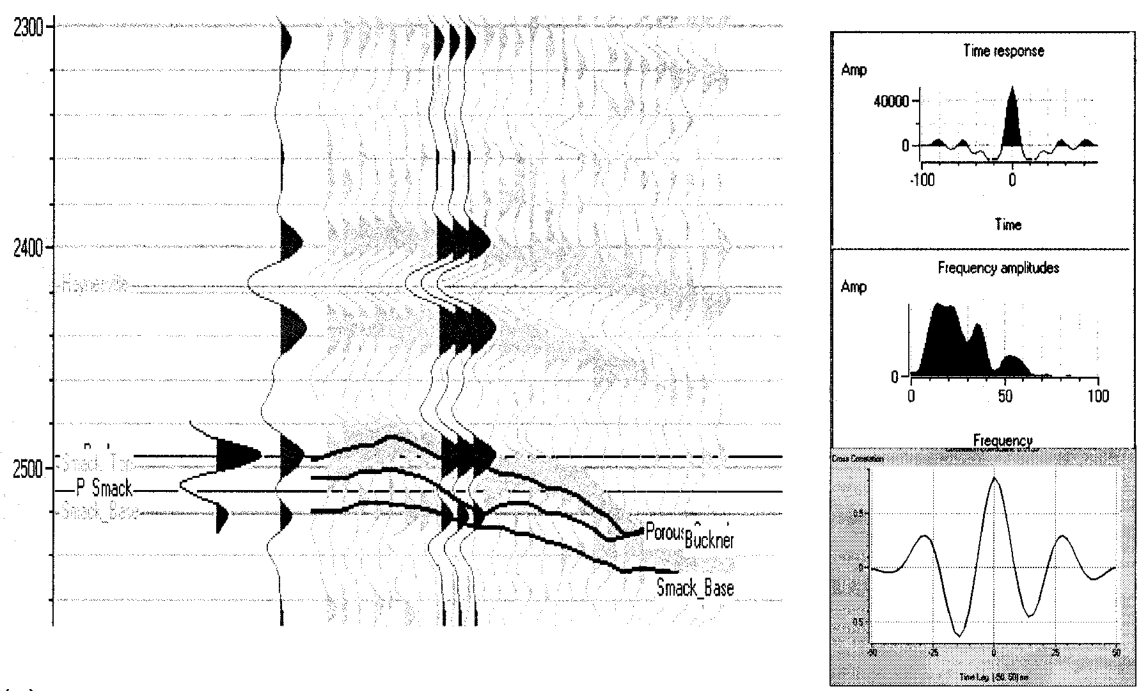

(a)

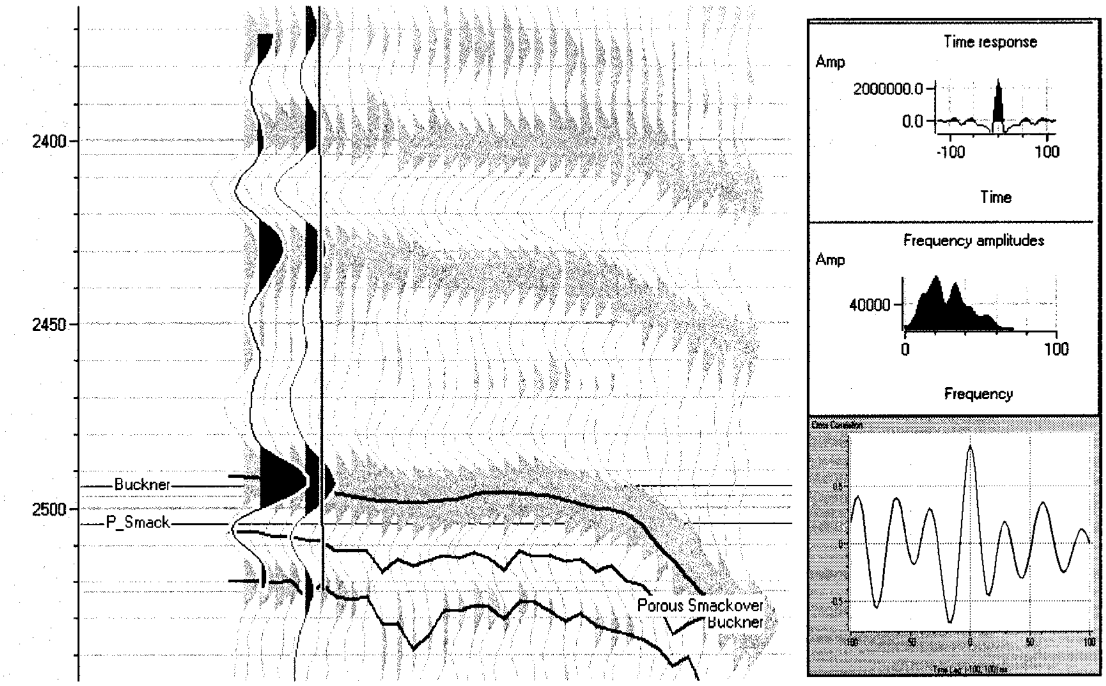

(b)

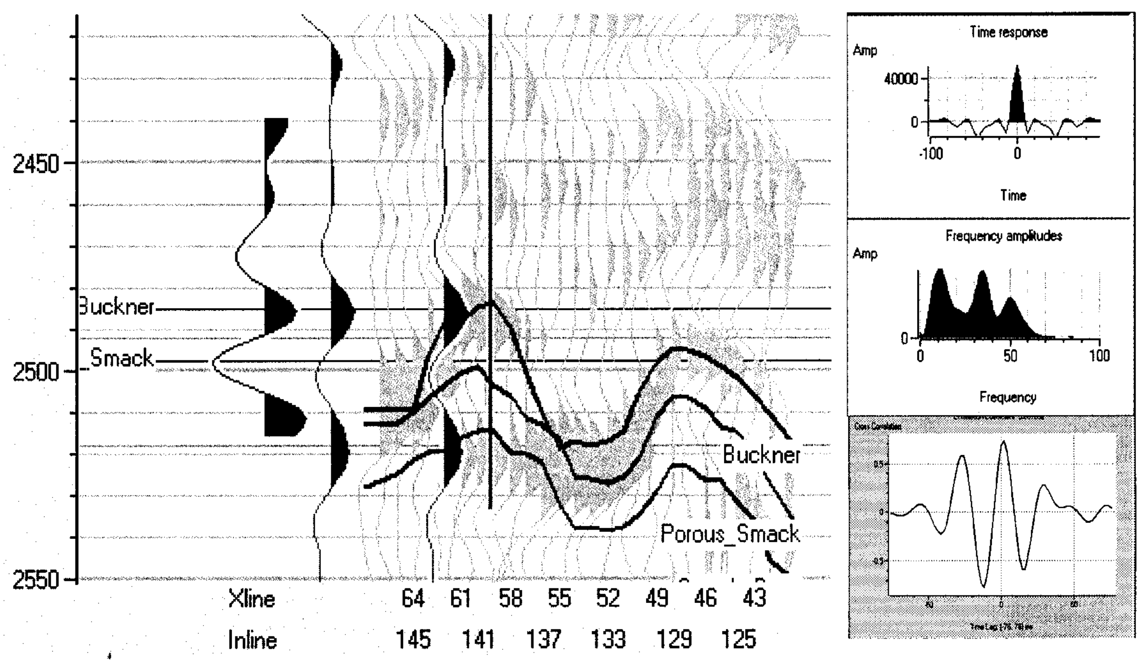

(c)

Figure B1: Synthetic seismograms of some wells showing good ties a = 3854, b = 3986, c = 4633B. Blue wiggle = synthetic, red wiggle = seismic trace extracted along the wellbore. Frequency, amplitude and time response of the seismic trace along with its seismic correlation has been included.

APPENDIX C

Seismic Modeling

The main components of the model were:

(i) Geometry/interval properties of velocity and density

(ii) Wavelet (obtained from the real seismic data)

The type of modeling carried out was stratigraphic, where the main objective was to model variations in physical property resulting from facies changes at the Appleton Field. It was meant to address the following questions (*c.f.*, Hart and Balch, 2000):

(i) What is the spatial (horizontal and vertical) resolution of the seismic data?

(ii) Can the event of interest, the porous Smackover, be characterized seismically?

(iii) Does this reflection event correspond to a peak, trough, zero crossing or something else?

(iv) Does polarity of this event change within the survey?

Model Parameters

Geometry and interval properties

Two structurally located wells (4835-B, 4633-B, Table C1) and an off-structure well (5138, Table C2) were used to define physical properties of the layers.

Calculations of tuning thickness, showed that in order for the top and the base of the porous Smackover to be resolved seismically, the porous Smackover had to be about 102ft (~31m) thick. Tuning thickness was calculated thus:

$$\text{Tuning Thickness} = V/4f_{dom} = \lambda/4 \qquad \text{C1}$$

$$v = d/t \qquad \text{C2}$$

$d = 12850ft, t = 1.26s$

→ $v = 12850/1.26 = 10198ft/s$

$v = f\lambda$, and $\lambda = v/f$ C3

→ $\lambda = 10198/25 = 408ft$

→ Tuning thickness (depth)= 408/4 = 102ft (~31m)

→ Tuning thickness (time) = d/v = 102/10198 = 0.01s = 10ms

where: f = frequency, λ = wavelength, v = Interval velocity, f_{dom} = dominant frequency, and t = average one-way time (s), d = average depth. Values used in calculations are estimated for the porous Smackover interval from logs and seismic data.

Wavelet

Wavelets were calculated from the seismic data; a statistical wavelet extracted from a 700ms window containing the Smackover Formation, and an Ormsby bandpass wavelet whose low and high cut frequencies were obtained from frequencies in the 3-D survey (Table C3, Table C4, and Figs. C3 & C4).

Table C1: On-structure well parameters

Formation	Velocity		Density	Depth (Cumulative)
(Name)	(ft/s)	(m/s)	(g/cc)	(ft)
Haynesville	14,925	4550	2.53	498.00
Buckner	19,354	5898	2.96	549.80
Non-Porous Smackover	20,513	6254	2.80	688.38
Porous Smackover	16,160	4927	2.65	854.00
Basement	19,803	6037	2.77	1180.70

Table C2: Off-structure well parameters

Formation	Velocity		Density	Depth (Cumulative)
(Name)	(ft/s)	(m/s)	(g/cc)	(ft)
Haynesville	14,925	4550	2.53	648.00
Buckner	19,354	5898	2.96	749.20
Non-Porous Smackover	20,513	6254	2.80	945.00
Norphlet	13,000	3963	2.60	1051.60
Basement	19,803	6037	2.77	1180.70

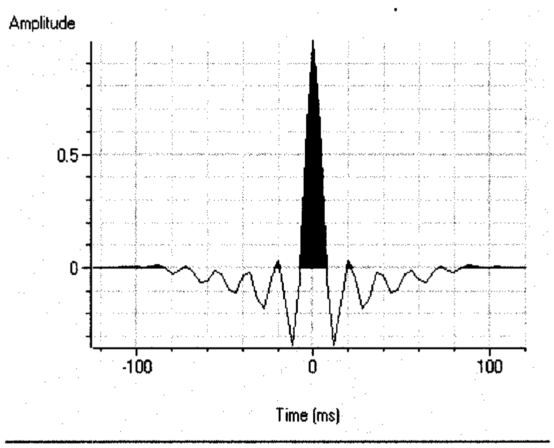

(a)

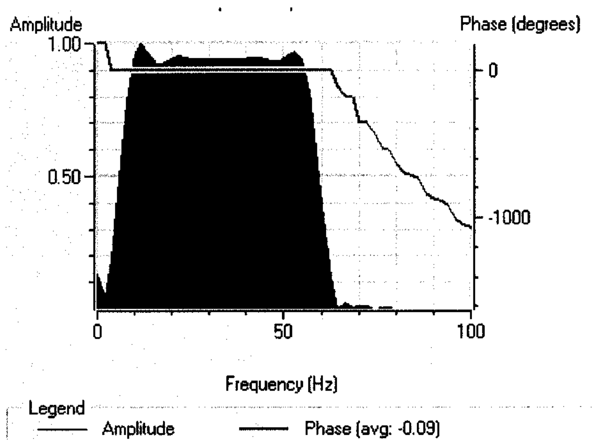

(b)

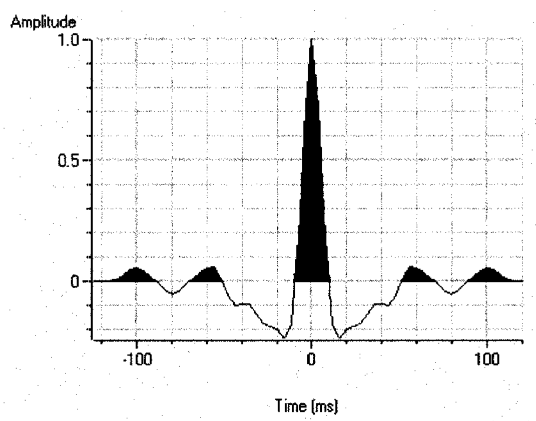

(c)

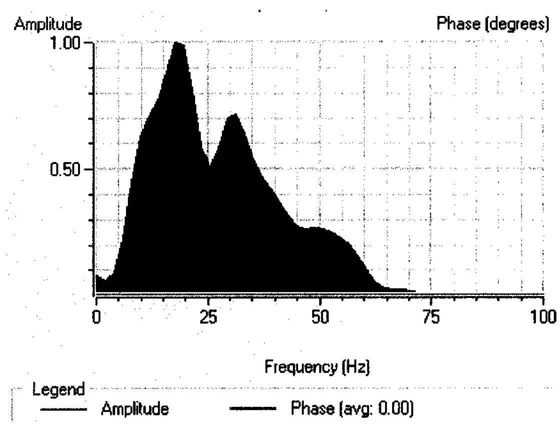

(d)

Figure C3: Model wavelets: Bandpass (a)& (b), Statistical wavelet (c) & (d). (a) & (c) show the wavelet shape, (b) & (d) show the phase and frequency range of the wavelet.

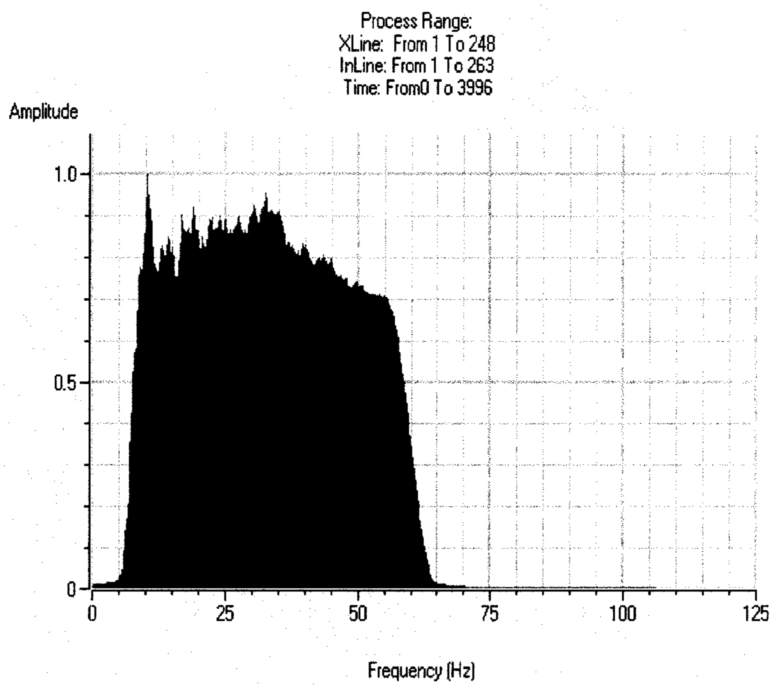

Figure C4: Amplitude spectrum showing available frequencies in 3-D seismic dataset

Table B3: Parameters used for extracting the bandpass wavelet (Ormsby). Range of frequencies obtained from frequency spectrum in Fig C4.

Wavelet phase type	Linear phase
Low Pass Frequency (Hz)	10
Low Cut Frequency (Hz)	6
High Pass Frequency (Hz)	55
High Cut Frequency (Hz)	65
Phase Rotation (degrees)	0
Sample Rate (ms)	4
Wavelet Length (ms)	250

Table B4: Statistical wavelet extraction parameters

Wavelet phase type	Constant Phase
Time Window (ms)	2100 - 2800
Crossline #	59 - 63
Inline #	139 - 144
Phase Rotation (degrees)	0
Sample Rate (ms)	4
Wavelet Length (ms)	250
Taper Length (ms)	50

Procedure adapted for study

(i) Two pseudowells were created from average log readings at known well locations (Table B1 & B2) using the Hampson and Russell® GEOVIEW package. Both pseudowells contained density (g/cc) and sonic (us/ft) logs with a sampling interval of 0.5ft, the same sampling rate as logs in the survey area.

(ii) These pseudowells were imported into the GMA LogM® Model Builder where stratigraphic correlations and model parameters (e.g., wavelet type, sampling interval, number of traces, etc.) were set (Fig. C5).

The following seismic responses of formation tops were deduced from the modeling (Fig. C6; Table 1 in Article).

- From calculating the thickness of the Porous Smackover unit from available well information (depth to the Smackover Base minus the depth to the Porous Smackover) it was determined that this unit was seismically resolvable (Table C6). Meanwhile, the Non-porous Smackover unit was found to be below tuning thickness, and together with the Buckner constitutes a high amplitude peak.
- There was a polarity reversal at the base of the Smackover, this was also observed by Hart and Balch (2000); this was characterized by a high amplitude trough where the Porous Smackover was underlain by the siliciclastic Norphlet Formation, and a low amplitude peak where underlain by the Basement.

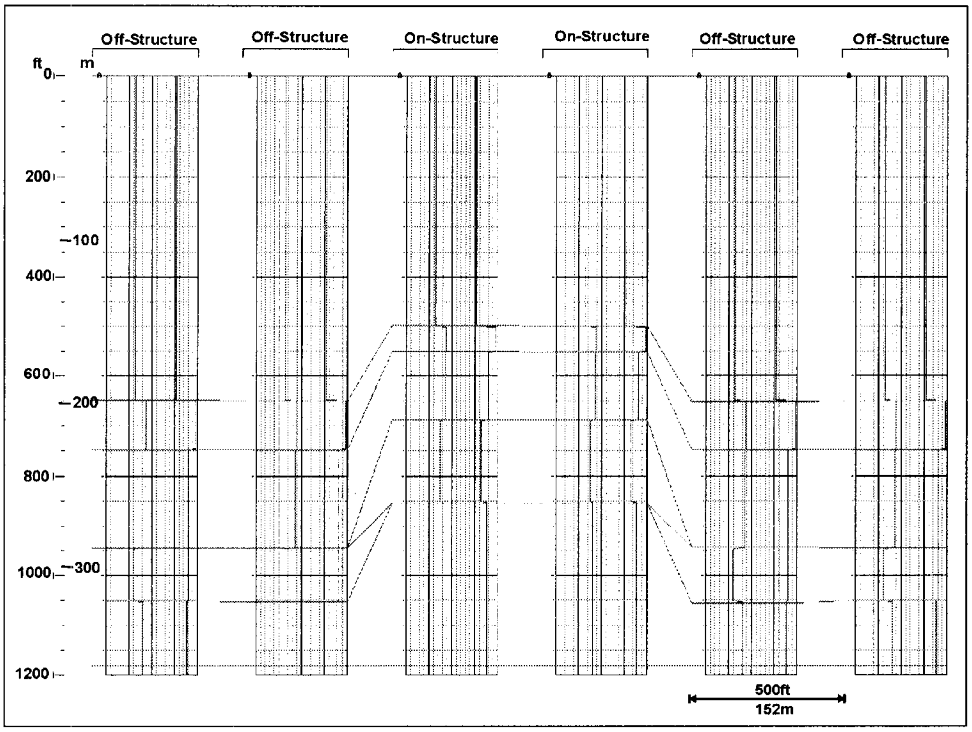

(a)

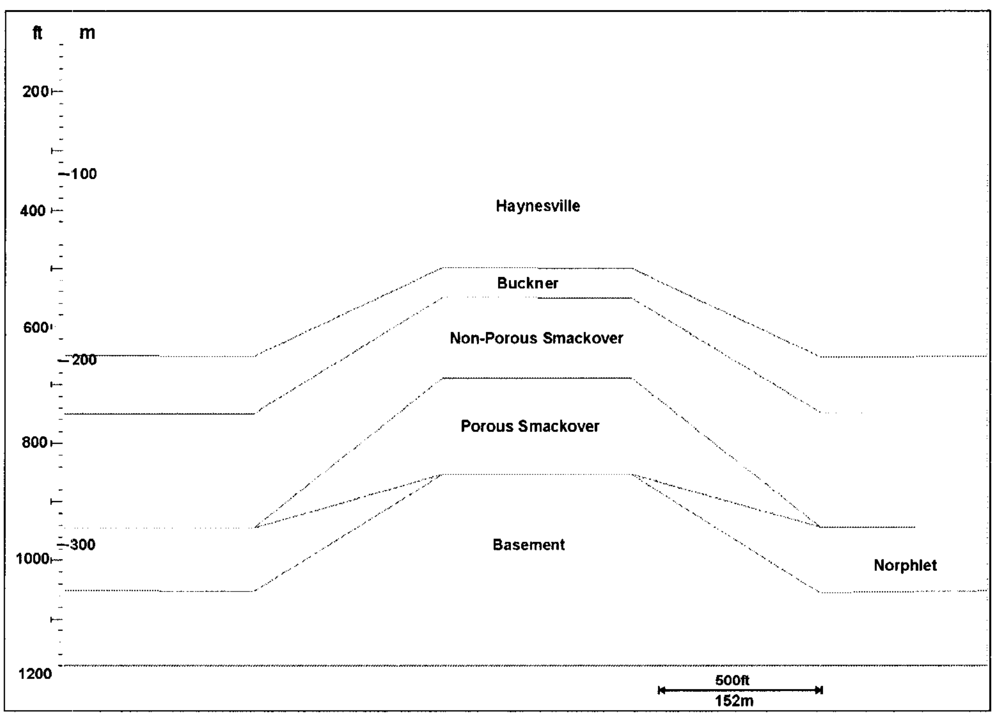

(b)

Figure C5: Model showing (a) Log correlation, (b) Stratigraphic relationship of Formations

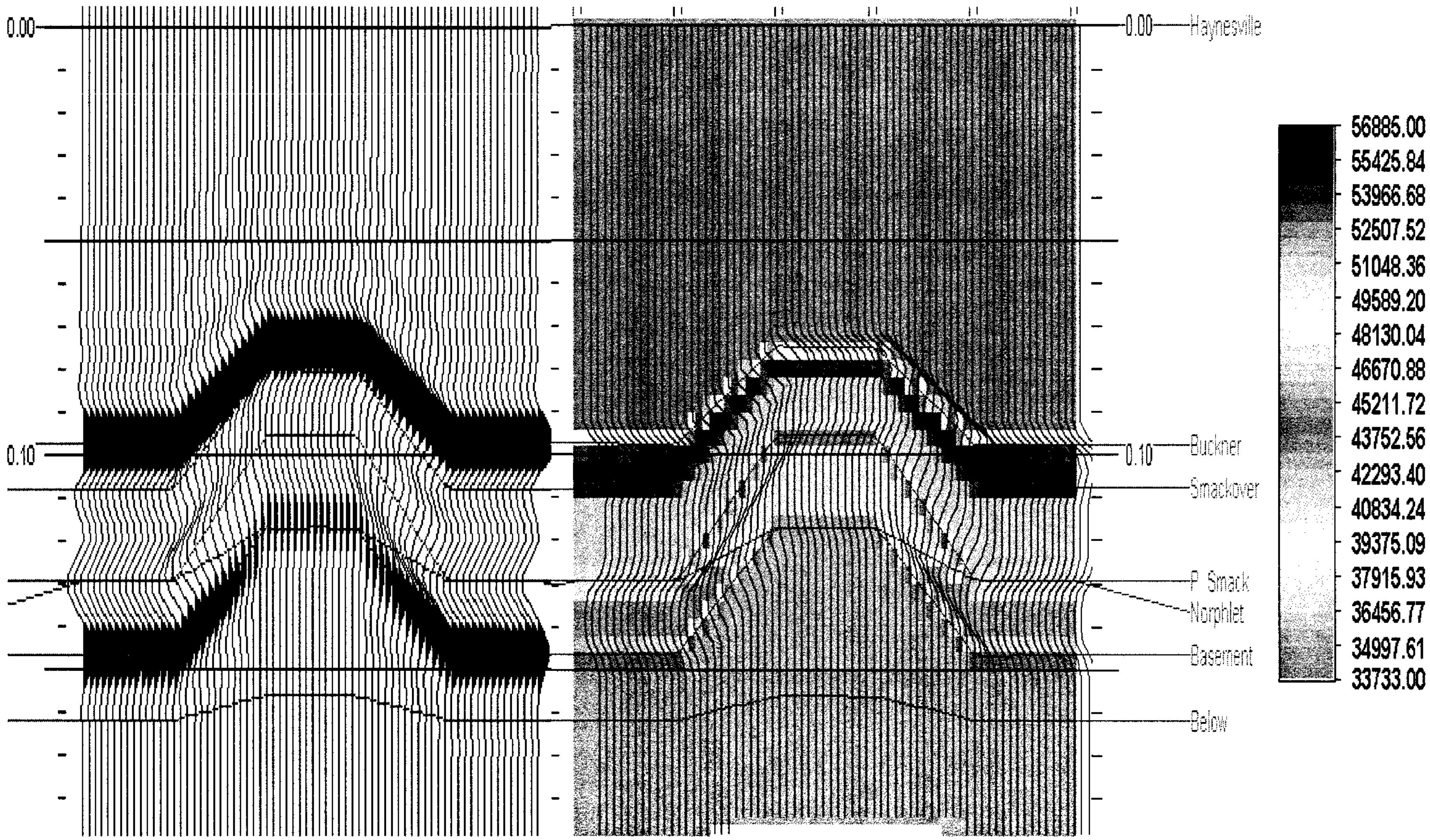

(a) (b)

Figure C6: (a) Synthetic Seismogram, (b) Impedance Model. Note the differences in amplitude at the Buckner, non-porous Smackover horizons in relation to the presence of paleostructure. Scale bar = acoustic impedance values of strata.

Table C6: Porous Smackover Thickness (well-based). See isopach in Figure D7.

Permit #	Porous Smackover Thickness (ft)/(m)
3854	170 52
3986	203 62
4633-B	142 49
4835-B	158 48
4991	154 (bottom hole in porous Smackover) 53
5089	- -
5138	- -
5224	205 62
5346	179 54
6247	95 29
6247-B	60 (bottom hole in porous Smackover) 18

Probable causes of differences observed between synthetic and real data

(i) The synthetic seismogram is developed from well log measurements; the well logs measures the vertical lithologic sequences around the borehole, while the real data averages a wider lateral extent, hence greater spatial variability.

(ii) The deviation survey for a given log may be incorrect; hence the resulting synthetic, since the log is not imaging the correct trace location, would be different from that of the seismic data.

APPENDIX D

Horizon Interpretation

Results obtained from modeling helped constrain the mapping of stratigraphic units within the Appleton 3-D seismic data. Mapping was carried out using a grid of seed lines (Fig. D1).

Mode of horizon picking depended on the continuity, stratigraphic complexity, strength of amplitudes, amount of noise in the data, etc. For the Buckner horizon, the most continuous and high amplitude peak, seed points were picked on a grid of lines (every 10th inline and crossline), these were then autotracked and later checked for misspicks. For discontinuous horizons like the Porous Smackover, picking was done manually. This, though slow and time consuming, ensured consistency and geologic plausibility of the picks. Picks were then crosschecked by examining loops and arbitrary lines. Picks were made using variable density displays; wiggle trace, and attributes (e.g., phase for edge detection). The result of this process were:

(a) Depth-structure maps (Figs. D2, D3 & D4) - showed the structural configuration of the horizons/formations with respect to the seismic reference datum (which was 0ft).

(b) Isochron/isopach map (Figs. D5-D8) - used to 'see' the variations in horizon geometries and hence determine the range in thickness, likely trends and probable causes of variations observed in the sediment package.

Geologic interpretation of the reservoir interval, the Porous Smackover, was based on the examination of the above maps, and the internal reflection configuration of the seismic data (discussed in the article).

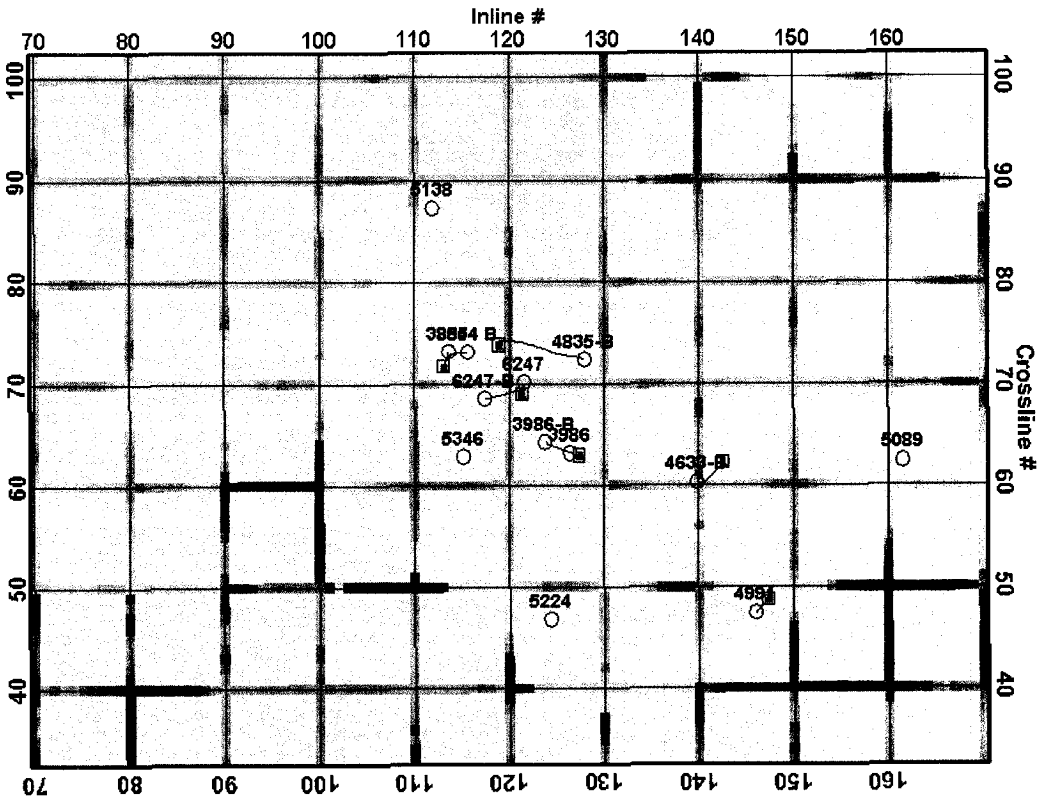

Figure D1: Grid of seed lines used in picking Buckner horizon. Circles denote well locations and connecting lines the wellbore path (for deviated wells).

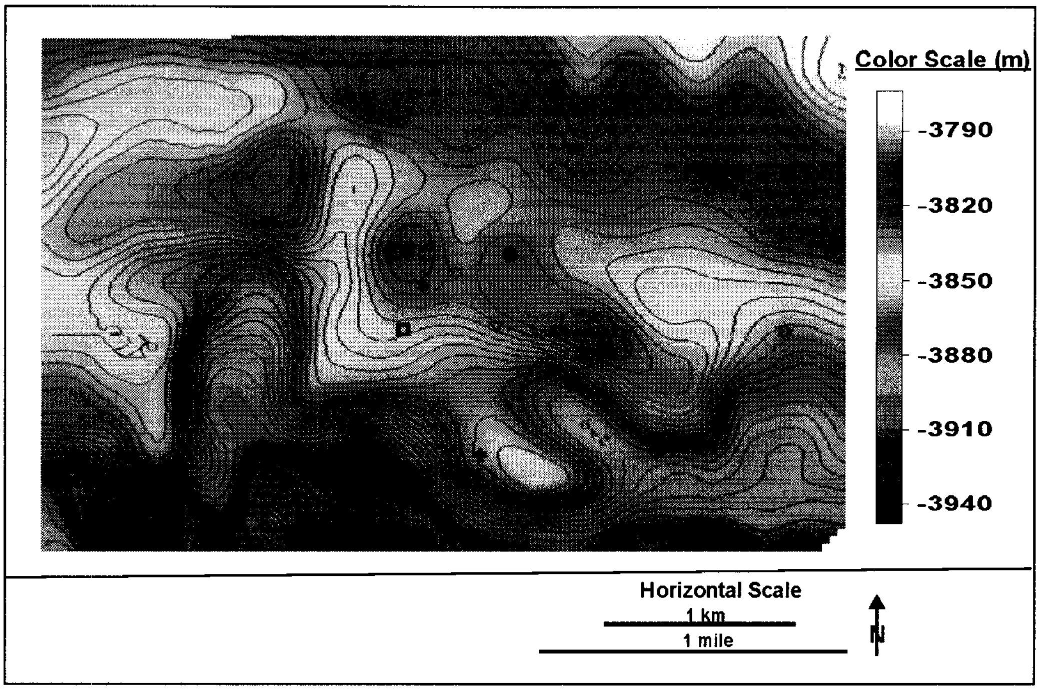

Figure D2: Depth sub-sea of Buckner/Smackover Formation: shows structural closure in the Appleton Field, two are penetrated by wells (4633-B and 3854-B). Closure to the south suboptimally penetrated by well 5224. No wells were available for the structural culmination to the NW and SW of the Appleton Field. For well names, see Figure 3/8.

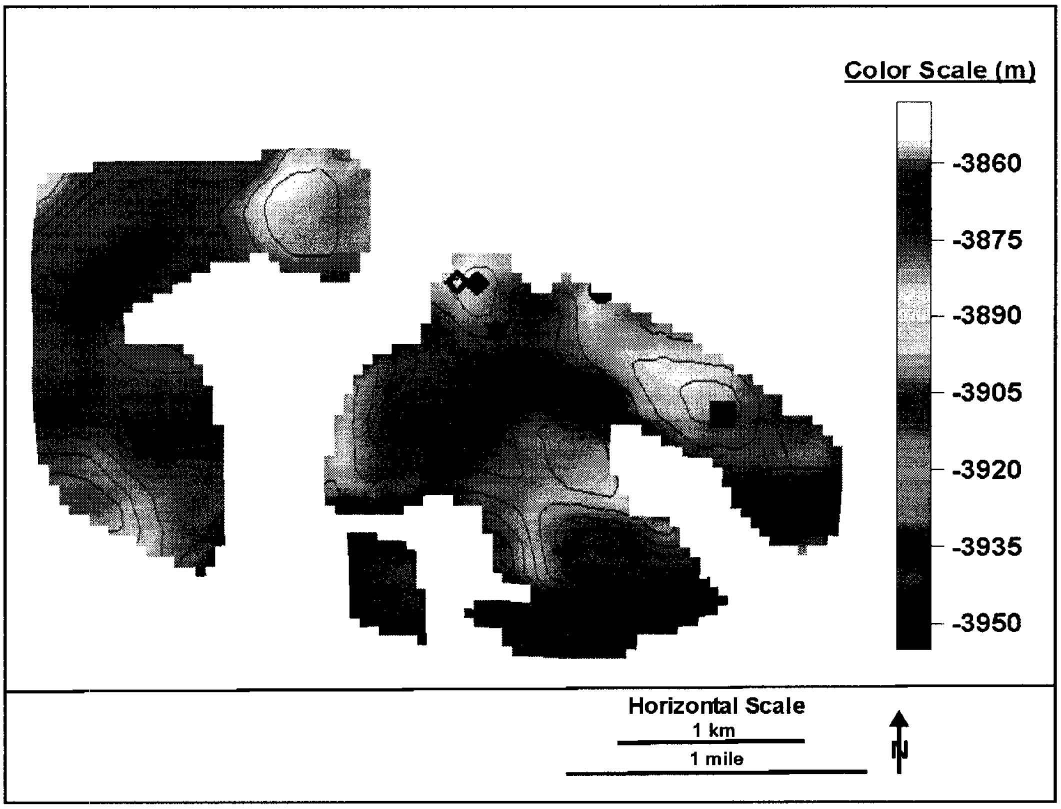

Figure D3: Depth sub-sea map of the Porous Smackover. Five main culminations observed. From this map, it is readily apparent that the Porous Smackover Formation is structurally influenced. For well names, see Figure 3/8 in article.

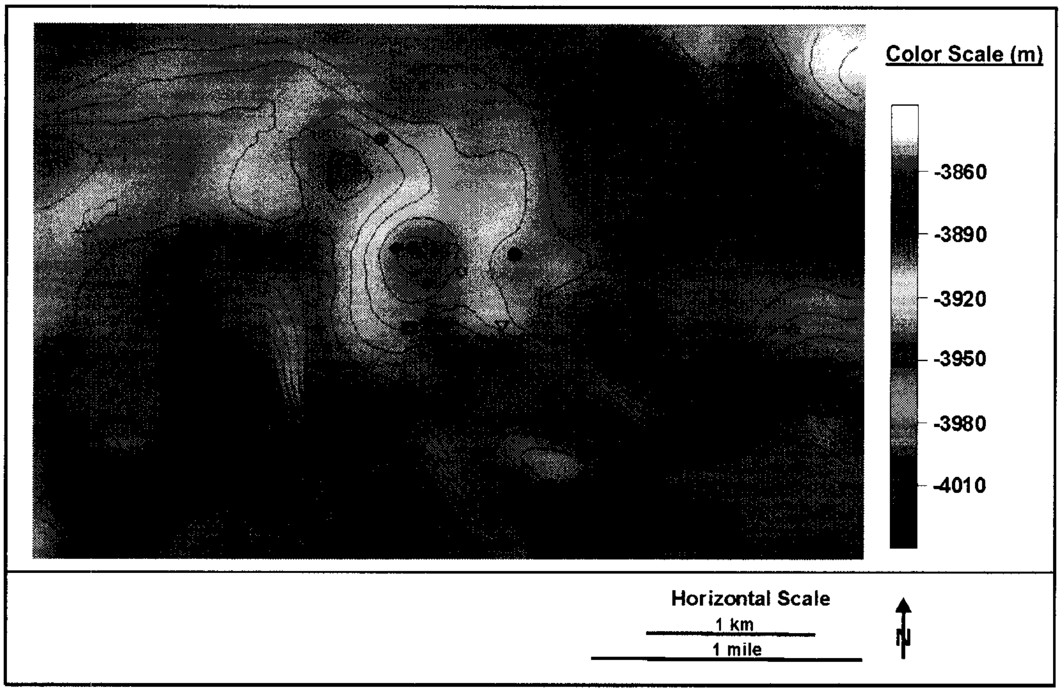

Figure D4: Depth sub-sea map of the Smackover Base. This maps shows existing culminations prior to Smackover depositition. It can be observed also that the paleohigh to the NW of the Appleton Field was structurally lower than those in the east. For well names, see Figure 3/8 in article.

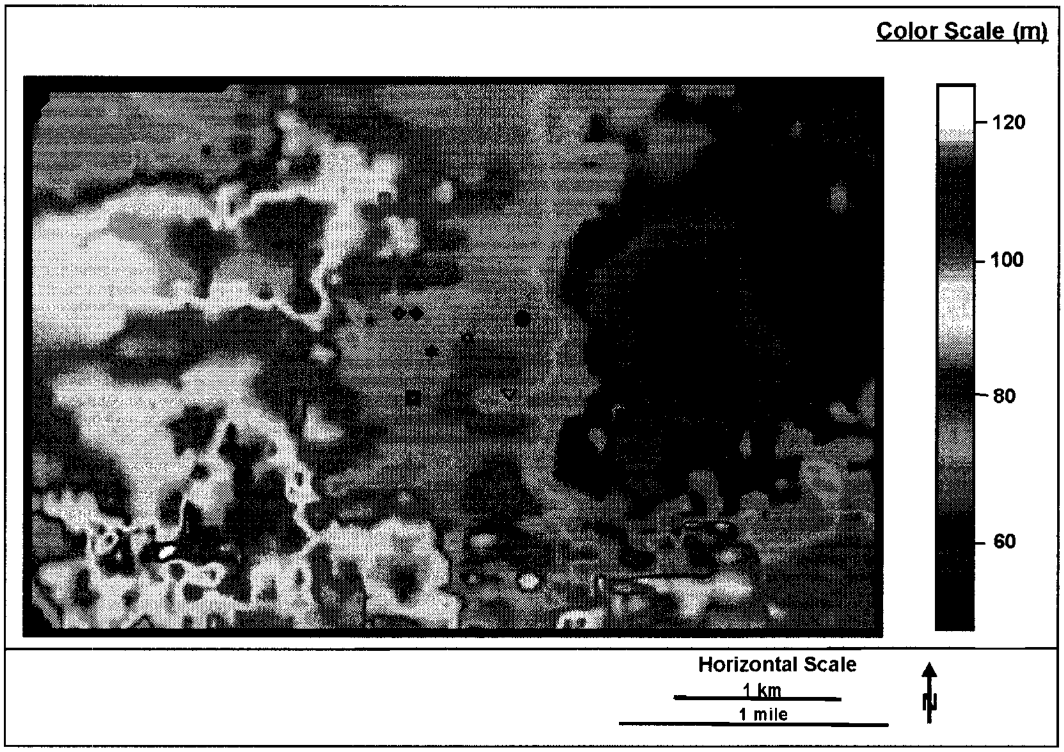

Figure D5: Smackover (top-base) Isopach. This thickness map shows that the Smackover Formation thickens basinward (SW) and thins landward (NE). For well names, see Figure 3/8 in article.

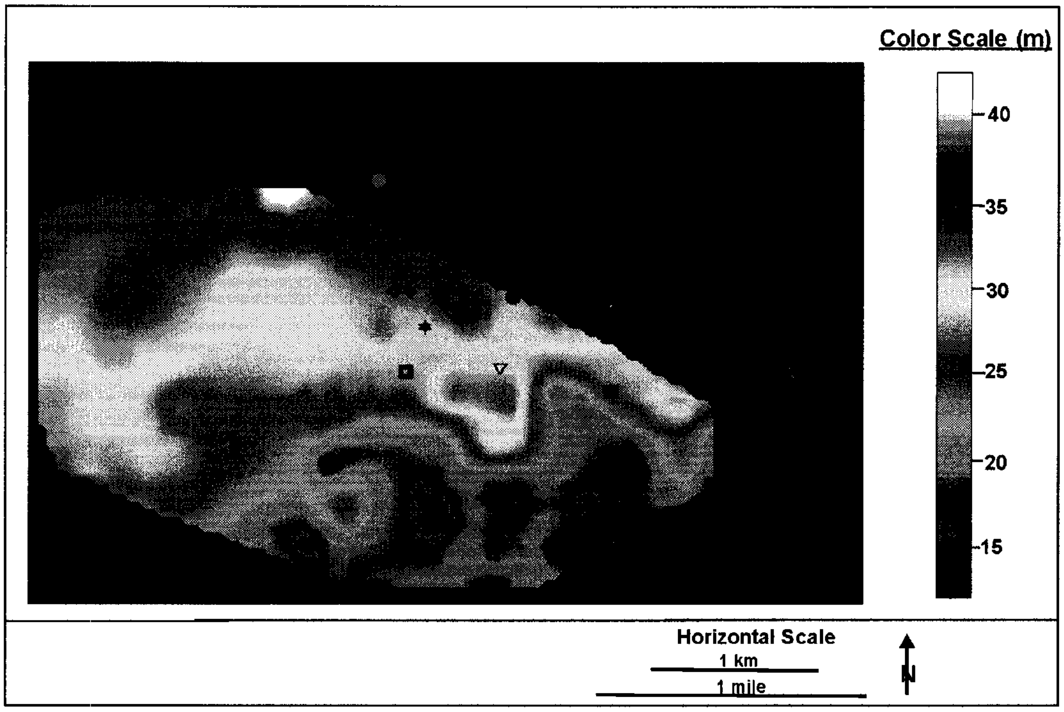

Figure D6: Buckner Isopach. This map shows that Buckner generally thickens away from structure, and decreases basinward. For well names, see Figure 3/8 in article.

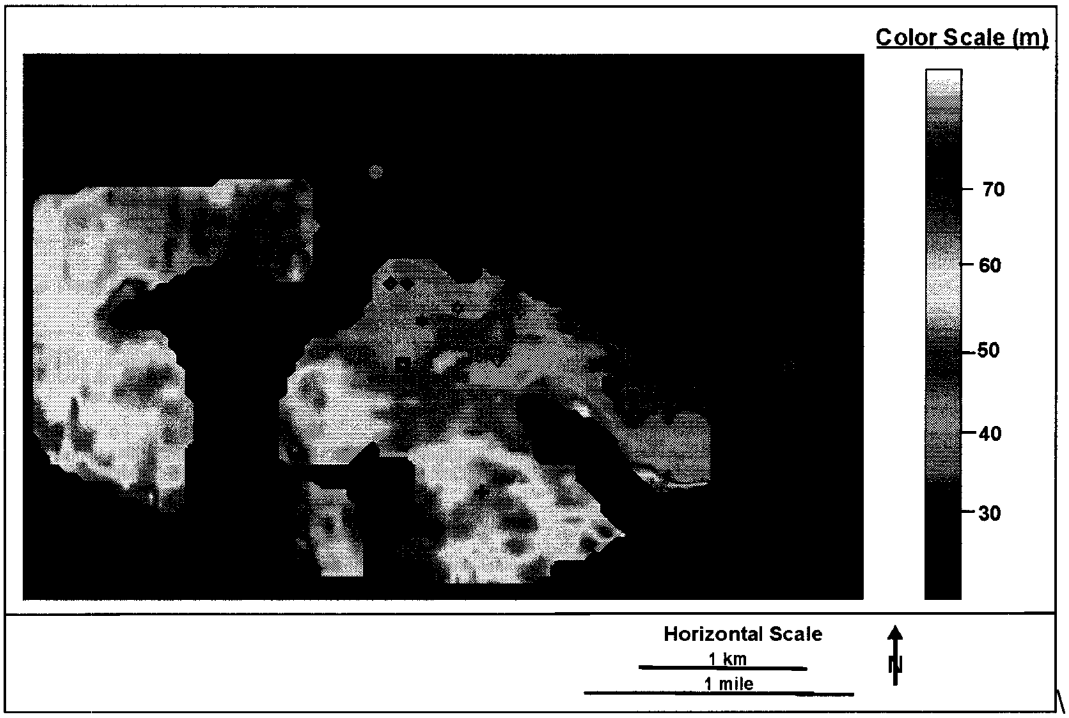

Figure D7 Porous Smackover Isopach. This thickness map shows the porous interval thickens basinward, and is thicker over lower relief paleohighs. For well names, see Figure 3/8 in article.

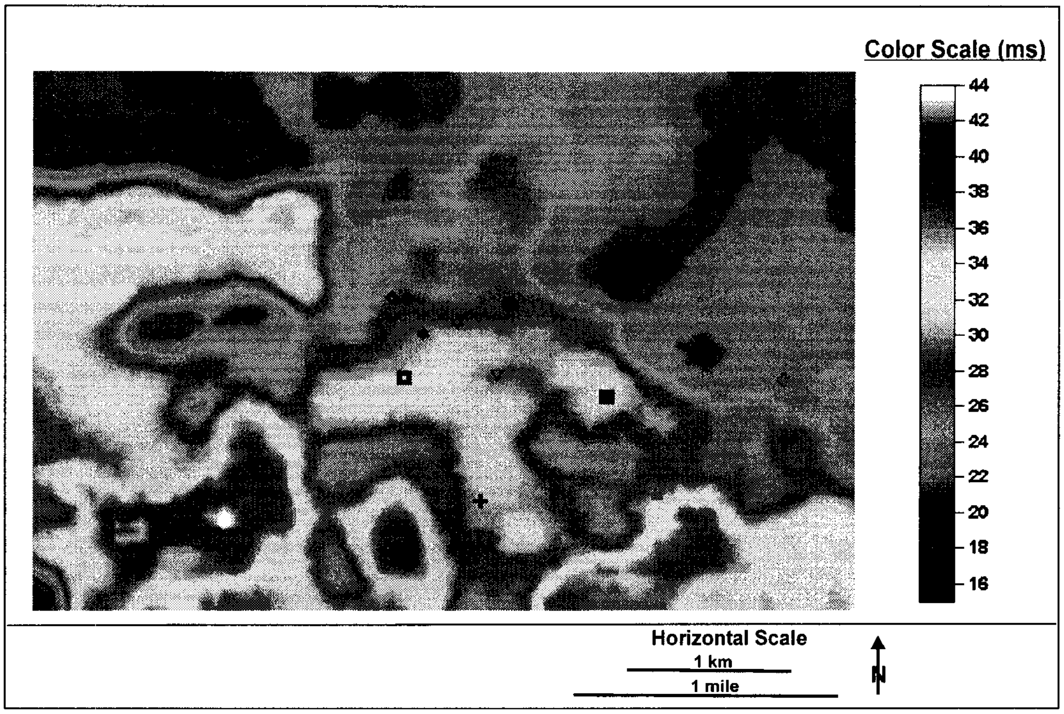

Figure D8: Buckner/Smackover to Base of Smackover isochron. This map also shows the structurally influence distribution of the Smackover Formation. Note similarity to porosity thickness maps obtained from seismic attribute studies (Figure 19 in article). For well names, see Figure 3/8 in article.

APPENDIX E

Trace Inversion

Fundamentals of seismic trace inversion

The seismic trace amplitude on a migrated CMP stack represents a 1-D primary p-wave reflectivity series (Yilmaz, 2001). The fundamental theory behind trace inversion is a reverse to that used in the computation of reflection coefficients from acoustic impedance (Lavergne and Willm, 1977). It involves the integration of the reflectivity series and can be summarized viz:

Seismic trace(s(t)) = wavelet (w(t))* reflectivity (r(t)) + noise E1

where: * = convolution

Reflectivity series (r(t); Eq. B4) is related to the impedance (see Eq. B2) of a series of layers in the earth. Acoustic impedance differences are used to characterize layers in the subsurface (Lavergne and Willm, 1977; Liner, 1999; Satindra Chopra, 2001), and can be converted to lithologic and/or reservoir properties (e.g. porosity, fluid fill; Mukerji et al., 1998). Thus acoustic impedance plays an exceptional role in reservoir characterization. Trace inversion converts seismic amplitudes directly into acoustic impedance and ensures the preservation of amplitude variations whose differences could be interpreted as resulting from geologic changes (Lavergne and Willm, 1977).

Because of the loss of low and high frequencies in the seismic process (by attenuation due to depth and lithologic changes, or processing), the frequency information which required for reconstructing impedance is absent in the stacked seismic data, hence the need for both seismic data (provides the high frequency component of interval in the velocity embedded in the reflectivity data, mapped horizons determine how these velocities are distributed at interwell areas), and well logs (mainly sonic) which supplies the low frequency component. The absence of these frequency components in the inversion will prevent the transformed impedance traces from having the basic impedance or velocity structure essential in making a good geologic interpretation.

Steps taken to ensure good inversion

(i) The seismic data, which was time-migrated, had no checkerboard look, coherent noise and was free of multiples. Thus each seismic trace was dependent on the reflectivity beneath it.

(ii) Horizons are used as lateral constraints.

(iii) Wavelet used contained the frequency and phase content derived from the seismic interval to be inverted and was time invariant.

From our inversion results we were able to categorize the spatial distribution of impedance at the Smackover Formation (Fig. E4). From these too, we could delineate areas of lowest impedance in the Porous Smackover, which we related to increasing porosity. Impedance was found to be generally lowest at the Porous Smackover unit. Some low impedance observed in the troughs i.e. off-structure, was attributed to the sandstones of the Norphlet Formation. Our impedance volume served as a template to verify and elucidate any anomalies we would observe in our porosity volume.

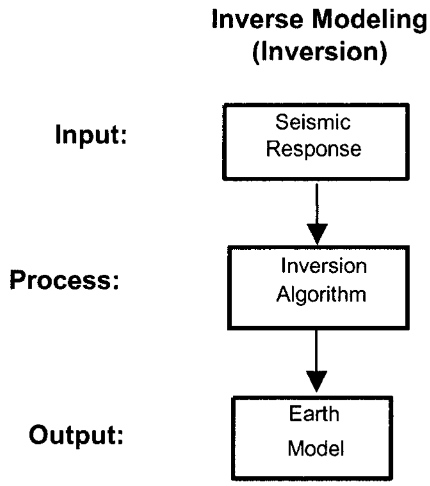

Figure E1: Simplified inversion workflow. Adapted from Hampson-Russell training manual.

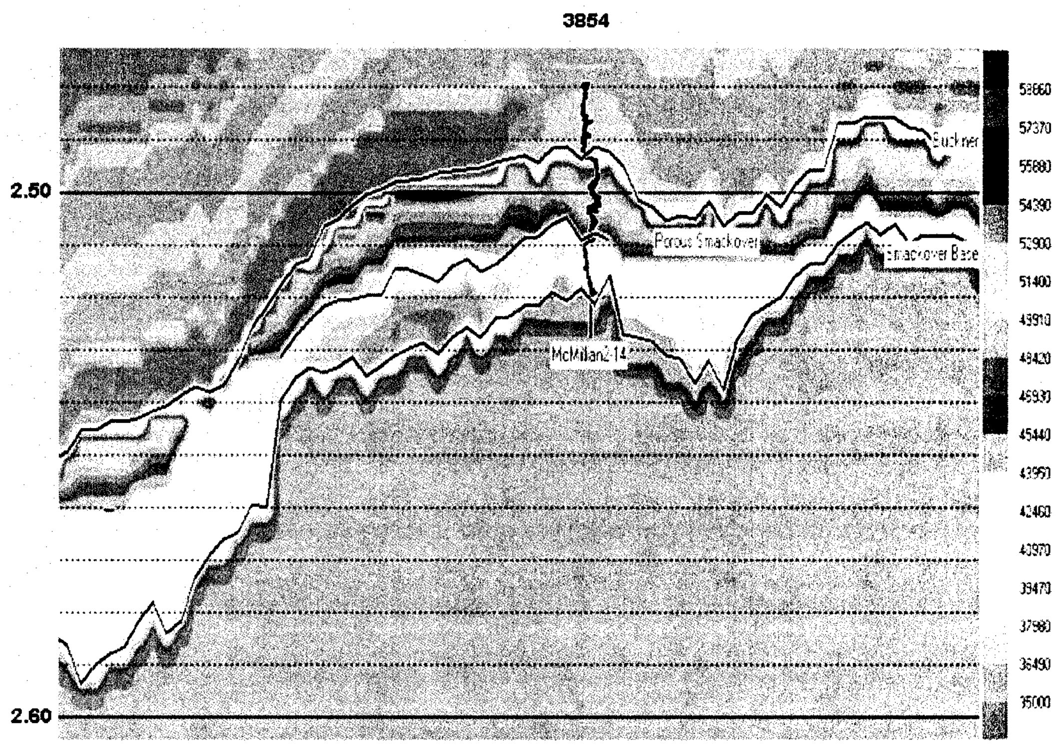

Figure E2: Initial Model – transect shows impedance structure at inline 114. Hotter colors have been used here to delineate areas of high porosity. This initial impedance model is created from sonic and density logs, using a statistical wavelet.

Table E1: Layer interpolation options to define relationship of stratigraphic units for modeling acoustic impedance.

Layer Interpolation Options	Stratigraphic Relationship
Above Buckner	Top Lap
Between Buckner and Porous Smackover	Conformable
Between Porous Smackover and Smackover Base	Base Lap
Below Smackover Base	Base Lap

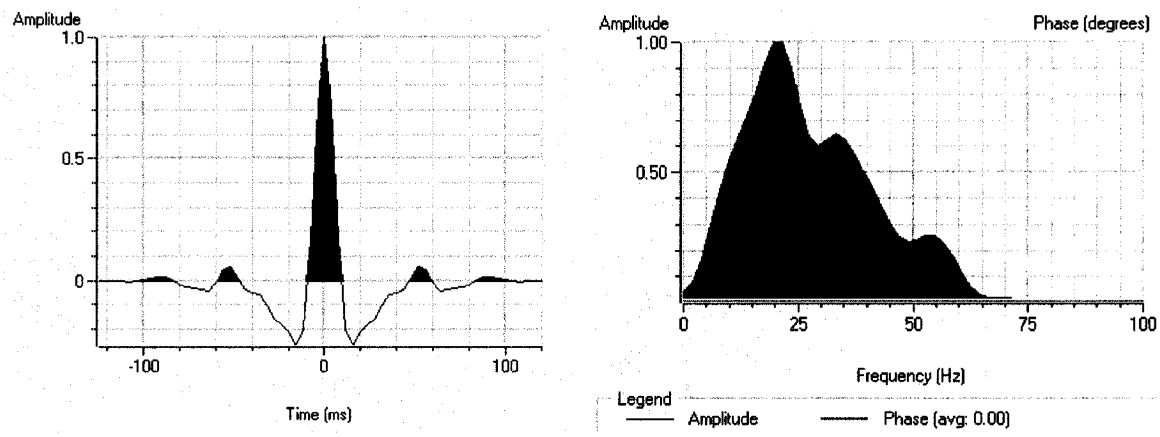

(a) (b)

Figure E3: Inversion wavelet was extracted from crossline 68-73 and inline 110-115. This wavelet shows same frequency spectrum as in C3 c&d. Though they were both extracted for the same interval, the number of inlines and crosslines used in their creation are different. This thus implies that this wavelet represents accurately the frequency spectrum within the porous Smackover.

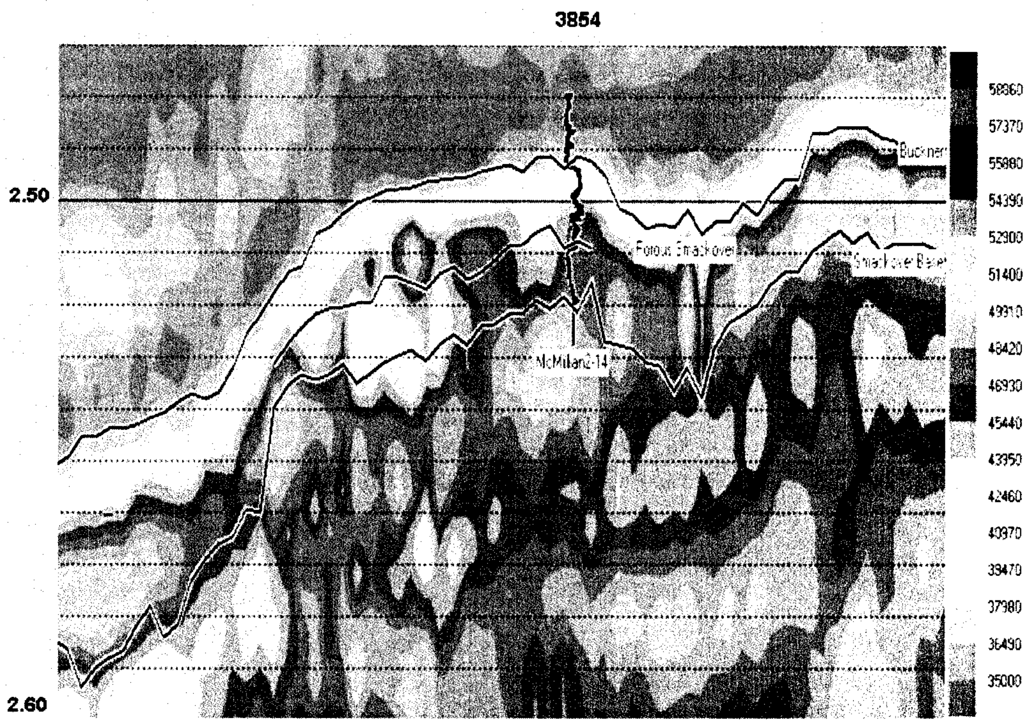

Figure E4: Impedance model from trace inversion. Same transect as in Figure E2. Note lower impedance downslope from the crest.

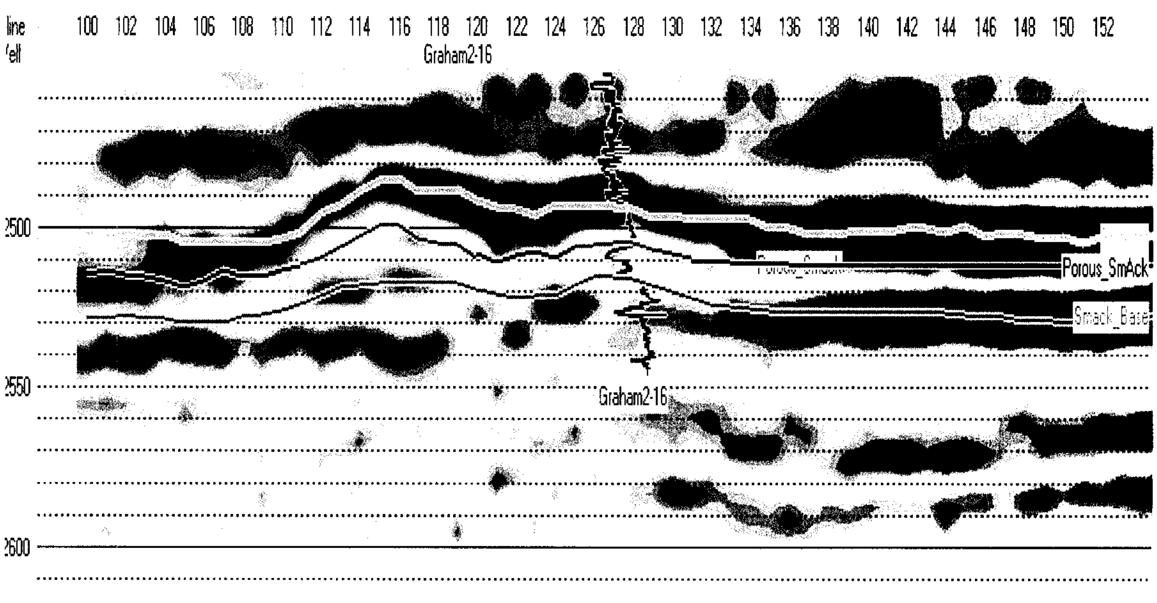

(a) Synthetic

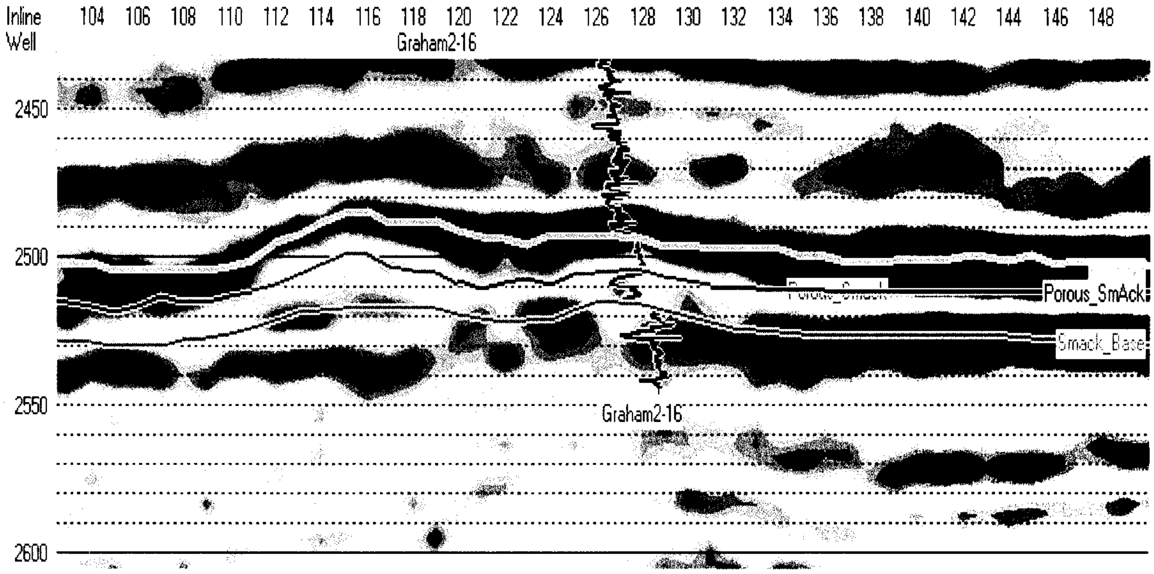

(b) Real Seismic

Figure E5: Comparison of modeled and real seismic data at crossline 72. Note how well the two sections correspond. Lines: yellow = Buckner/Smackover, Red = porous Smackover, pink = Smackover base.

APPENDIX F

Multi-attribute Analysis

Principles and methods of seismic attribute studies

A seismic attribute is defined as:

" A derivative of a basic seismic measurement which may be extracted along a horizon or summed over a time window" (Brown, 1996a)

They are also termed transforms and are commonly non-linear to the seismic data from which they are derived. The three main attributes are called 'instantaneous attributes'. These are the estimated amplitude envelope, phase, and frequency at any given seismic sample (Fig. F1, Table F1). These attributes are derived from the complex trace (Eq. F1), which is composed of the seismic trace (s(t)) and its 90^0 phase rotated image the Hilbert transform (h(t)) (Taner *et al.*, 1979; Barnes, 1998). This can be written in the Cartesian form as:

Complex trace $C(t) = s(t) + jh(t)$ F1

(Taner et al., 1979)

where: h(t) = Hilhert transform (projection in imaginary plane), s(t) = seismic trace (projection in real plane).

Attributes can be horizon or volume-based and are classified based on the type of seismic information they are derived from i.e. amplitude, frequency, phase, time or integral. Table F1 defines the volume-based attributes used in EMERGE and how they are calculated.

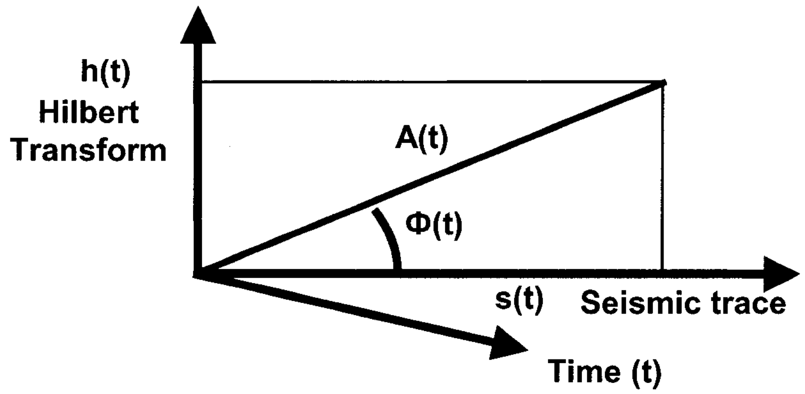

where: A(t) = amplitude envelope (perpendicular distance from helix to time axis), Φ(t) = phase (angle between line along which A(t) is measured and the horizontal).

Figure F1: The complex trace in polar form, defines the main seismic attributes.

The goal of a multi-attribute analysis is to predict physical properties distribution in the seismic data at well and interwell locations. The rationale behind this is that all features (amplitudes, wavelet behavior etc.) of seismic signals are directly caused by rock physics phenomena (Schultz et al., 1994).

The mode of attribute extraction is of considerable importance and depends on: -

(i) The goal of study; i.e. the quality of information required and the physical property investigated.

(ii) The thickness and stratigraphic complexity of the interval of interest.

(iii) Data quality and precision required from study.

Two foremost modes of attribute extraction (Brown 1996b) are horizon–based and volume-based. Horizon attributes are extracted along interpreted structural horizons and requires only the definition of the interval of interest, hence fewer constraints imposed. Volume/window–based attributes on the other hand are extracted over a window that could be defined by:

(a) two structurally interpreted horizons,

(b) a structural horizon and a constant time interval above and below it,

(c) a constant time window (statistical slice).

Attribute studies could be deterministic, where a physical relationship is known to exist between seismic data and property (Schultz et al., 1994; Russell et al., 1997); or data-driven, where an empirical relationship is sought between the attribute and physical property estimated. For this analysis a workflow like the one shown below was used (Fig. F2).

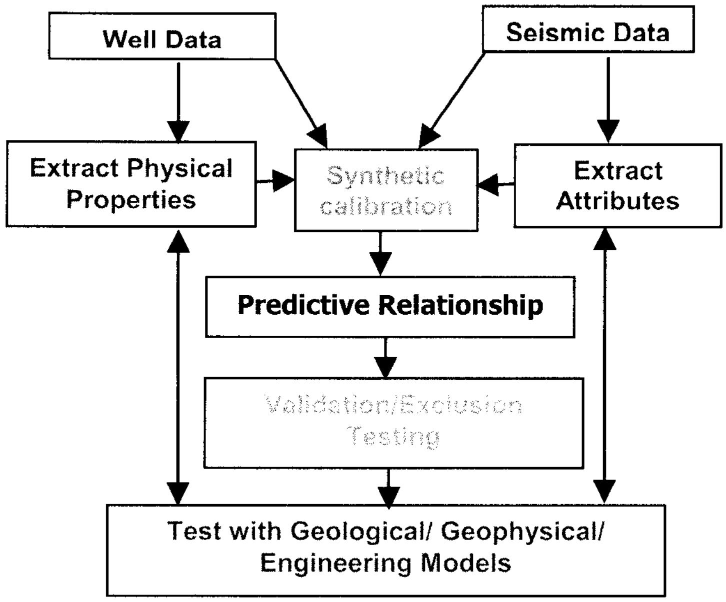

Figure F2: Simplified workflow of multiattribute analysis. Adapted from Schultz et al. (1994).

Procedure adopted for study

(1) Well Selection - Several limitations are placed on the choice of wells to use for multi-attribute studies.

(2) Analysis Window - This refers to the interval for which porosity is being measured (Schultz et al., 1994). EMERGE had the capability of detecting the time window based on well-seismic ties. The attributes were averaged both areally and vertically between the upper and lower surface of the time zone around the well intersections.

(3) Attribute Selection - The question that arises now is 'how do we identify what attributes to use?' The choice of what attribute to use is the most crucial in any attribute studies because of the probability of spurious correlations between any attribute and the well log property (type 1 error; Kalkomey, 1997).

The following procedure was used for attribute selection:

(a) Crossplots of wells and attributes - Most prediction methods require making inferences from seismic data (larger sample population) at a small number of wells (smaller population), thus comparing two data sets with different sampling populations. Crossplots indicates the presence and nature of relationship between two variables, which do not necessarily have the same sample size. An example of such indication can be seen when crossplotting density porosity at wells with seismic attributes (Table F3, Fig. F3). Some attributes had better correlations with porosity while others did not, though were indications of better correlations given a non-linear relationship.

Table F2: Wells used for multi-attribute analysis

Well Name	Permit #	Well Status
McMillian 12-4 #3	4633-B	Producer
McMillian 2-15 #5	6247	Abandoned
McMillian 2-14 #1	3854	Producer
McMillian 11-3 #1	5346 (Sonic log estimated)	Dry Hole (?)
McMillian Trust #12-1	5089	Dry Hole
McMillian 11-1	3986	Abandoned

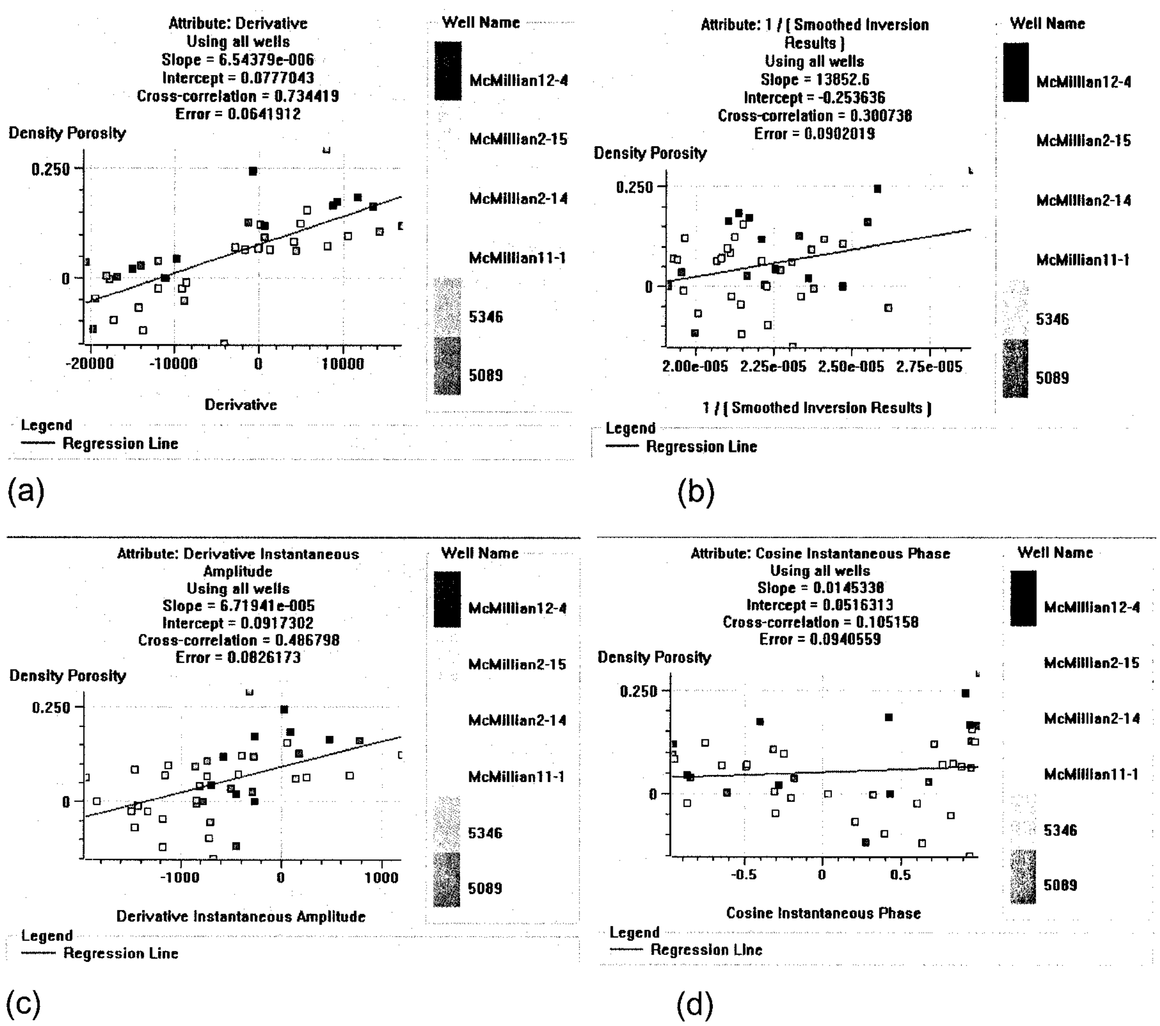

Figure F3: Examples of crossplots of attributes and density porosity at wells.

Table F3: All well correlation of seismic attributes and density porosity (check values in EMERGE).

Attributes	Transform	Error	Correlation to Density Porosity
Derivative	None	0.083754	0.515
Apparent Polarity	None	0.088127	-0.432
Integrate	None	0.089078	-0.411
Amplitude Weighted Phase	None	0.089547	-0.400
Amplitude Envelope	None	0.089599	-0.399
Second Derivative Instantaneous Amplitude	None	0.089730	-0.396
Second Derivative	None	0.092181	-0.332
Instantaneous Phase	None	0.093082	-0.304
Amplitude-Weighted Frequency	None	0.094016	-0.273
Derivative Instantaneous Amplitude	None	0.094064	0.2707
Integrate absolute Amplitude	None	0.094070	-0.2706
Instantaneous Frequency	None	0.095258	0.223
Amplitude-Weighted Cosine Phase	None	0.096247	-0.173
Raw Seismic	None	0.096323	-0.168
Smoothed Inversion	1/X	0.096834	0.134
Smoothed Inversion	Log	0.097031	-0.118
Smoothed Inversion	Sqrt	0.097115	-0.111
Cosine Instantaneous Phase	None	0.097177	-0.105
Smoothed Inversion	None	0.097190	-0.104
Smoothed Inversion	**2	0.097315	-0.090
Time	None	0.097622	-0.044

From these crossplots, derivative (see Fig. 10 in article) was obtained as the best single-predicting attribute. The well logs were time-shifted to optimize this correlation (Table 4). It was however observed that some of the relationships were non-linear; also not all the wells had good correlations with the same attribute(s). Hence there was a need for a statistical relationship involving multiple attributes to strengthen correlations and thus increasing the robustness of our prediction.

(b) Step-wise multilinear regression - The above listed single attributes were trained using stepwise linear regression to predict the best combination of 8 attributes (Table F5) that best define porosity, with the assumption that first attribute is the best single attribute and the next best two attributes include the first attribute and so on. At each time sample, the target log is modeled as a linear combination of several attributes (Fig. F4). As was observed, and is characteristic to this method (Hampson et al., 2001), the final set of attributes used in the prediction which is decided by the validation plot (Fig. 9 in article) does not reflect individual correlation of each attribute and the log property. This is because an attribute with a good correlation can be the linearly scaled version of another, which implies adding this attribute to the equation does not necessarily improve the fit.

Table F4: All well correlation of seismic attributes and density porosity after optimization with the best single-predicting attribute.

Attributes	Transform	Error	Correlation to Density Porosity
Derivative	None	0.06419	0.734
Amplitude-Weighted Cosine Phase	None	0.07989	-0.535
Integrate	None	0.08207	-0.497
Derivative Instantaneous Amplitude	None	0.08261	0.487
Instantaneous Phase	None	0.08494	-0.439
Apparent Polarity	None	0.08760	-0.377
Second Derivative Instantaneous Amplitude	None	0.08902	0.338
Smoothed Inversion	1/X	0.09020	0.300
Smoothed Inversion	Log	0.09067	-0.284
Smoothed Inversion	Sqrt	0.09089	-0.276
Smoothed Inversion	None	0.09110	-0.269
Amplitude Envelope	None	0.09125	-0.263
Smoothed Inversion	**2	0.09149	-0.253
Instantaneous Frequency	None	0.09204	-0.230
Second Derivative	None	0.09301	-0.181
Integrate absolute Amplitude	None	0.09332	-0.162
Amplitude-Weighted Frequency	None	0.09368	-0.137
Time	None	0.09402	-0.108
Cosine Instantaneous Phase	None	0.09405	-0.105
Raw Seismic	None	0.09408	-0.102
Amplitude Weighted Phase	None	0.09414	-0.096

Table F5: Multiattribute list showing the best predicting 8 attributes and their acronyms, prediction error decreases with the addition of each attribute

No. of attributes	Target	Final	Error
1	Density	Derivative (D)	0.0642
2	Density	Derivative Instantaneous Amplitude (DIA)	0.0616
3	Density	Cosine Instantaneous Phase (CIP)	0.0586
4	Density	1/Smooth Inversion Results (1/SIR)	0.0554
5	Density	Amplitude Weighted Frequency (AWF)	0.0539
6	Density	Integrate (I)	0.0515
7	Density	Apparent Polarity (AP)	0.0508
8	Density	Integrate Absolute Amplitude (IAA)	0.0499

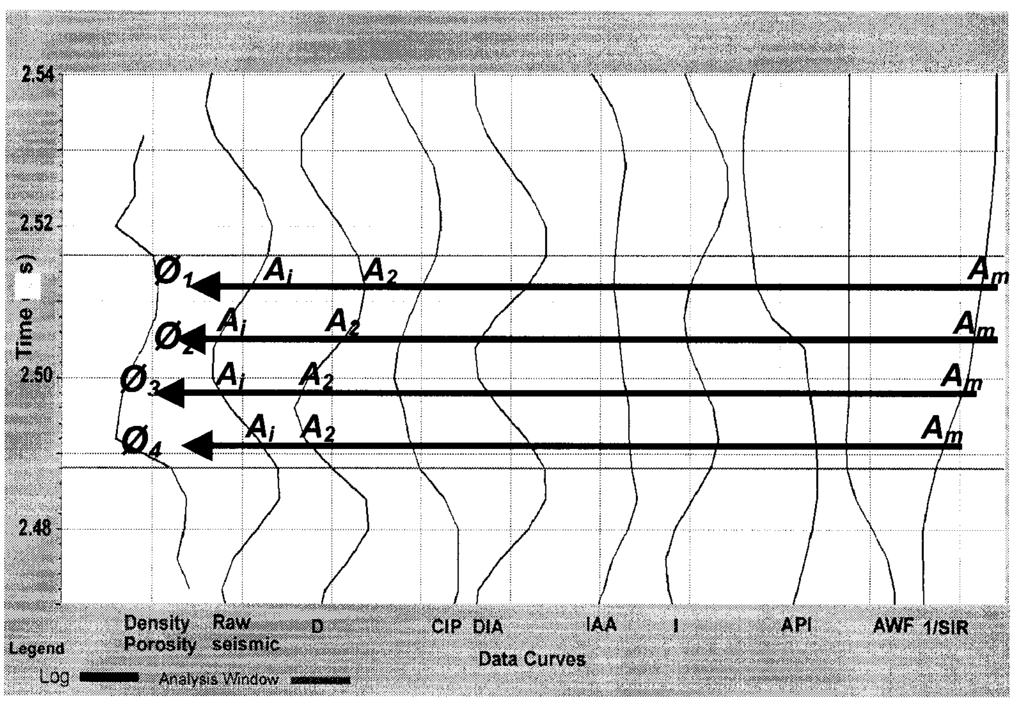

Figure F4: Above figure of well 4633-B shows an example of attribute extraction at well locations. The predicted log is modeled by a combination of several attributes including the seismic data.

The weights, constants, along with the multi-attribute transforms (Article Table 2) were used in the creation of an empirical relationship of the form:

$$P_{MLR}(z) = C + W_i\,(X\,(z)) + \ldots + W_m(Y\,(z)) \qquad \text{F2}$$

Where: P =predicted property, X & Y = attributes, W (i = 1...m) = weights, z = time, C = constant

This relationship was then applied to the seismic data to give a porosity log at each trace location (Fig. 13 in article).

(b) Probabilistic neural network was used to account for the non-linearity in correlation observed in crossplots of attributes and density porosity logs (Fig. F3). The 4 attributes obtained from MLR were trained ("learning" process of Liu and Liu, 1998) using probabilistic neural network to improve resolution PNN (Fig. F5) is a mapping technique in which we solve for the unknown property (P_0, e.g. porosity) by comparing previously known relationships, in this case derived from MLR, between this property and a given set of attributes. It is similar to linear regression in that; the exponential functions (weights in MLR) from each training point is multiplied by the known log values and divided by the sum of the exponential functions to determine the unknown log values (Eq. F3). PNN training transforms *any* given input to an output without any established physical correlation, thus there is the probability of over fitting the training data (Schuelke, et al., 1997). The use of the previously determined MLR relationship in our PNN analysis overcomes this shortcoming.

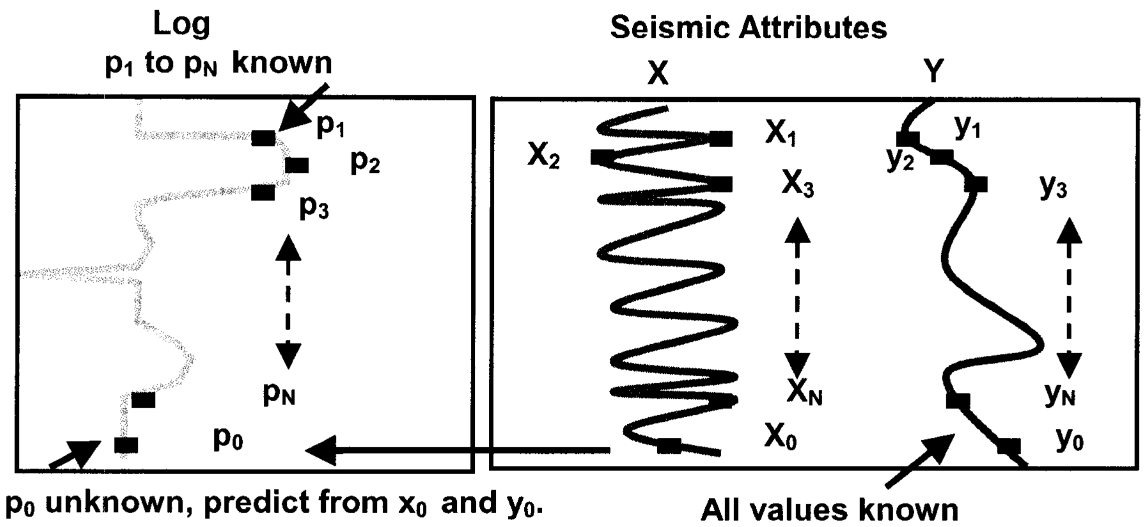

Figure F5: Schematic representation of Probabilistic Neural Network technique (Hampson-Russel, 2001).

$$P_{PNN}(z) = \frac{[P_1 e^{\wedge}(-d^2{}_1/\sigma^2) + P_2 e^{\wedge}(-d^2{}_2/\sigma^2) + P_3 e^{\wedge}(-d^2{}_3/\sigma^2)]}{[e^{\wedge}(-d^2{}_1/\sigma^2) + e^{\wedge}(-d^2{}_2/\sigma^2) + e^{\wedge}(-d^2{}_3/\sigma^2)]} \qquad \text{F3}$$

where: P_{PNN} = predicted property at each sample, $P_{1\text{-}3}$ = actual porosity value, $d^2{}_1$ = distance between input point and the training data $[(X_1 - X_0)^2 + (Y_i - Y_0)^2]$, σ is a scalar.

Both PNN and MLR volumes were created. Because of the flexibility in display offered by the volume-based method, we were able to view sections and slices though the data. Also for a quantitative interpretation, we generated thickness maps (phiH) maps by calculating the cumulative thickness of porosity greater than 12%, the accepted cutoff value for this field. To account for rapid facies changes and hence velocity variation within the Smackover we used a range of velocity values obtained from inversion. We observed that variations in velocity, which is expected because of facies changes within this formation, affected the overall thickness values depicted by our porosity thickness maps (Fig. F6). We however chose to use the average velocity of the porous interval since it was the most porous and thus most affected by velocity changes (Fig. F7a).

Figure F6 and Figure 19 (in article) show the porosity thickness values calculated for the Smackover Formation, while Figure F7 shows that for the Porous Smackover unit. As can be seen, the bulk of porosity in this field is found in the Porous Smackover unit and preferentially to the forereef flanks. Additionally, the trend of increasing porosity thickness basinward (also seen in Fig. D7) that was predicted by this analysis was also found prevalent in other data (i.e., core and well log) available for this field. This goes to further confirm the robustness of our predictions. Differences in thickness observed in core data results mainly because only a limited extent of the logs was cored.

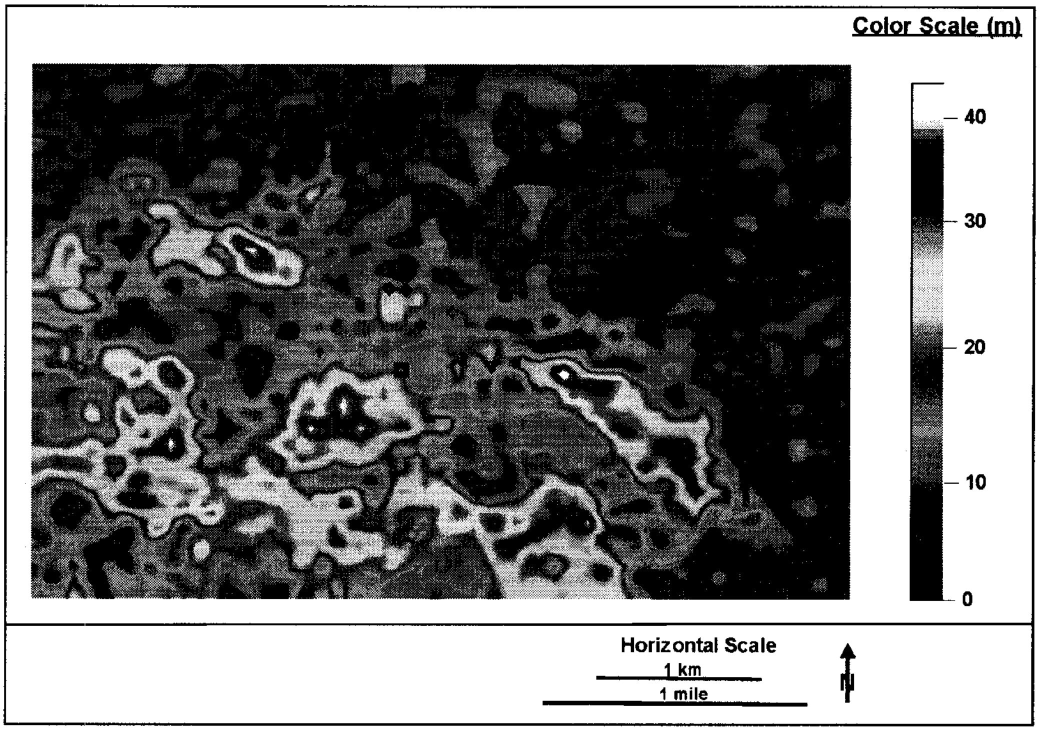

Figure F6

(a) Porosity thickness calculated using an average velocity of 4420m/s.

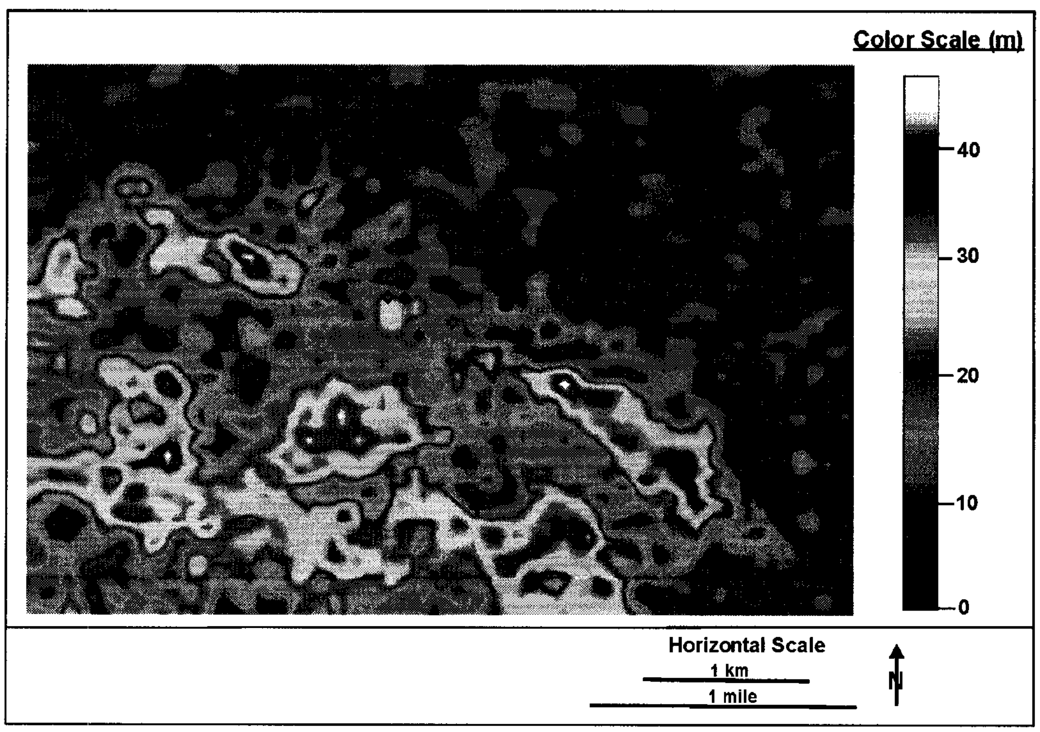

(b) Porosity thickness calculated using an average velocity of 4927m/s.

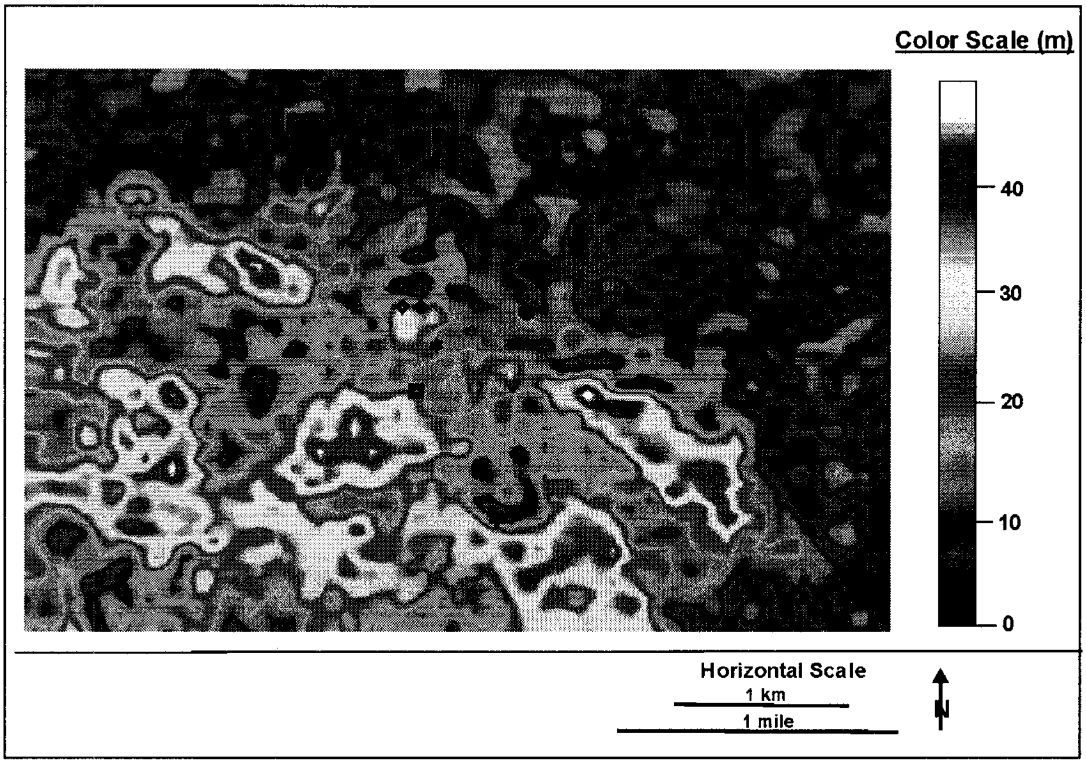

(c) Porosity thickness calculated using an average velocity of 5319m/s.

Figure F6: Porosity thickness maps created from PNN volume using a varying velocity values. Note differences in thickness with velocity value used. At first glance, because of the color scale, it could be thought that varying the velocity has no effect on the ensuing thickness changes. For well names, see Figure 3/8 in article.

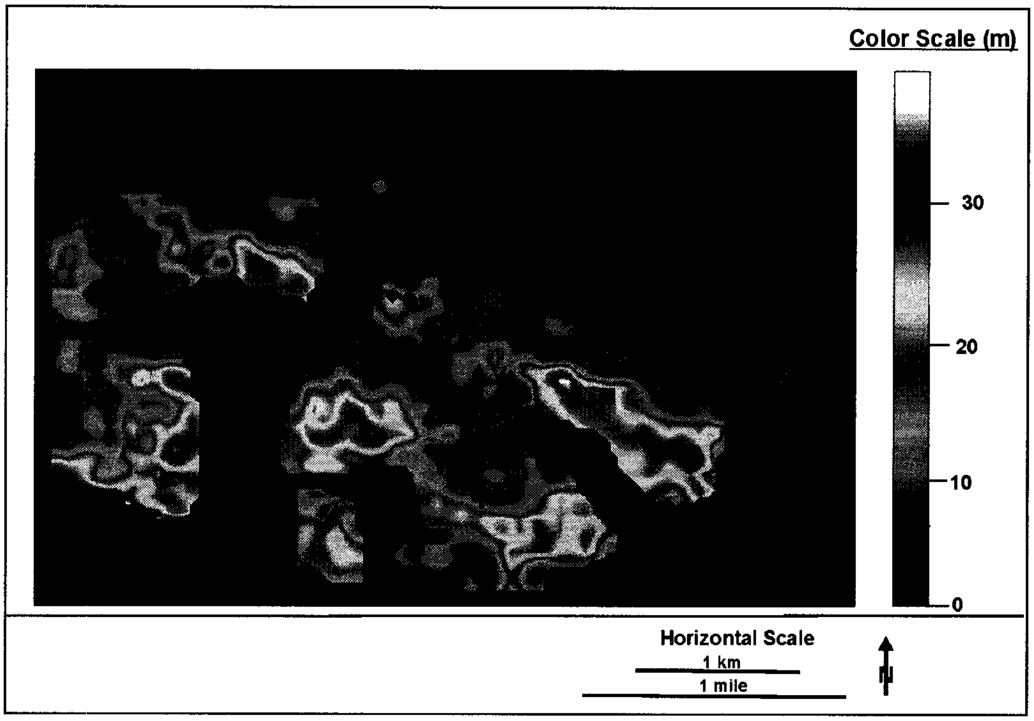

Figure F7

(a) PNN-derived porosity volume.

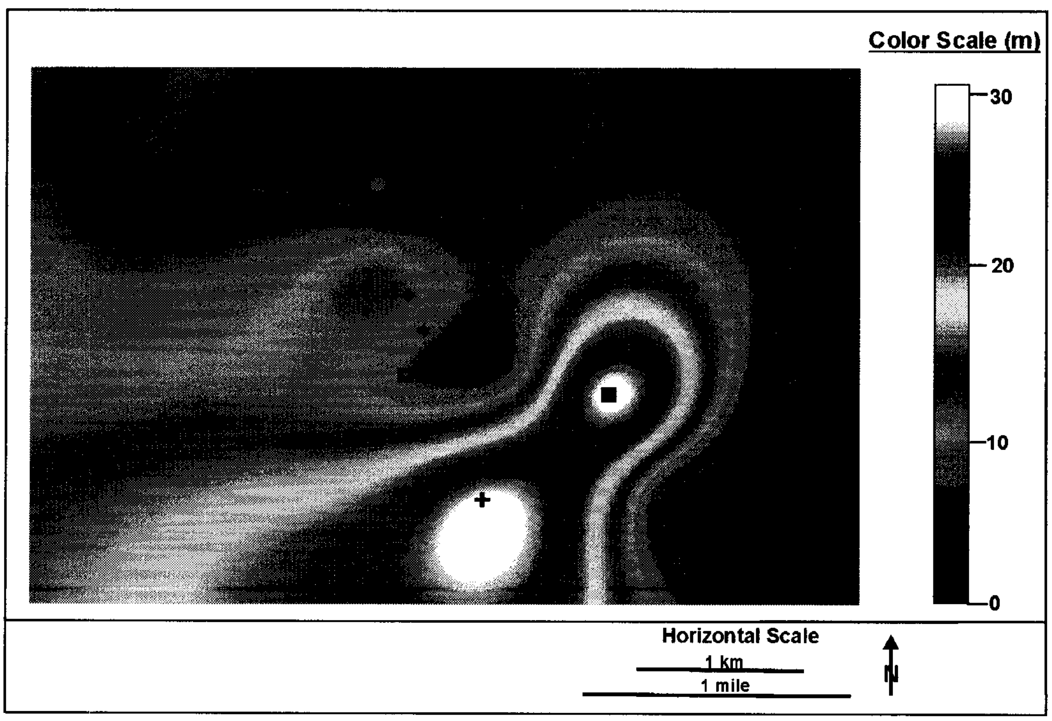

(b) Well-based porosity values.

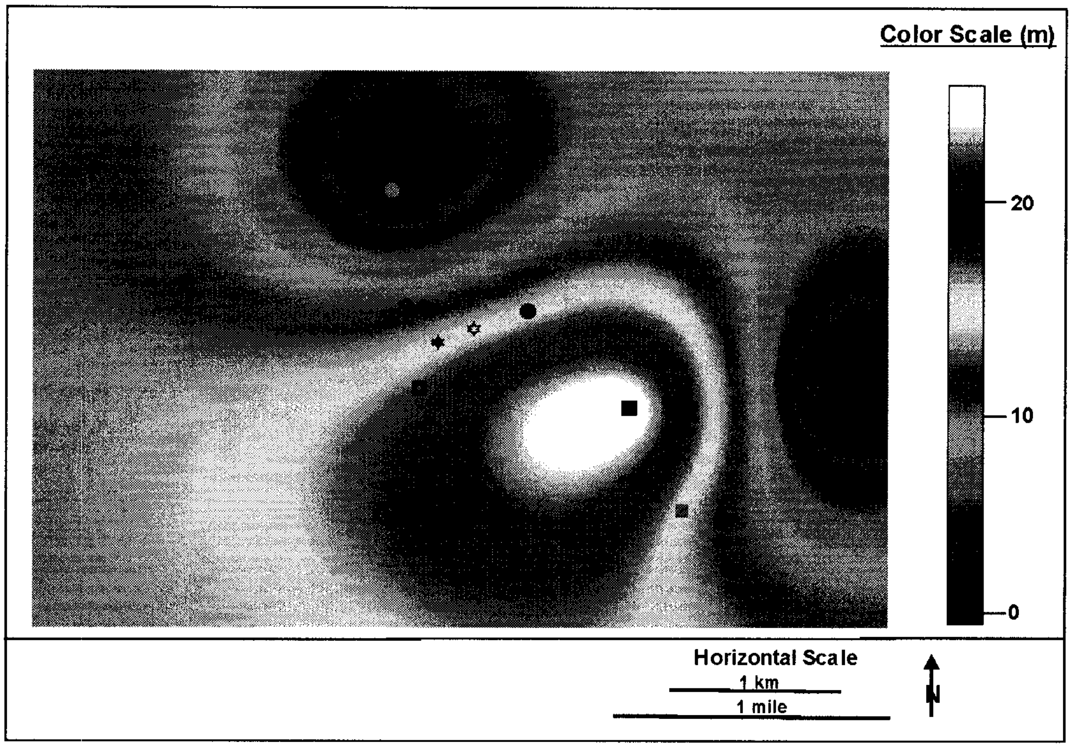

(c) Core-based porosity values. Note not all length of the porous unit was cored.

Figure F7: Porosity thickness maps calculated from different sets of data available for this analysis. Note the overall trend of porosity thickness, which is persistent in all the data. Porosity general decreases landward (NE) and increases basinward (SW). For well names, see Figure 3/8 in article.

Attribute Modeling

Model parameters

Table F6: Equal thickness model. Geometry of the stratigraphic units are equal, what varies here is the interval transit time obtained from sonic logs. DT average is the average transit time to stratigraphic units obtained from log measurements, and served as a standard to which other estimated log values (DT) were compared

Depth (m)	Porous Smackover Velocity			Base of Smackover Velocity	
	Increases (m/s)	Standard (m/s)	Decreases (m/s)	Increase (m/s)	Increase (m/s)
0	4550	4550	4550	4550	4550
152	4550	4550	4550	4550	4550
167	5898	5898	5898	5898	5898
209	6254	6254	6254	6254	6254
259	4984	4927	3963	3963	3963
365	6037	6037	6037	6080	6150

Table F7: Varying thickness model. Geometries of the stratigraphic units are equal, what varies here is the thickness of the Porous Smackover. A thickness of 35m (115 ft) served as a standard to which other estimated log values were compared. Tuning thickness for the Porous Smackover is 31m (102ft)

Average Velocity (m/s)	Varying thickness at the Porous Smackover							
	3.04m	6.1m	15m	27.4m	35m	50m	61m	76m
4550	0	0	0	0	0	0	0	0
4550	152	152	152	152	152	152	152	152
5898	167	167	167	167	167	167	167	167
6254	209	209	209	209	209	209	209	209
4927	212	215	224	237	259	259	270	285
6037	365	365	365	365	365	365	365	365

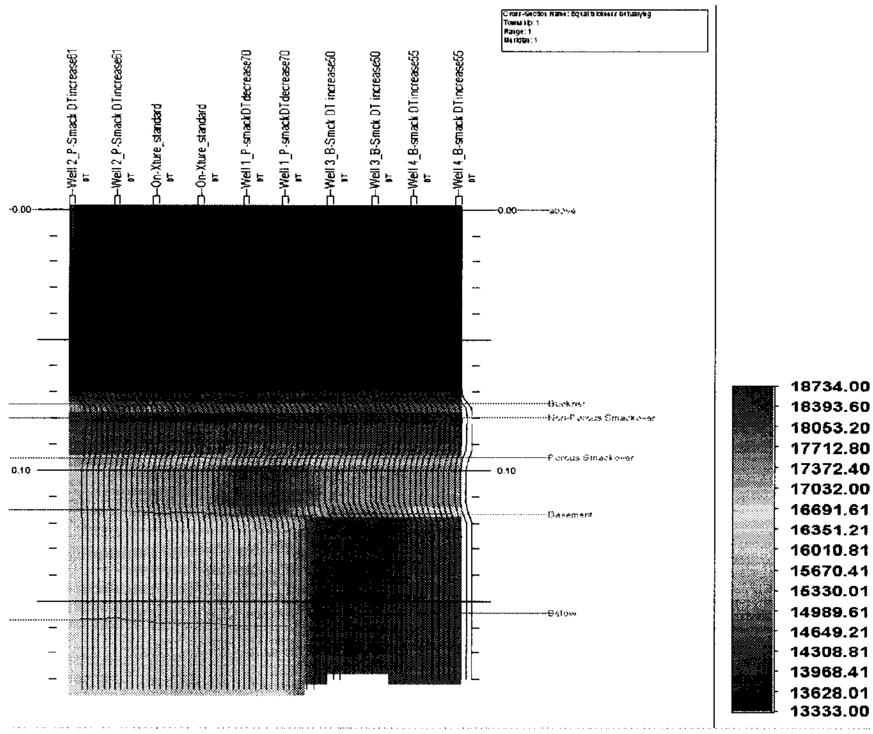

Figure F8: Equal thickness model. This shows the impedance structure across the porous Smackover.

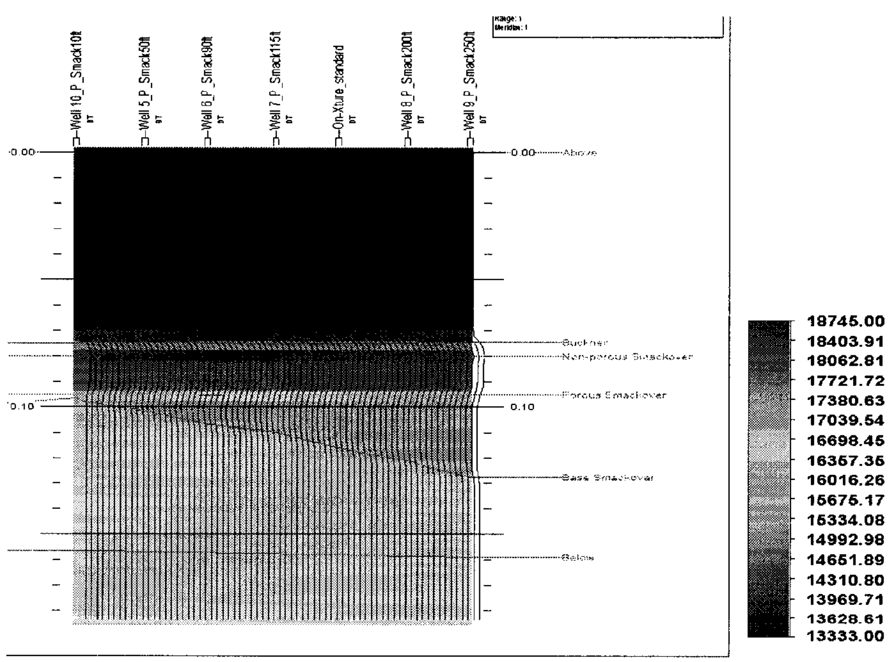

Figure F9: Varying thickness model. Varying thickness but constant acoustic impedance across the porous Smackover.

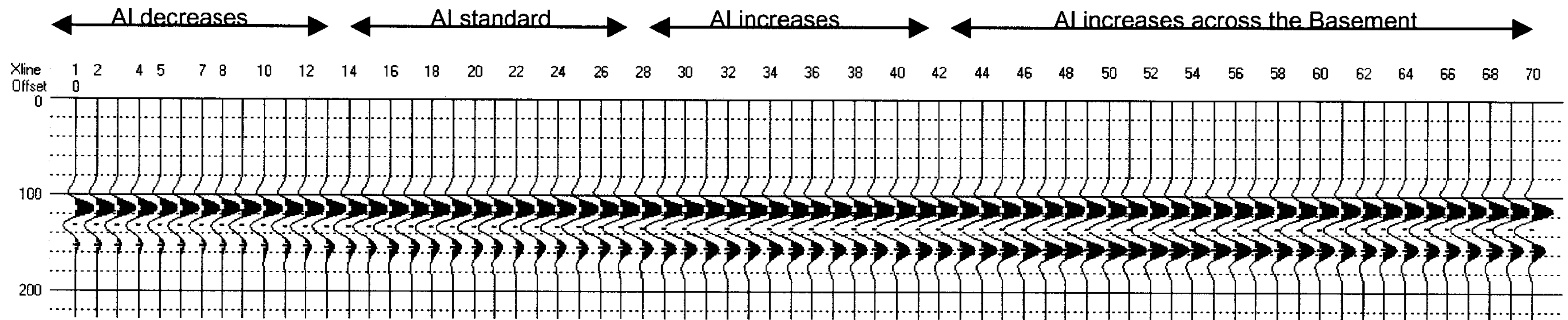

Figure F10 (a) Synthetic seismogram from modeled logs

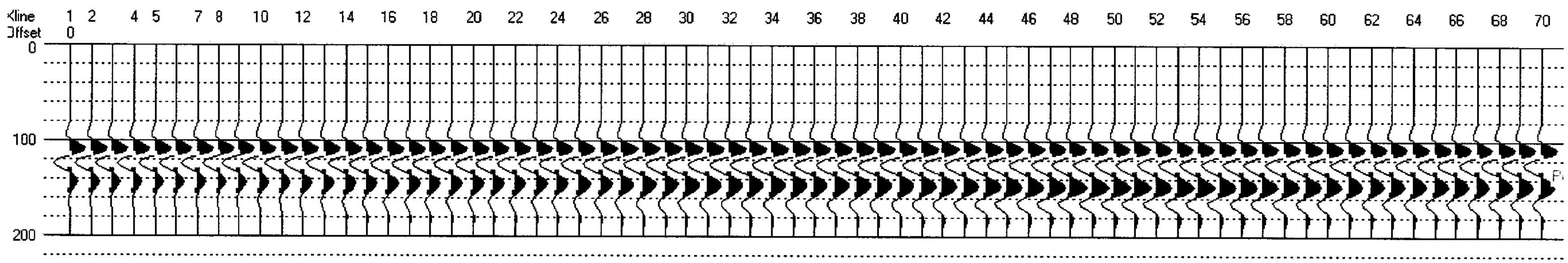

(b) Derivative attribute

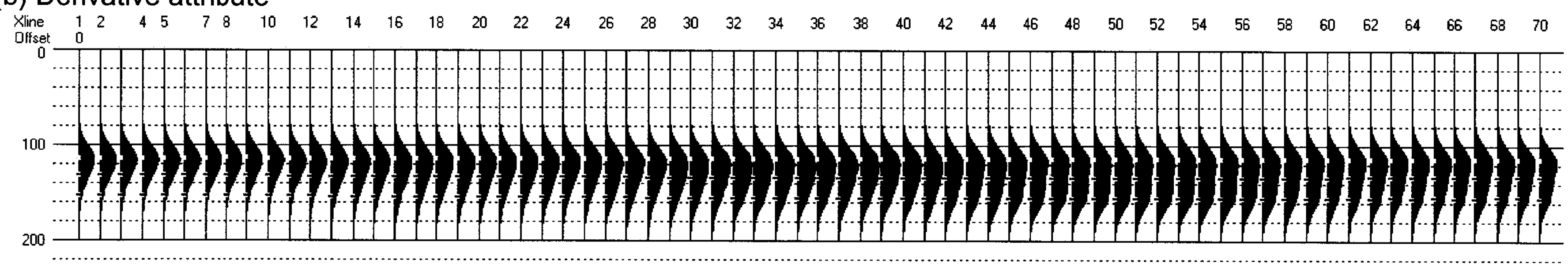

(c) Amplitude Envelope

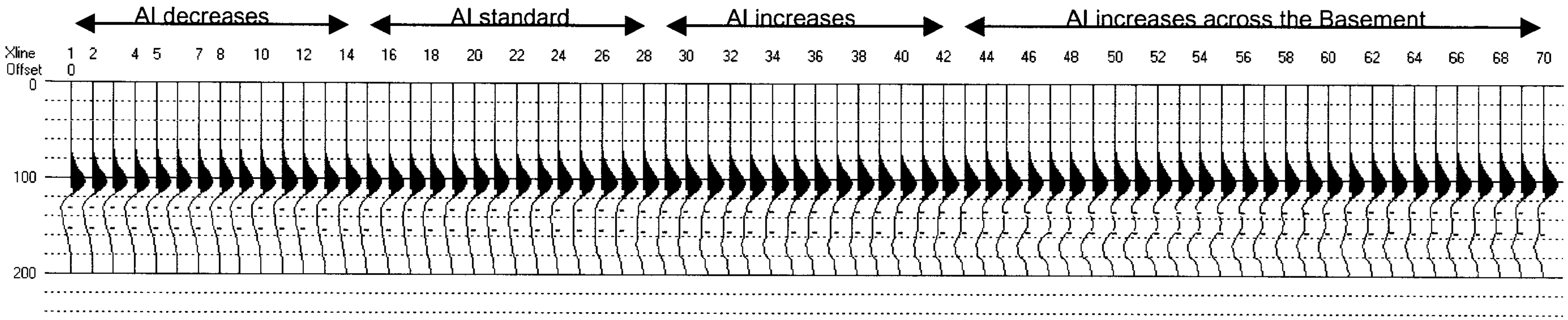

(d) Derivative Reflection Strength

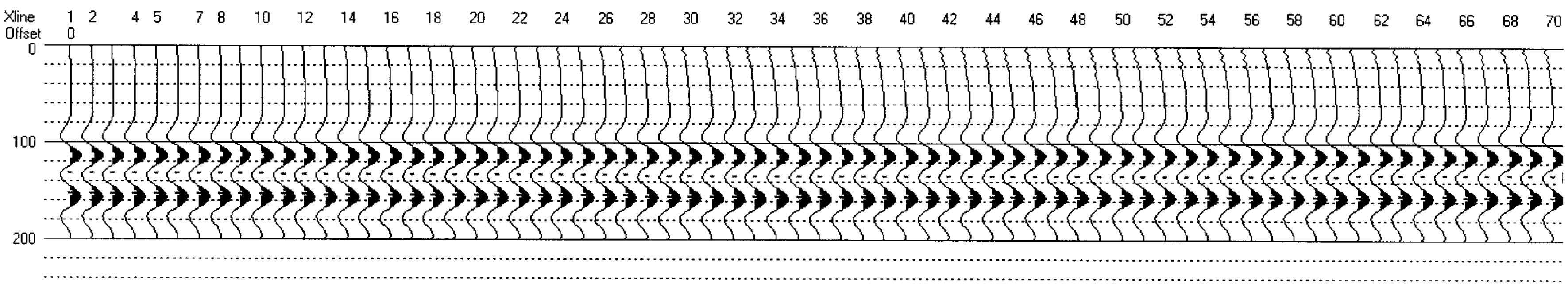

(e) Cosine Instantaneous Phase

Figure F10: Equal thickness seismic model and extracted attributes. Note the effect of varying impedance across the porous interval on the predicting attributes. Lines: Yellow = Buckner/Smackover Formation, Pink = Porous Smackover unit of the Smackover Formation, Red = Smackover base. AI = Acoustic impedance.

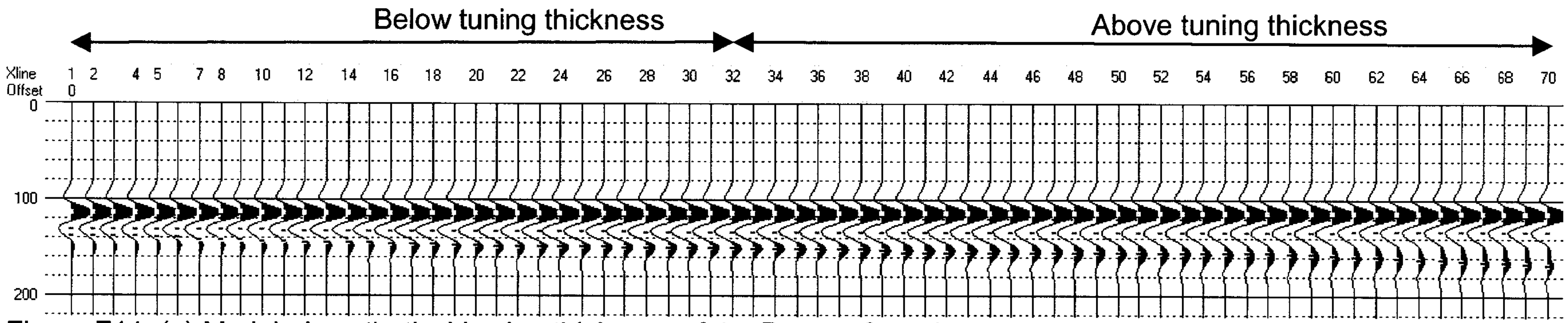

Figure F11: (a) Modeled synthetic: Varying thickness of the Porous Smackover

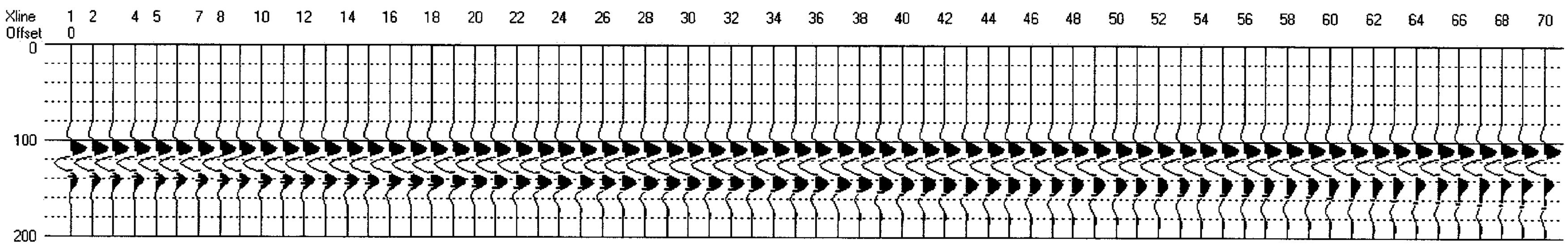

(b) Derivative

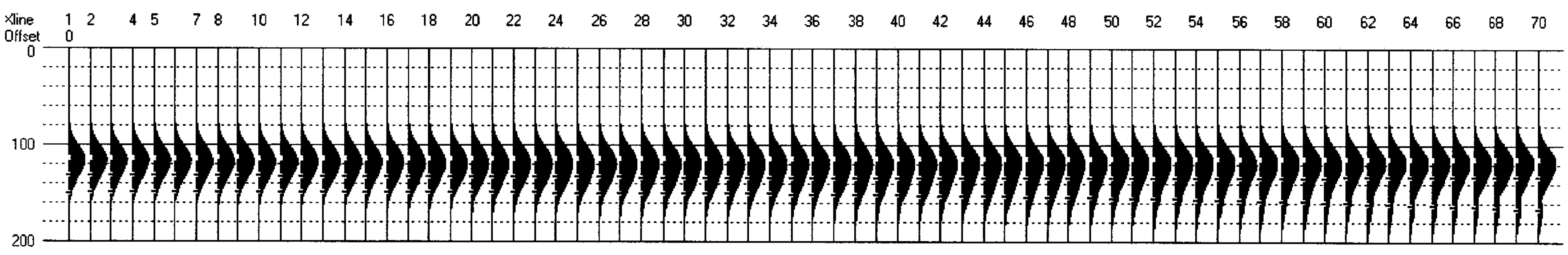

(c) Amplitude Envelope

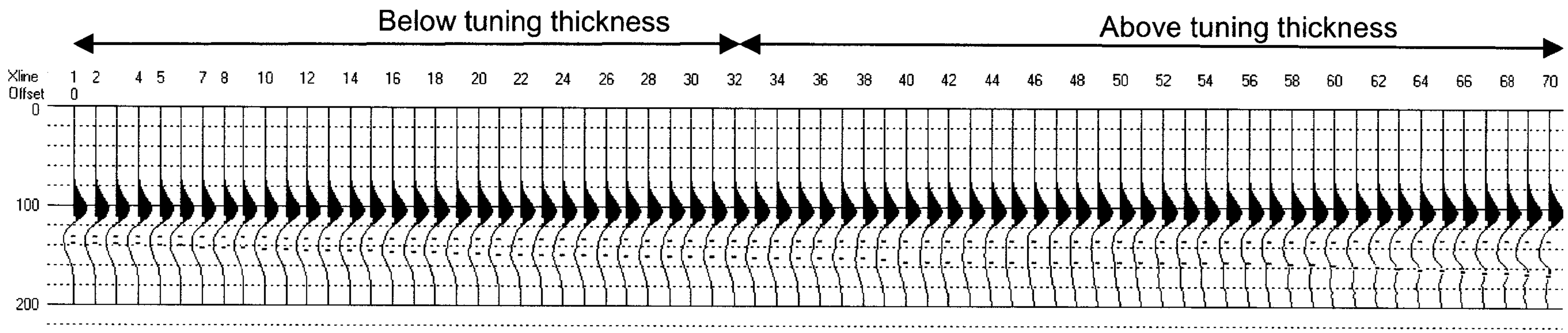

(d) Derivative Reflection Strength

Figure F11: Varying thickness model and extracted attributes. Note the effect of varying thickness of the porous interval on the predicting attributes. The Derivative Reflection Strength is the most affected of all the attributes extracted.

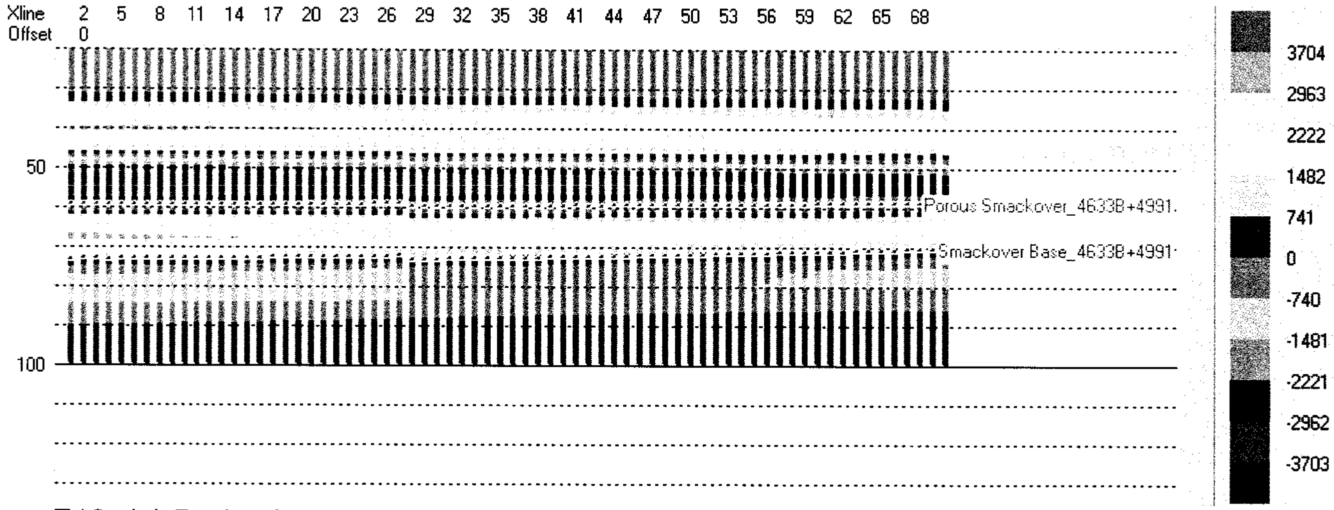

Figure F12: (a) Derivative

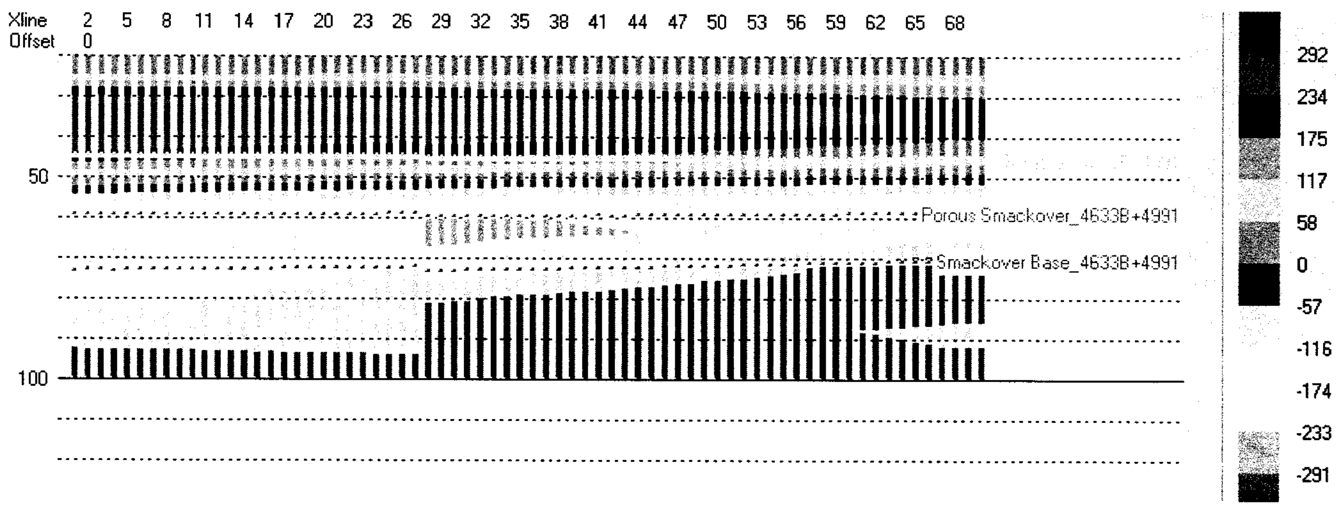

(b) Derivative Reflection Strength

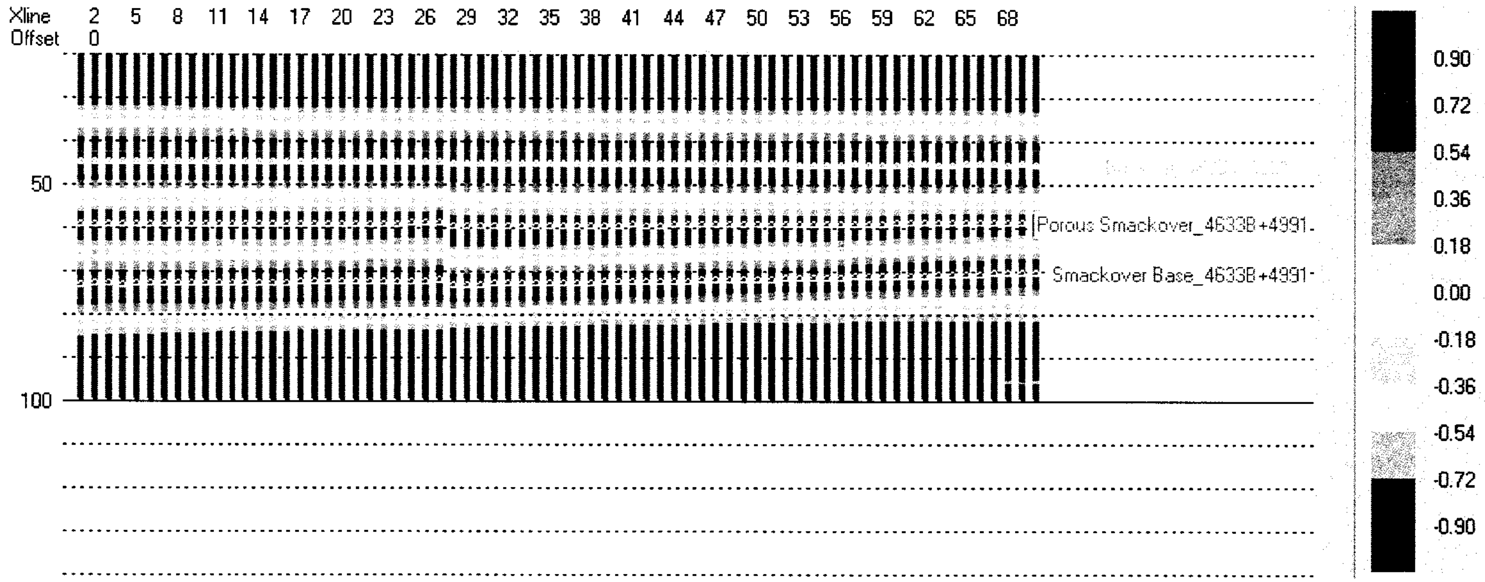

(C) Cosine Instantaneous phase

Figure F12: Well specific model, created using wells 4633-B and 4991 to account for changes in porosities on the forereef flanks. A change in amount of dip, around crossline (trace) 29 shows an abrupt change in the extracted attributes at this location. This change wasn't readily apparent on the seismic section (Article Figure 6a, 16a, 17a).

APPENDIX G

Carbonate Sedimentology and Sequence Stratigraphy

Definition and characteristics

Reefs can be defined as biologically influenced carbonate accumulation, large enough during formation to have possessed some topographic relief (Tucker and Wright, 1990). They are potentially wave resistant and stabilized syndepositionally by organic growth and/or submarine cementation (James, 1989). Reefs commonly form where there is prevalent slope within deeper water of platform interiors (James and Macintyre, 1985). The structures observed at the Appleton Field are termed carbonate build-ups. These buildups are circumscribed body of carbonate, which display topographic relief above equivalent strata, and differs in nature from surrounding rocks (Heckel, 1974).

There are two main types of reefs; skeletal/frame-built reefs formed by calcareous metazoans, and reef mounds which are mainly biogenic and formed by trapping and binding (James *et al*, 1985). These reef mounds can further be divided into microbial, formed by cyanobacteria and algae, and mudmounds formed by metazoans or metaphytes (James and Macintyre, 1985). The carbonate build-ups at Appleton Field are microbial reef mounds and composed mainly of thrombolitic facies.

Reef geometry is controlled by internal and external factors. Internal factors such as, biological and paleoecological changes, represent the most important. Changes in accommodation space due to sea-level fluctuations and/or changes in total subsidence as well as variable sediment production and input constitute important external factors for reef development. Variations of any factor result in e.g. aggradational, progradational or retrogradational stratal patterns of reefs or in "drowning". These internal and external factors further control the geometries of reefs, the development, and different types of carbonate platforms (Fig. G1; ramps, shelves, etc.).

Reefs have been known to form in a variety of depositional settings ranging from lagoonal to deep marine. Main site of carbonate formation are shelves and platforms, where favorable conditions of water depth, water clarity and temperature, wave action and availability of carbonate saturated water exist (Fig. GI; Moore, 1985). Several processes are responsible for reef formation and their subsequent modification, these are:

(i) Constructive – this mainly by action of organisms such as, cyanobacteria and algae, through the action of sediment baffling and binding.

(ii) Destruction – by action of wave and bioeroders e.g., crustaceans.

(iii) Cementation – this is responsible for the creation of reef profiles, and is pervasive on crest and front of reefs where wave action is dominant. Early cementation aids in reef stabilization and prevents against compaction. Cementation thus influences reef form and reservoir potential (James and Guinsburg, 1979; James *et al.*, 1976).

Sedimentation – This depends on the condition of the ocean (i.e., $CaCo_3$ saturation). Sediment source could be autochthonous (from erosion of reef, secretions of reef dwellers), and allochthonous (Fig. G2). Further controlling factors of sedimentations are: proximity to continent, shallow water carbonate organisms rate of production, changes in tectonic plates which

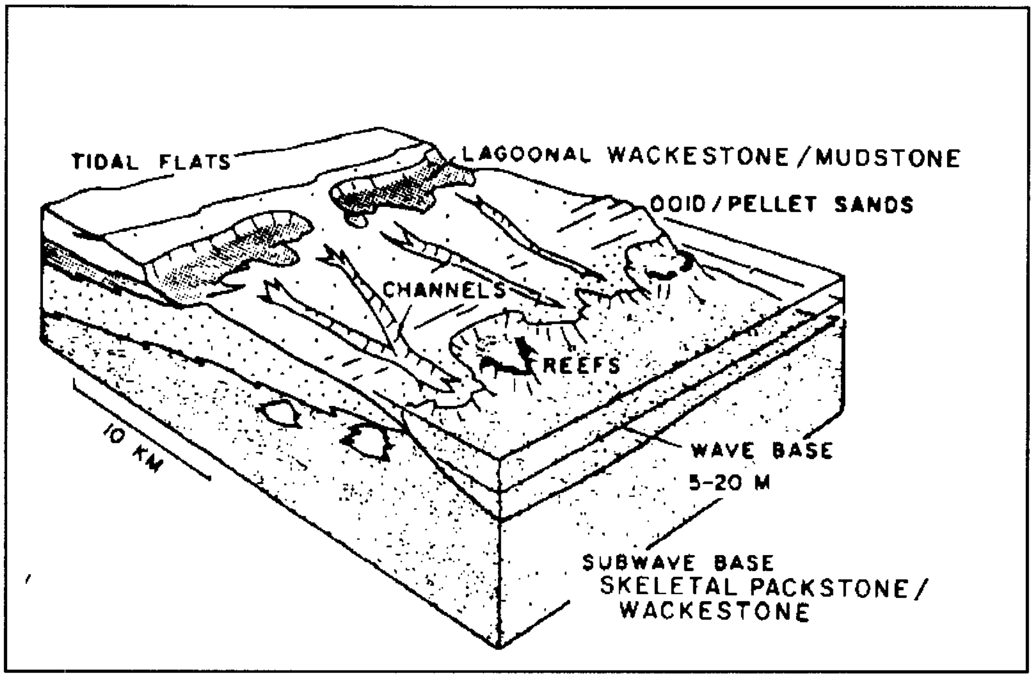

(a) Platform model: ramp, and their associated depositional environments.

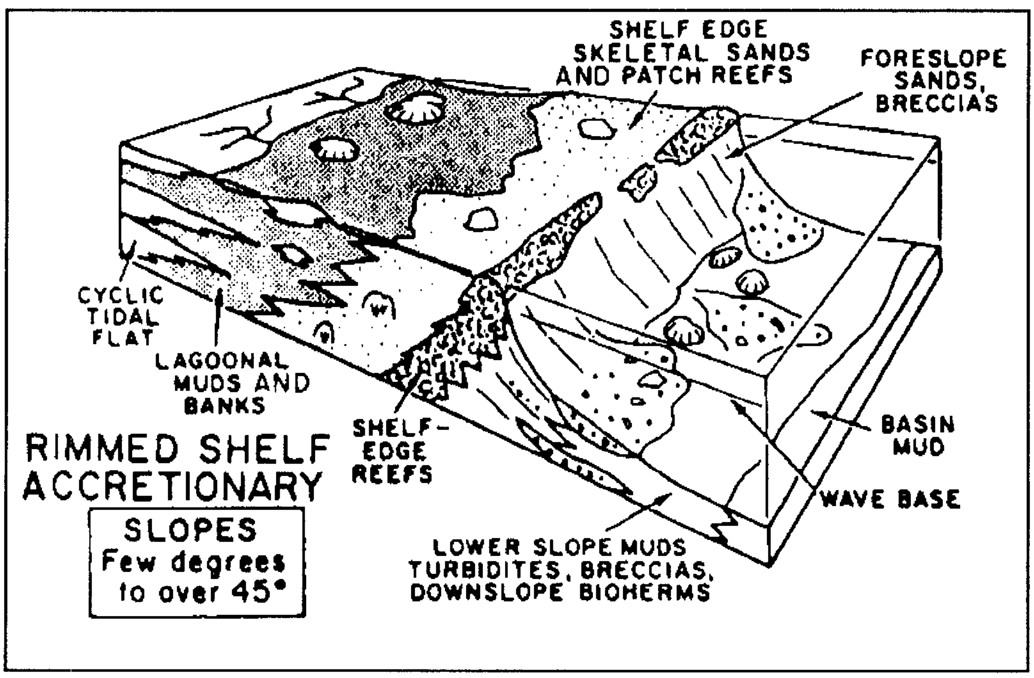

(b) Platform model: rimmed, and sub-environments (Read, 1985).

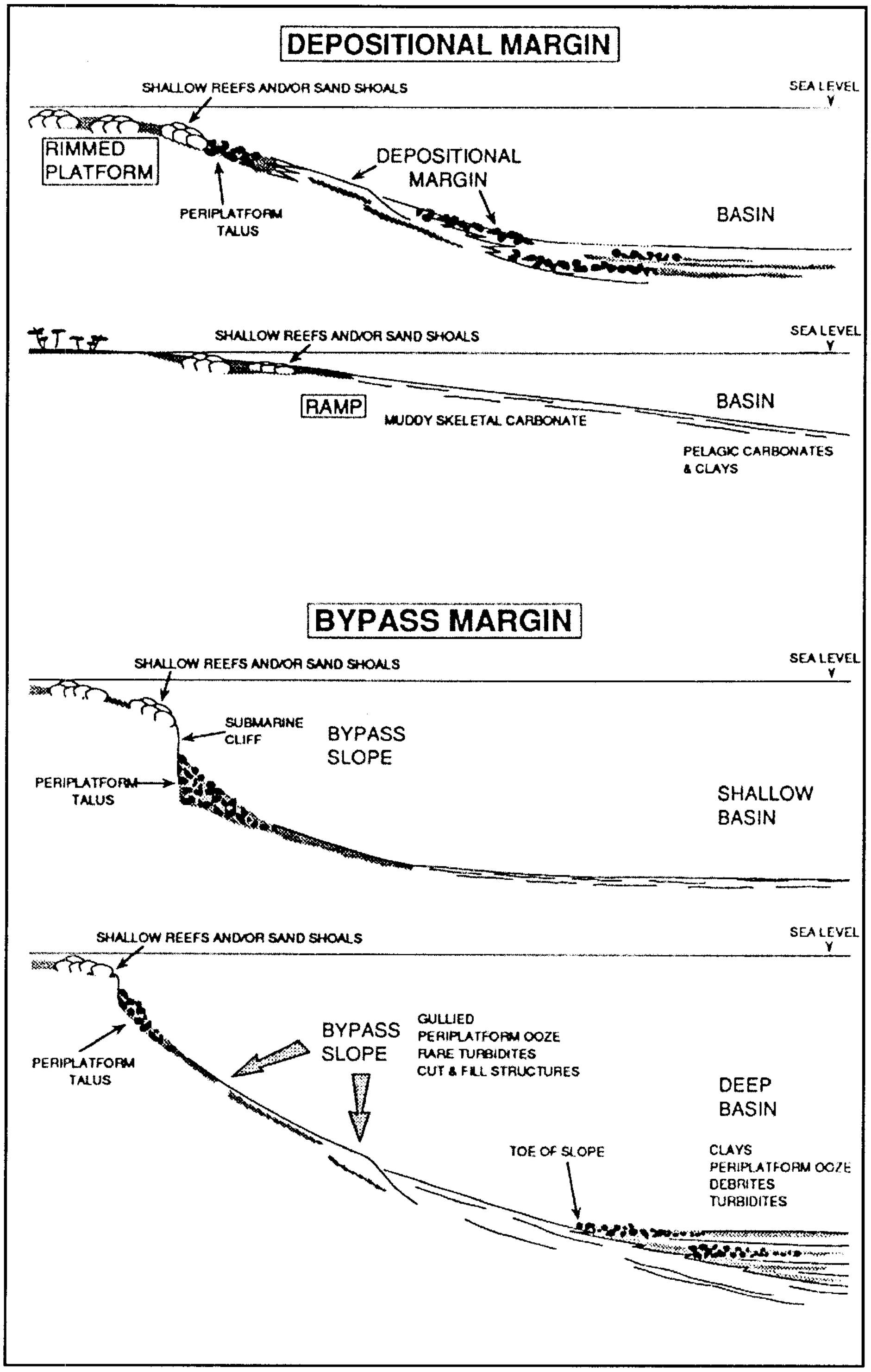

C. Depositional margin types and their associated deposits

Figure G1: Platform types and depositional Margins. From Read (1985) and Tucker and Wright (1990).

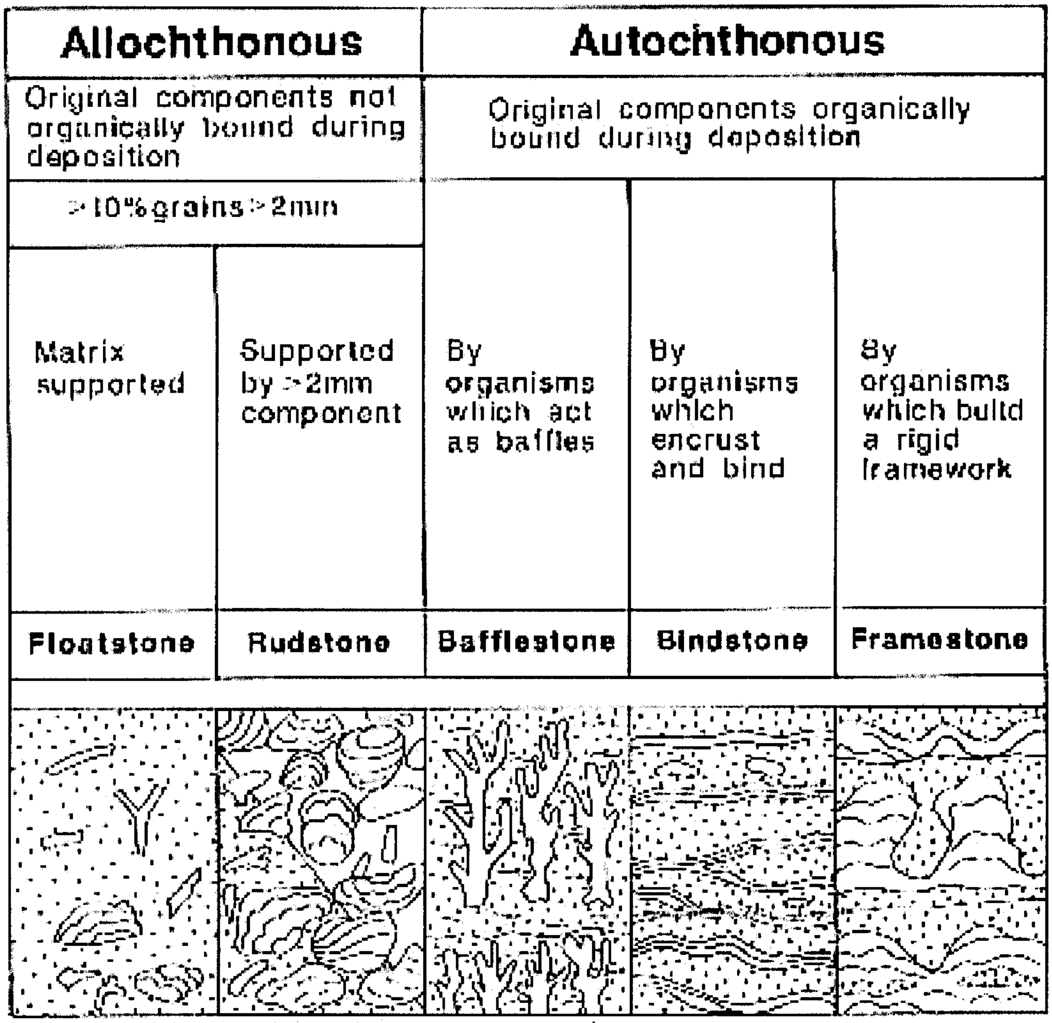

Figure G2 Sediment source and textural classification of reef limestone from Embry and Klovan, (1971); James (1984).

may effect carbonate production, evolution of reef-building organisms, oceanographic setting.

Reef morphology

Major controls on reef morphology

(1) Biological productivity – a function of water depth, salinity, nutrient level, etc.

(2) Topography – carbonate sedimentation decreases with increase in relief; a result of biological productivity.

(3) Sea level changes- this results mainly from eustatic sea level changes and tectonism.

Effects of changing sea levels:

(a) Rising sea level (James and Macintyre, 1985; Tucker and Wright, 1990)

  (i) Give-up - sea level increase is greater than carbonate production and accumulation (Fig. G4.1).

  (ii) Back-step – carbonate production and accumulation slower than sea-level rise. Reef grows in stages, transgressing to shallower and higher position on the platform margin (Fig. 4.2).

  (iii) Keep-up (accretion) – carbonate production and accumulation (growth) increases with increase in sea level (Fig. G4.4).

  (iv) Catch-up – carbonate growth rate higher than sea level increase (Fig. G4.3).

(b) Falling sea levels – this leads to progradation of reef due to decreasing water depth (Fig. G.4.5). Falling sea levels also leads to dolomitization due to mixing of fresh and marine waters, or, as at Appleton, evaporite formation.

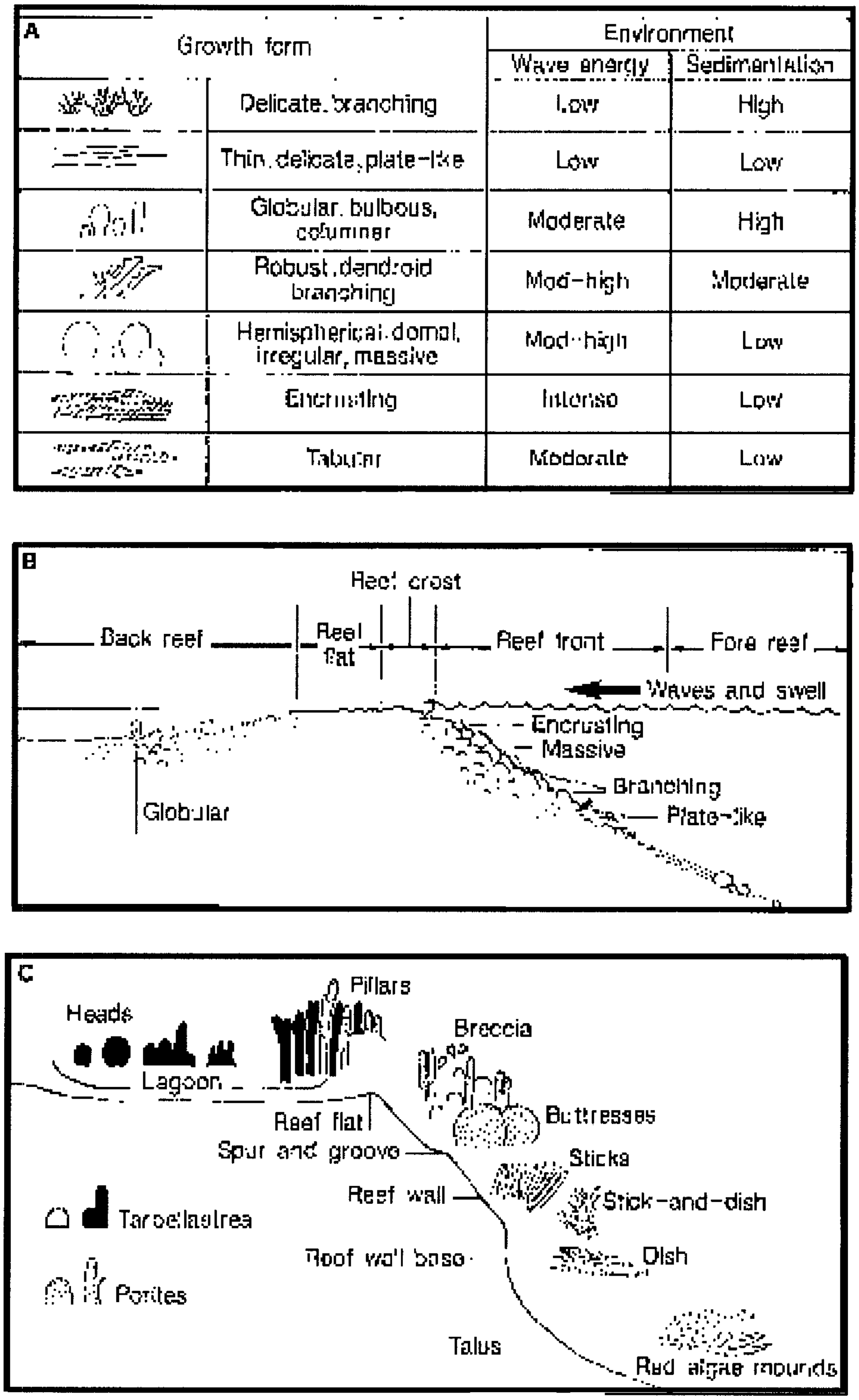

A Growth form		Environment: Wave energy	Environment: Sedimentation
	Delicate, branching	Low	High
	Thin, delicate, plate-like	Low	Low
	Globular, bulbous, columnar	Moderate	High
	Robust, dendroid branching	Mod-high	Moderate
	Hemispherical, domal, irregular, massive	Mod-high	Low
	Encrusting	Intense	Low
	Tabular	Moderate	Low

Figure G3: Hypothetical section illustrating morphology of reef builders. After James (1984).

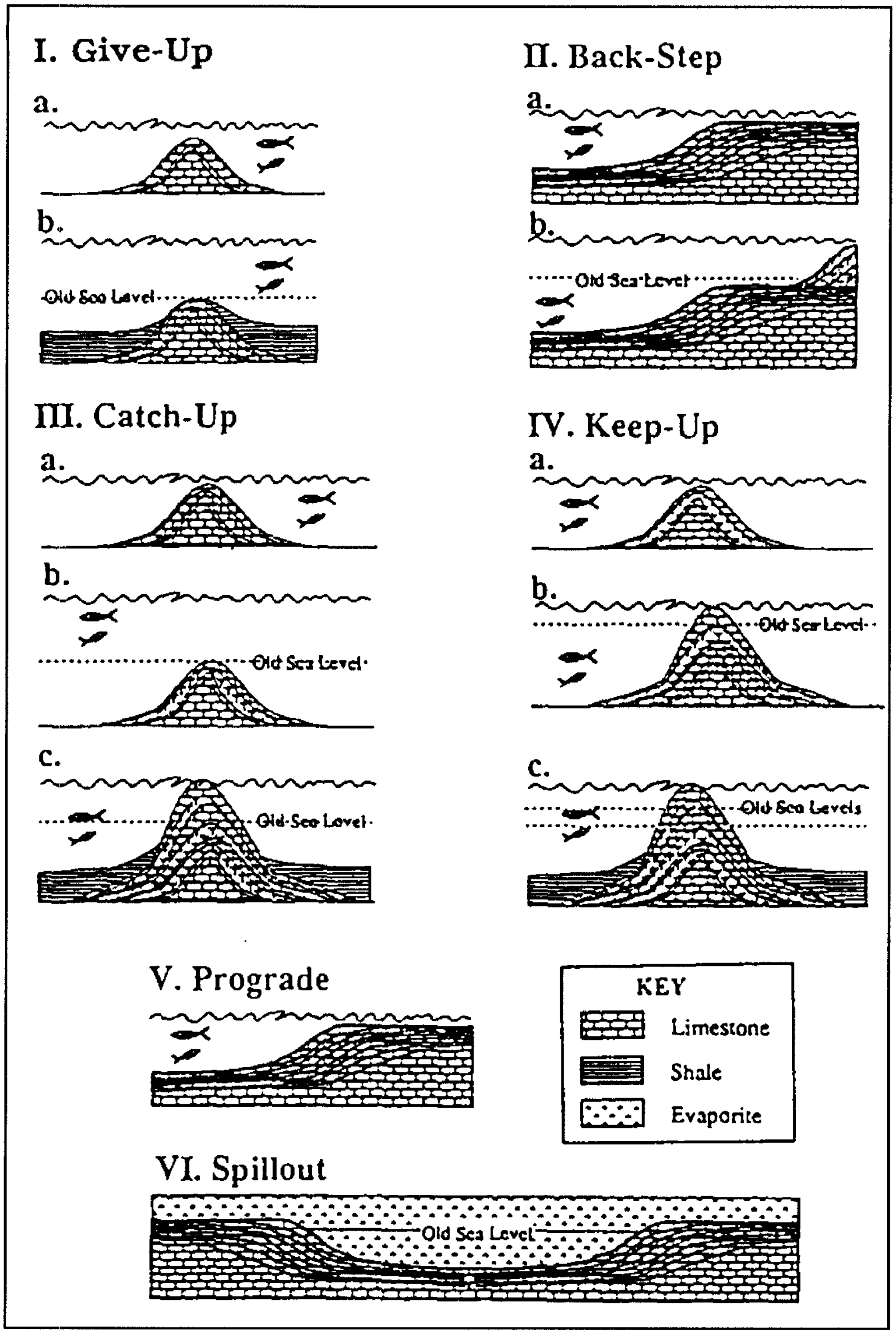

Figure G4: Effect of sea level changes on the morphology of reefs. After Kendall *et al.* (1991).

The potential space available for sediment to fill is determined from the combined movement of the sea surface (eustasy) and movement of the sea floor. Therefore, accommodation is a function of changes in relative sea level. (Sarg 1988, Posamentier and James, 1993). Thus accommodation is not only a function of eustasy and tectonic movement but also of sedimentation. It is this hypothesis that governs the concept of sequence stratigraphy, and can be illustrated thus (Fig. G5):

a) Sea level rise and zero or low sediment flux results in transgression.
b) Sea level rise and there is a low rate of sediment flux, leads to retrogradation of the coastal parasequences.
c) Sea level rises and the rate of sediment flux equals sea level rise, then aggradation of the coastal parasequence results.
d) Sea level rises and the rate of sediment flux exceeds the sea level rise, then progradation of the coastal parasequence results.

Changes in sea level greatly affect slope morphologies by influencing sediment availability, type, transport, deposition, and erosion. Sea level and carbonate slope development can be broken down into system tracks based upon slope development and sea level changes resulting from climatic variances and tectonic subsidence (Van Wagoner *et al*, 1988).

TST: In the transgressive sequence system tracks the sedimentation rate and sediment influx exceeds sea level rise, resulting in sediments being deposited closer to shore along margins, on the platform and farther up slope reducing the sediment availability. In transgressive system tracks, sea level rise results in an increased sediment influx and the “start-up phase” in which carbonate accumulation. This is followed by the “catch-up phase” which results in a prograding shift of sediments being deposited onto the slopes. The transgressive systems track peaks with the “keep-up phase” in which sediment accumulation closely matches the rate of sea level rise (James and Macintyre, 1985)

HST: In Highstand system tracks, sea level rise reaches maximum, the inundated self has continued prograding and carbonate sedimentation and accumulation reached a maximum. These highstand system tracks retain the sediment shift of the types of sediments being deposited onto the slopes receiving an increase in carbonate sediment from the excess shelf carbonate accumulation. Sea level rise also shifts carbonate transport further out onto the slope thus increasing the surface area for deposition. As highstand progresses the on-lap at maximum transgression or highstand often leads to sediment starvation.

LST: In lowstand system tracks in comparison to highstand system tracks and transgressive sequences are reversed. Sea level reaching maximum drop stage, the rate of subsidence still less than the rate of sedimentation, which initially resulted in an increased sediment influx seaward because the sediments are being deposited further away from shore along margins on the platform. Lowstand system tracks result in a shift of the types of sediments being deposited onto the slopes to an increase in siliclastic input of sediments. Sea level drops also shifts the type of transport further out onto the slope also decreasing the surface area onto which the sediment may be deposited resulting in retrograding shelves (Fig.G5). Slope failure occurs frequently at times of lowstand and as a result debris-flow, grain-flow deposits primarily thickened wedges and fans develop. Additionally, the winnowing and erosion of platform corals, sediments and shallow water sediments exposed at lowstand and are deposit seaward along the slope. Toward the end of the lowstand system initial phase shifts in subsidence and seal transition to a transgressive systems track.

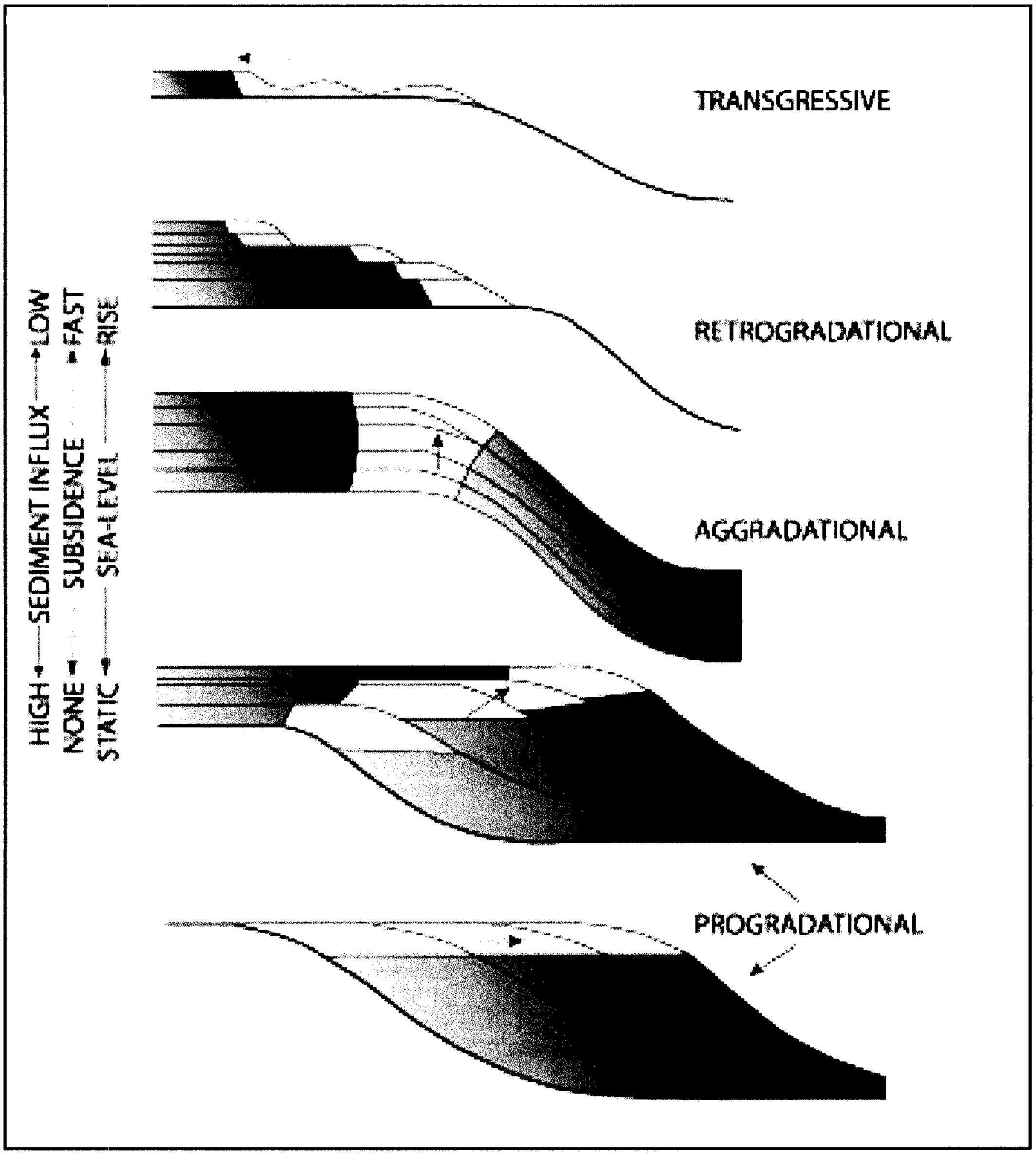

Figure G5: Depositional architecture as a function of accommodation volume and sediment supply (from Emery, 1999; after Galloway, 1989)

This change in sea level led to diversity in reef organisms and growth forms. For patch reefs, there are five main stages of growth seen in Figure G6:

(i) Initial growth or stabilization stage. These are characterized by framestone.

(ii) Vertical growth or reef colonization stage, characterized by bafflestone and floatstone. At the Appleton Field the boundstone facies (thrombolites) dominate at this stage (see Fig. G7). For patch reefs, this is also a stage for biodiversification. Growth forms range from domal to encrusting (see Fig. G3)

(iii) Wave action- energy gradients (windward dir = higher energy bindstone on crest, leeward = lower energy).

(iv) Higher energy gradients. Rudstone (Fig. G2) and grainstone facies dominate (see Fig. G6).

(v) Sediments undergo diagenesis (e.g., lithification).

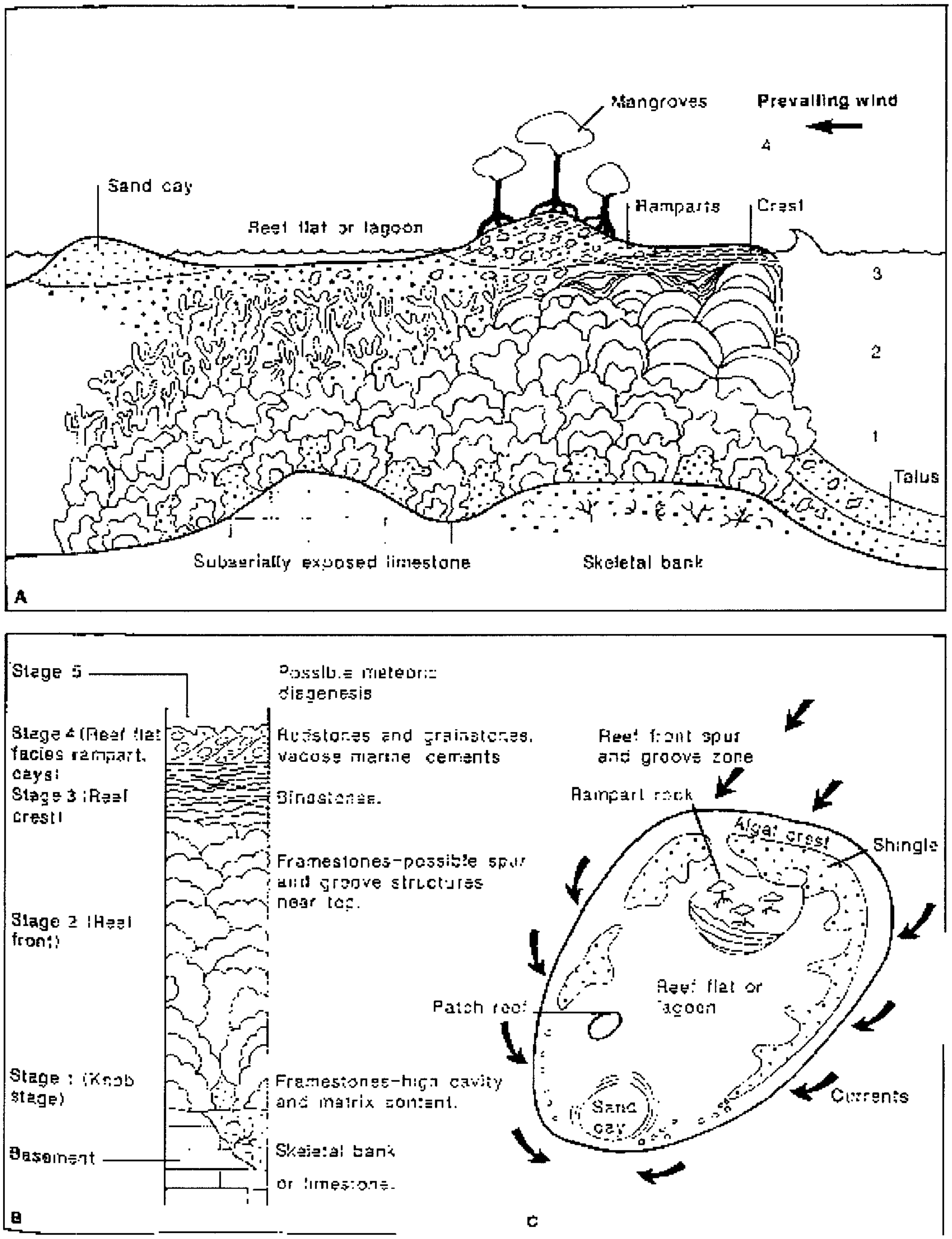

Figure G6: Schematic development of a patch reef (a & b show transects through reef, and c is a horizontal slice across the reef).

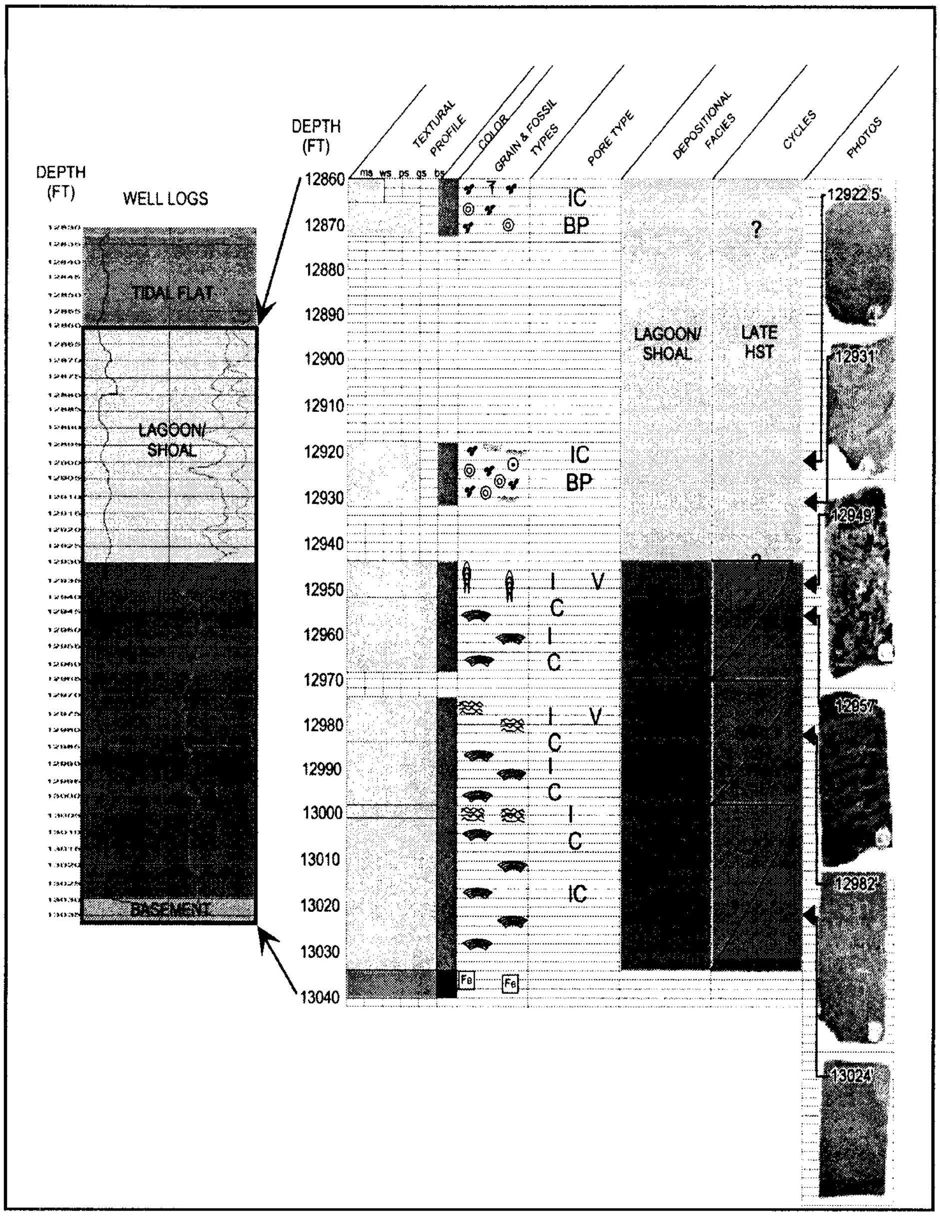

Figure G7

(a) Well 4633-B

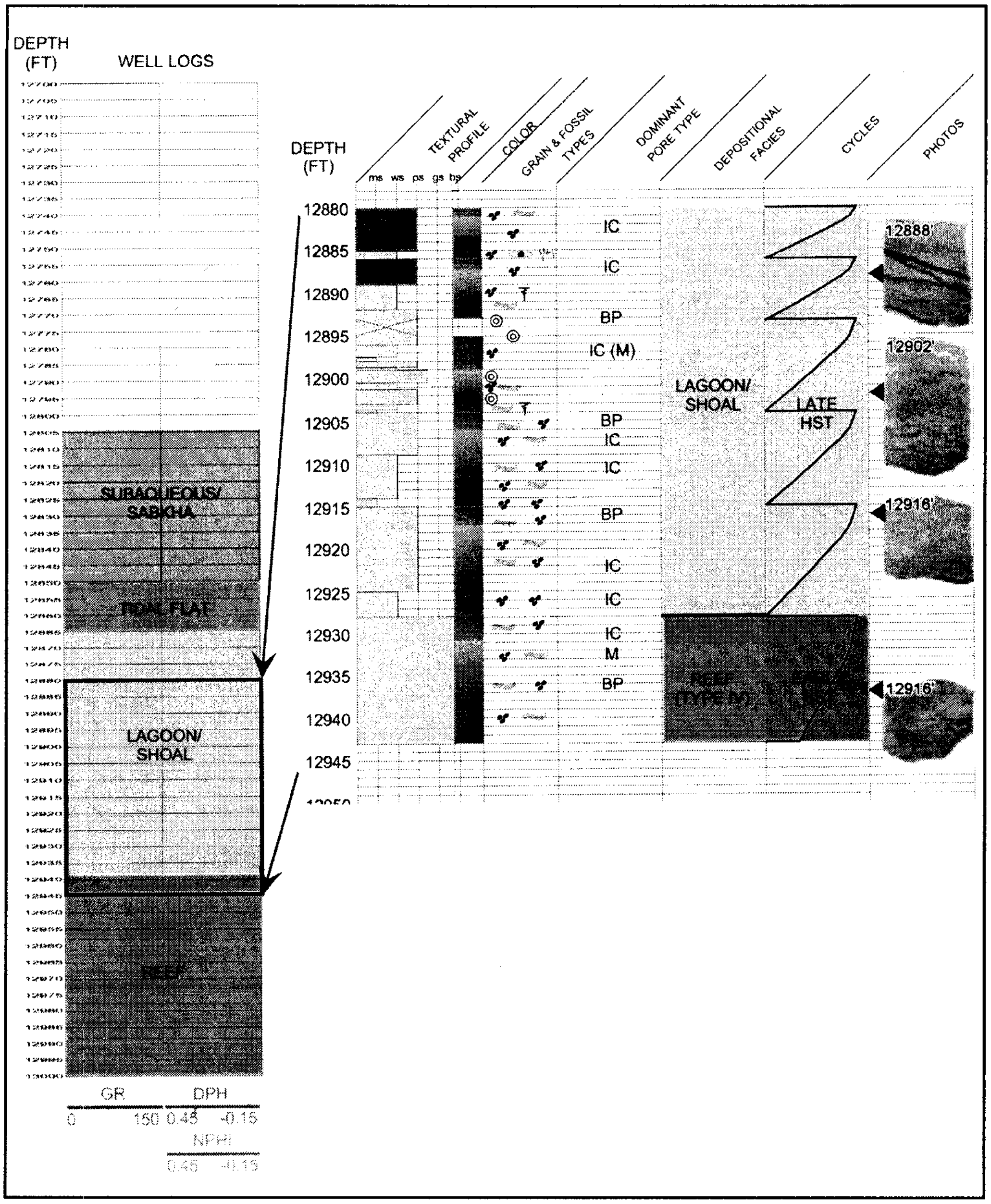

(b) Well 3854

Figure G7: Graphic logs. These show the facies types and their sequence stratigraphic relationship. These can be easily related to the different stages of patch reef growth in Fig. G6 (After Parcell, 2000).